Supplementary Information for

Ecological causes of uneven diversification and richness in the mammal tree of life

Nathan S. Upham, Jacob A. Esselstyn, and Walter Jetz

Nathan S. Upham
Email: nathan.upham@yale.edu

This PDF file includes:

Table of Contents
Supplementary Methods
Supplementary Results
Figs. S1 to S24
Tables S1 to S12
Captions for Datasets S1 to S7
References for SI reference citations

Other supplementary materials for this manuscript include the following:

Datasets S1 to S7

Table of Contents (click to navigate)

Supplementary Methods

0. Experimental design

0.1 Overview of tree-building strategy

We reconstructed the evolutionary history of extant Mammalia aiming to maximize the accuracy and comparability of temporal information (branch lengths) across lineages in a posterior set of time-calibrated phylogenies. Our goal was to enable macroevolutionary questions to be addressed in a rigorous and replicable way across the tree of all mammals, while also considering uncertainty in divergence timing and species relationships. We devised a multi-step strategy for tree-building (Fig. S1) to: (i) sample and vet available DNA sequences for extant and recently extinct species into a 31-gene supermatrix (sections 1–3); (ii) build a global maximum likelihood (ML) tree from that DNA supermatrix (section 4); (iii) include species unsampled for DNA in the phylogeny via taxonomic completion methods (PASTIS (1), section 5); and (iv) integrate fossil data at nodes and tips to compare methods of calibrating molecular divergence times among clades (section 6). Adapting the 'backbone-and-patch' strategy of Jetz et al. (2), we split the full diversity of Mammalia into non-overlapping subclades ('patches'), estimated their phylogenies separately in relative-time units, and then rescaled and joined patches to fossil-calibrated backbones (section 7). Grafting together the full tree in this way was designed to unify the time scales of all species, so that all branches in the tree are comparable across clades, biomes, and other units of biological interest.

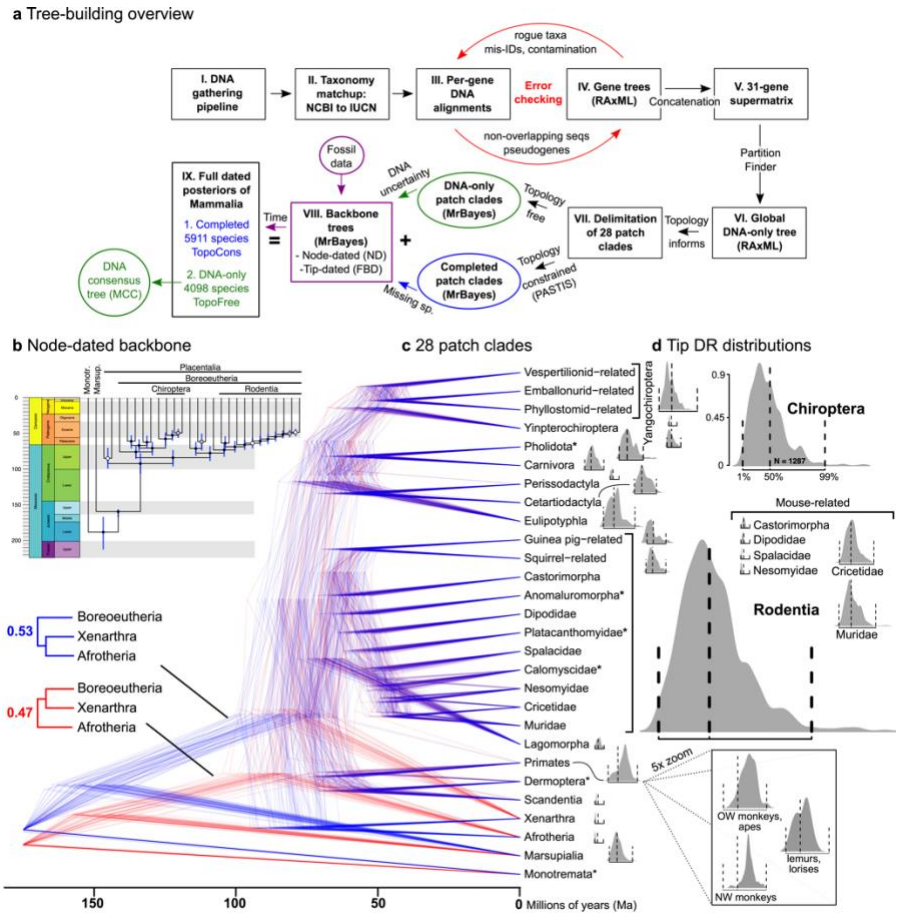

Fig. S1.
Multi-step strategy for building the supermatrix-based Mammalia phylogeny. (a) Schematic overview of DNA sequence gathering from NCBI, taxonomic reconciliation and error checking, and building a global maximum-likelihood (ML) tree from the resulting supermatrix (31 genes, 4098 species). A two-part strategy estimated and assembled subclade (patch) phylogenies and fossil-calibrated backbone trees to yield posterior samples of 10,000 fully dated phylogenies, either with 5911 species and the global ML tree topology constrained (Completed trees, TopoCons) or with 4098 DNA-sampled species and no topology constraints (DNA-only trees, TopoFree). Node- and tip-dated backbones were used, and maximum clade credibility (MCC) trees were estimated for the DNA-only trees. (b) Backbone trees were pruned to representatives of (c) 28 patch clades where an assumption of hard monophyly could be made. Shown is the topological uncertainty across the backbone (sample of 100 trees), highlighting the unresolved base of

Placentalia, slightly favoring the Atlantogenata hypothesis (blue) versus Exafroplacentalia (red). (d) Density plots of tip-level diversification rate (tip DR) scaled in proportionate size to the number of species in that clade and shown relative to the 0.01, 0.50, and 0.99 quantiles for all mammals (dotted lines). Clades with < 140 species are equally sized for visibility, while those < 10 species are marked with asterisks and not shown. Monotr., Monotremata; Marsup., Marsupialia; X., Xenarthra; Chiropt., Chiroptera; OW, Old World; NW, New World.

0.2 Our tree relative to other inference methods

The decision to divide Mammalia into smaller clades for analyses – rather than perform tree-wide dated inference – is based on trade-offs in the following factors:

(i) computational limits to adding tips in phylogenetic analyses;
(ii) propagating uncertainty in inference; and
(iii) propagating uncertainty in models of evolution.

We found the maximum tree size for Bayesian inference in MrBayes v.3.2.6 (3) was ~800 species in our trial runs. Near this maximum, our largest patch (Muridae, 778 species) took 3.7 weeks to finish 33,330,000 generations in parallel on 16 BEAGLE-enabled compute nodes. We suggest a current hard limit of < 1000 species for reasonable convergence of Bayesian supermatrix analyses (matrix complexity was also a key determinant of run times, see section 5.1). Our goal of including full uncertainty of divergence times and species relationships was best suited to Bayesian inference, where the likelihood of parameter estimates is reflected by their posterior frequency (4–7). In contrast, maximum-likelihood and parsimony approaches to find the single 'best' point estimate effectively collapse tree uncertainty and can increases type I error (4). The ideal of using the multi-species coalescent to co-estimate genealogies and the species tree (8) is unfortunately limited to ~25 species (e.g., *BEAST (9, 10)). ML-based models (e.g., ASTRAL-II (11)) have extended applications of the coalescent to larger trees, but analyzing the breadth of Mammalia is still not feasible. We instead based our backbone-and-patch subdivision of the tree on the supermatrix approach (12) using Bayesian inference and partitioned gene regions.

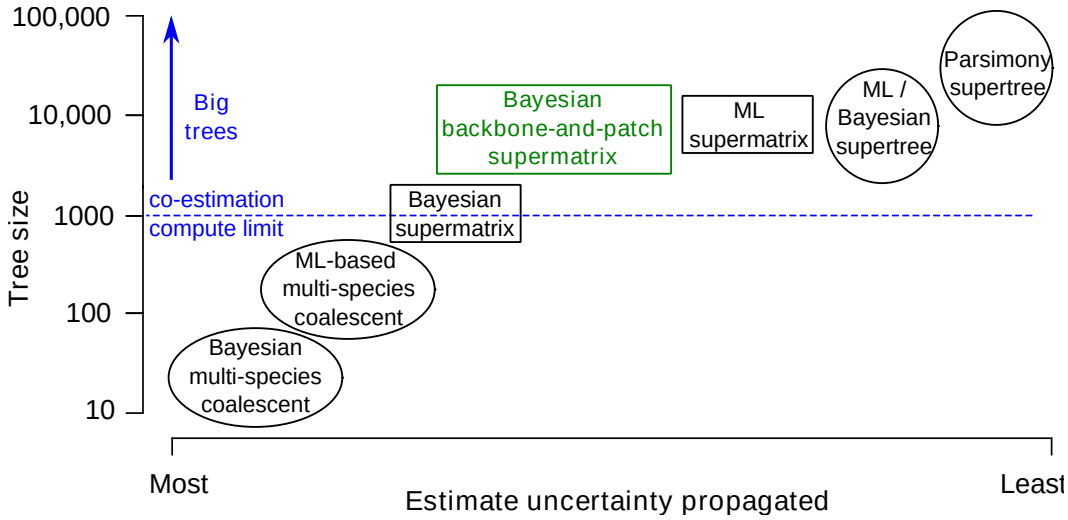

Fig. S2.
Trade-off between tree size and statistical uncertainty in the tree. Computational costs increase with tree size and the realism of the evolutionary models, resulting in reduced ability to propagate estimate uncertainty in larger trees. We suggest a current upper limit of ~1000 species for Bayesian co-estimation, beyond which performing supermatrix analyses requires our backbone-and-patch approach (green) to divide the tree into smaller sub-analyses. Note that the supermatrix approach uses multiple model partitions (e.g., GTR+G, HKY) to co-estimate molecular evolutionary parameters with tree topology, while supertrees merge and re-scale a collection of independently estimated trees.

Overall, we emphasize that the 'big tree' territory beyond ~1000 species requires new types of phylogenetic assumptions to overcome computational limits to co-estimation (Fig. S2). Parsimony supertrees were developed for this purpose (e.g., matrix representation parsimony (13)) and first implemented on large scales across Mammalia (Bininda-Emonds et al. (14) and its updates (15, 16)). However, supertrees add artifacts of short branch lengths every time merged source trees disagree (e.g., >50% of nodes in Bininda-Emonds et al. (14)), and are thus biased to infer rapid radiation at regions of the tree with the greatest phylogenetic and temporal uncertainty (e.g., some results of Stadler (17) are attributable to a series of polytomies in rodents and bats; see Supplementary Results for a comparison of tree shapes). For this reason, we aimed to depart from the supertree paradigm, which was also used for two recent mammal supertrees (18, 19), instead aiming to measure tree-wide diversification rates and their uncertainty using the backbone-and-patch supermatrix approach detailed below.

1. DNA gathering pipeline

1.1. Targeted gene fragments

We targeted 31 gene fragments (Table S1) that are commonly sampled across mammalian species and thus useful in a comparative phylogenetic framework. The genetic sampling of Meredith et al. (20) served as our starting point since it included most extant families for 27 nuclear genes (nDNA; 22 exons and 5 non-coding [NC] regions). Although Meredith et al. (20) analyzed RAG1 as a single region, we treated it as 2 non-overlapping regions (RAG1a and RAG1b) to match how researchers have most commonly published these sequences and avoiding an alignment gap between them (e.g., a 357-base pair [bp] gap separates the *Didelphis virginiana* RAG1 sequences DQ865890 and AY011864 as aligned to the RAG1 entry for this taxon in TreeBase submission S11872 (20)). We additionally targeted four protein-coding genes from the mitochondrion (mtDNA; cytochrome-b [CYTB], cytochrome oxidase I [COI], and NADH dehydrogenase I [ND1] and II [ND2]) to help us maximize the species-level sampling in the resultant supermatrix and downstream phylogeny.

1.2. BLAST-based gathering of DNA sequences

To assemble data useful for Mammalia-wide phylogenetic analyses, all public DNA sequences gathered from GenBank needed to be: (i) homologous and orthologous to our targeted gene fragments; and (ii) associated with accurate taxonomic information. Ideally, all sequences would be annotated directly as a vouchered museum specimen, but in practice, GenBank and museum data are not well associated (e.g., the "specimen_voucher" field is often empty, or contains collector not museum numbers, inconsistent formats, or unrelated identifiers). Much work is needed to improve links between museums, NCBI, taxonomic authorities, and trait aggregators like IUCN (21). However, to improve mammalian phylogeny at the present time, we devised bioinformatic solutions to this key problem of matching public DNA sequences to recognized taxon names. We used the BLAST algorithm (Basic Local Alignment Search Tool; (22)) for verifying standards of homology and orthology among gathered sequence data, and to efficiently query a local copy of NCBI's nucleotide (nt) database (downloaded on 20 April 2015).

For each gene, we used a set of pre-vetted sequences or "DNA baits" as queries for extracting homologous gene fragments from the NCBI database. Given that these per-gene DNA baits were the basis for all downstream work, each bait set was carefully curated to ensure the valid homology of sequences to the targeted gene (e.g., robust alignment, absence of stop codons) while sampling up to 1 sequence per mammalian family. Nuclear DNA baits were taken

from the mammal portion of Meredith et al. (20)'s DNA alignment, as subset to 1 family representative per gene. We constructed our own mtDNA baits on a per-gene basis by parsing for the longest vetted sequence per family from an output of general NCBI search terms [e.g., for ND2: "((((((txid40674[ORGN] ND2) NOT genome) NOT tRNA) NOT COI) NOT COIII) NOT cytb) NOT d-loop"].

We performed separate per-gene BLAST searches on the nt database subset to the NCBI GI list for mammals (38,442,994 entries for Mammalia), using the "blastn" executable (BLAST+ version 2.2.31). We set the per-gene BLAST searches to use a coarse E-value of 10 when querying the DNA baits to ensure broad taxonomic coverage. We used the XML2 output format to assign taxonomic information to each resulting hit for subsequent parsing.

1.3. Parsing output for redundancy

For each gene, the aligned hits and taxonomic metadata returned from BLAST were parsed for redundancy and quality, keeping only the unique longest hit per NCBI taxon ID that was greater than 200 bp in length. We accomplished this using custom Bash scripts (including the utilities *awk*, *sed*, *sort*, and *join*). Table S1 documents the extent of redundancy that was successively reduced using this procedure, and during steps of taxonomic matching and error checking (see below).

This BLAST-based pipeline initially yielded a sampling of ≥ 1 targeted genes for 6247 unique taxon IDs at the ranks of species and subspecies, out of a possible 7319 such names (85%, as based on the NCBI taxonomy of 20 April 2015). Unaligned FASTA-format files for each gene were then subjected to a taxonomic matchup prior to alignment and further vetting.

Table S1.

Results from BLAST searches for each of the 31 gene fragments used in this study. Successive steps to parse results to unique NCBI species and subspecies names, match NCBI names to initially accepted names in the master taxonomy, and then manual addition (+) and removal (-) steps of error checks to yield per-gene final accepted species (excl. = excluded).

Gene	Region	(1) Unique BLAST hits	(2) Unique NCBI taxa	(3) Initial species	(4a) Added manual (+)	(4b) Stop codons (-)	(4c) Rogue taxa (-)	(4d) Visual errors (-)	(5) Final species	Error-check excl.
A2AB	exon	792	343	323	0	0	19	15	289	34
ADORA3	exon	746	500	476	1	0	46	3	428	48
ADRB2	exon	662	245	235	0	0	16	2	217	18
APOB	exon	1480	681	603	4	1	17	3	586	17
APP	NC	1028	472	453	0	0	39	0	414	39
ATP7	exon	670	506	485	0	0	17	0	468	17
BCHE	exon	462	340	324	0	0	16	0	308	16
BDNF	exon	1241	625	590	5	4	84	0	507	83
BMI1	NC	400	243	232	0	0	40	1	191	41
BRCA1	exon	2350	1095	992	5	0	25	3	969	23
BRCA2	exon	522	326	309	0	0	3	0	306	3
CNR1	exon	744	399	378	0	0	23	0	355	23
COI	mtDNA	49049	2326	1852	0	0	158	9	1685	167
CREM	NC	1889	403	385	0	0	51	3	331	54
CYTB	mtDNA	89218	5375	3787	41	3	237	8	3580	207

DMP1	exon	684	455	434	0	0	14	5	415	19
EDG1	exon	655	359	341	0	1	26	2	312	29
ENAM	exon	372	262	249	0	0	2	0	247	2
FBN1	NC	422	345	331	0	0	26	4	301	30
GHR	exon	2113	1141	1071	19	0	113	0	977	94
IRBP	exon	3361	1534	1412	0	0	67	1	1344	68
ND1	mtDNA	32483	1212	1007	0	0	45	1	961	46
ND2	mtDNA	32902	1175	1014	6	0	37	1	982	32
PLCB4	NC	922	554	526	0	0	48	0	478	48
PNOC	exon	701	482	460	0	0	47	3	410	50
RAG1a	exon	1234	727	682	0	0	44	0	638	44
RAG1b	exon	1871	1066	983	31	0	75	4	935	48
RAG2	exon	2139	1108	1018	4	0	131	3	888	130
TTN	exon	764	375	363	0	0	19	0	344	19
TYR1	exon	690	380	363	0	0	28	0	335	28
VWF	exon	1276	866	826	19	0	23	2	820	6
	Total sequences		13486	22504	135	9	1536	73	21021	1483
	Total unique taxa		6247	4217	.	.	.	.	4098	119

2. Taxonomic matchup of mammalian species names

Coherency among species names and their associated data is central to the integrity of any species-level comparative analysis, and especially so for this macro-scale Mammalia study. The NCBI taxonomy of our genetic data in many cases contained synonymous names, and so needed to be vetted against an authoritative list of accepted mammalian species. We chose to base this matchup on the IUCN mammal list (23) because it: (i) followed closely the authority of Mammal Species of the World vol. 3 (MSW3; (24)); (ii) was updated in several cases from MSW3; and (iii) remains tied to geospatial (23) and species trait (25) resources for downstream analysis.

2.1 NCBI to IUCN

The IUCN base taxonomy contained 5513 species as downloaded 15 April 2015. We next used a synonym list compiled from several sources (Catalog of Life, MSW3, IUCN; total of 195,562 unique equivalencies; updated from Meyer et al. (26)) to match the NCBI species and subspecies names to IUCN names. This initial procedure yielded direct matches for 4725 of the 6247 NCBI names (75%) that our BLAST search returned. Of the remaining unmatched NCBI names, we matched 765 via manual reference to the literature, often by consulting paper appendices where given sequences were published. These names were ranked as species (304), subspecies (410), or had ambiguous epithets (51; "cf.", "sp.", etc.). We manually assigned per-gene accession numbers for 77 species (135 sequences) where the corresponding NCBI taxon ID included sequences for multiple species (denoted as "added manually" in Table S1 and Dataset S1). The total of 5490 NCBI names matched included 1273 species synonyms, resulting in a starting list of 4217 accepted species with ≥ 1 targeted gene sampled (3954 IUCN species + 263 added species; Fig. S3). These DNA data were the basis for parsing.

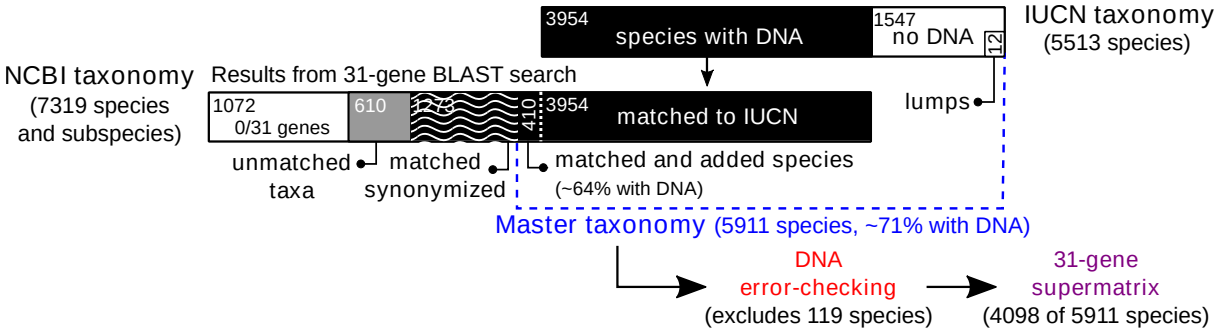

Fig. S3

Our master taxonomy merges the mammal lists of NCBI (genetic data) and IUCN (name authority). Bars representing each taxonomic list are sized proportionately to the number of names in each list category. We conducted a baited BLAST search of NCBI using 31 genes, from which data was returned for ~85% of the NCBI names (6247 of 7319; list of 20 April 2015). Steps of synonym matching and taxon addition to the IUCN list resulted in our master taxonomy of 5911 species. Black corresponds to the 4217 species initially with DNA, including 410 species we added to the IUCN list (newly described species, domestic forms, or recently extinct), which was reduced to 4098 species after error-checking steps. See Dataset S2 for name reconciliations and Dataset S1 for DNA error-checking.

2.2 Master taxonomy for this study

We used a complex NCBI-to-IUCN taxonomic matchup system (Fig. S3) that produced our master taxonomy of 5911 mammalian species. We retained 5501 species names from the 5513 species in the original IUCN list, synonymizing 12 species within existing IUCN names ("lumps"). We added 410 species to the IUCN base taxonomy, as follows: (i) 367 new species that were described since the ~2008 cutoff for most of the IUCN list (about 200 updates were made between 2009-2014); (ii) 13 domestic species; and (iii) 30 recently extinct species. The Mammal Diversity Database ((27, 28); https://mammaldiversity.org), which includes 6495 extant and recently extinct species as of 15 August 2017 (version 1.0), was an outgrowth of our project and continues to update mammalian taxonomy as new literature is published.

For the new species, we integrated these names to the master taxonomy either as derived from portions of existing IUCN names ("splits"; 33 species), or else as new discoveries ("de novo"; 334 species). All splits had associated DNA sequences published with their taxonomic changes, while 56% of de novo species had DNA sampling for 1 or more of our targeted markers. Domestic species were in most cases sampled for all targeted loci (e.g., guinea pig, camel, sheep, goat) and therefore helped anchor their wild relatives in the phylogeny. Each of the recently extinct species that we added were sampled for at least 1 of our targeted loci and therefore were useful for dividing long branches in the tree (e.g., *Archeolemur*, *Mammut*, *Mylodon*). However, we did not attempt to add every Pleistocene extinct mammal (as did (18)). We also matched 17 of the 77 extinct species from the IUCN list (either extinct in the wild or overall) with 1 or more DNA sequences, yielding DNA for 47 of 107 extinct species in our list. We additionally followed recent taxonomic revisions to give new genus assignments to 76 species in the IUCN list (denoted as "name transfers" in Dataset S1; see file for full accounts and references of taxonomic changes and the master taxonomy used in this study). Our master taxonomic list contains 5804 species considered extant out of 5911 species total, which is nearly 400 more than MSW and IUCN (Table S2).

Table S2.
The master taxonomy of this study vs. existing authoritative lists. Common authorities for mammals are Mammal Species of the World, vol. 3 (24) (MSW3), International Union for the Conservation of Nature (29) (IUCN), and the Mammal Diversity Database (MDD(27)). See Fig. S3 for a conceptual breakdown of the input sources to the master taxonomy and Dataset S1 for full documentation of changes.

Taxa	MSW3 2005	IUCN 2008	MDD v1 2017	Master taxonomy (this study)
Species				
Total	5,416	5,513	6,495	5,911
Extinct	1	77	96	107
Living	5,415	5,436	6,399	5,804
Living wild	5,415	5,436	6,382	5,791
Genera	1,230	1,226	1,314	1,283
Families	153	149	167	162
Orders	29	24	27	27

3. Error-checking via iterative DNA sequence alignment and gene tree construction

The abundance of annotation errors on GenBank (e.g., incorrect taxon or gene identifications; (30–32)) is well-known. To address this, we used a per-gene approach to iteratively clean DNA data via (i) alignment, (ii) trees, and (iii) error-checking (Fig. S1a).

3.1 DNA alignments and pseudogenes

For the 26 coding fragments (mtDNA and exons), we aligned each to the appropriate amino acid reading frame using MACSE v1.0 (33), aiming to minimize stop codons with reference to per-gene guide alignments (e.g., from Meredith et al. (20)). This procedure allowed us to identify 30 sequences with stop codons that we confirmed as nuclear mitochondrial copies (numts) or pseudogenes; of these, 21 were replaced with another sequence from GenBank while the remaining 9 had no appropriate replacement. Gene sequences of ENAM and IRBP containing known loss-of-function stop codons were retained for enamel-absent (e.g., baleen whales, xenarthrans) and blind (e.g., blind mole-rats) species of mammals, respectively. Additional sequence alignment was performed in MAFFT version 7.245 (34) with manual checking.

We aligned the 5 non-coding (NC) nuclear genes using PRANK v.140603 (35), an algorithm which is able to distinguish between insertions and deletion events in the alignment. Ambiguity in the resulting alignments was reduced using the "-gappyout" method in trimAl v1.2b (36) to exclude the most gap-rich columns of the alignment. We visually inspected all alignments for clear errors in homology, and in several cases excluded unaligned (entirely non-overlapping) sequences. The full list of excluded sequences is in Dataset S1.

3.2 Gene tree construction and rogue taxon identification

We generated maximum-likelihood (ML) gene trees for several additional rounds of sequence verification. We used RAxML v.8.2.3 (37), the GTRCAT model of DNA evolution, and the "-f a" option to specify 1000 rapid bootstrap replicates for all gene trees. Outgroup selection was a key step of this process since sequences of the same outgroup taxon were not

available across all 31 gene fragments. In fact, the analyses of Meredith et al. (20) suffered from the same problem: 10 of the 27 gene fragments in their concatenated analyses lacked a non-mammalian outgroup (3, 4, or 5 outgroup taxa were sampled for their remaining genes; Table S3). When available (for 21 genes), we used the lizard *Anolis carolinensis* as the outgroup to mammals, since together they form the clade Synapsida (38). Otherwise, for 4 genes we used a monotreme outgroup (*Ornithorhynchus anatinus*) to a therian ingroup, and for 6 genes a marsupial outgroup (*Monodelphis domestica*) to a placental ingroup (Table S3). For those 10 genes, we pruned alignments to the ingroup and single outgroup for purposes of sequence validation, but in downstream analyses retained all mammals.

Rogue taxa are defined as those that "jump around" beyond a desired threshold in a sample of phylogenetic trees and reduce nodal support (39, 40), a problem we sought to minimize within per-gene alignments. This phenomenon is attributable to ambiguous or inadequate phylogenetic signal in a particular sequence (41), often due to an insufficient extent of sequence overlap, too few informative sites, gene mis-identification, or paralogy (42). We expected the number of rogues in an alignment to be related to the site-by-taxon coverage pattern, and to corresponding metrics of fractional decisiveness used to measure a matrix's power to distinguish between terraces of phylogenetic trees with similar likelihood (43). By pruning out rogues, we were able to improve the overall information content of resulting gene trees as measured using the relative bipartition information criterion (RBIC) (40). This procedure was therefore conservative.

For each gene, we identified rogue taxa using RogueNaRok v1.0 (40) on the best-scoring ML tree and bootstrap sample of 1000 trees as input. The number of rogues identified per gene varied from 2 (ENAM; 0.8% of input sequences) to 237 (CYTB; 6.2%), with a mean of 49.6 rogues per gene (6.8%). In total, we identified 1537 rogues that, when excluded from each alignment, improved mean per-gene RBIC by 0.014 (max: 0.025 in ADORA3). To test whether excluding additional rogue sequences might further improve alignments, we built a second round of ML gene trees on the rogue-pruned alignments as input for RogueNaRok. We found that a mean RBIC improvement of 0.002 per gene could be obtained by excluding 354 more rogues (mean of 11 per gene). However, given this small change we decided instead to retain those DNA sequences to maximize taxon sampling.

3.3 Visual error-checking of gene trees

We identified an additional 73 erroneous sequences by visually examining each ML gene tree after rogue-taxon exclusion. We flagged sequences based on expectations of monophyly in established higher clades (e.g., orders), and then investigated each flagged sequence for errors in labeling or alignment. Of these sequences, 28 were NCBI author-based errors of sequence contamination or mislabeling (including four cases of *Rattus* contamination), as well as four additional pseudogene sequences. We also note that four sequences from Meredith et al. (20) appear to be mis-annotated: COI: *Sapajus apella* (Primates; JN380205) as identical to *Canis lupus* (Carnivora; KF661058); CREM: *Pecari tajacu* (Artiodactyla; JN633478) as highly similar to *Ailuropoda melanoleuca* (Carnivora); RAG2: *Cratogeomys castanops* (Geomyidae; JN633333) as more similar to *Octodontomys gliroides* (Octodontidae; JN633335) than other Geomyidae; and VWF: *Ctenomys boliviensis* (Ctenomyidae; JN415078) as more similar to *Proechimys* (Echimyidae) than other Ctenomyidae. All erroneous sequences were excluded from downstream analyses. See Dataset S1 for the full details of erroneous sequences (pseudogenes, stop codons), rogue taxa, and contaminants detected, with accession numbers.

In total, our error-checking steps excluded 1618 sequences across all genes (i.e., 7.2% of the 22,504 individual DNA sequences; Table S1). This corresponded to excluding 119 species from the 31-gene supermatrix due to unreliable data, yielding 4098 species with at least 1 gene fragment present and validated in the final supermatrix.

3.4 Final gene alignments and gene trees

Our procedure of DNA-baits searching, curation, and alignment of sequences from the NCBI database resulted in taxon sampling that ranged from 191 (BMI1) to 3581 (CYTB) species per gene (Table S3). The mtDNA genes were generally sampled for more species than the nDNA genes (means of 1803.0 vs. 512.3 species), although 3 nDNA loci (IRBP, GHR, and BRCA1) were sampled more frequently than ND1. Per-gene matrices were most completely sampled for BMI and TYR (>98% ungapped sites) and most incomplete for DMP1 (41% ungapped), while the best mean coverage of species per site was found in CYTB, COI, and IRBP (3318.0, 1657.4, and 1231.9, respectively; Table S3). Final gene trees were calculated in RAxML with the GTRCAT model and 1000 rapid bootstrap replicates. These large phylogenies were plotted in the R programming language (44) using the function "splitplotTree" in the phytools package (45), and with nodal support values annotated using the phyloch package (http://www.christophheibl.de/Rpackages.html; final gene trees and plotted versions are available in Dataset S2).

Gene trees were not separately considered in subsequent analyses (e.g., as under the multispecies coalescent; (8)) for 2 reasons: (i) our primary aim was not upon the best species tree topology for Mammalia, but rather consistently estimating tree-wide branch lengths for this group; and (ii) current methods cannot handle more than 1000 species (e.g., ASTRAL-II; (11)). Instead, we focused on analyses of the concatenated DNA supermatrix, first for global RAxML analyses (section 4) and then as subset taxonomically for each of the subclades ("patch" clades; section 5), and subset by lineage representatives for the time-scaled backbone (section 6). Finally, the patch and backbone phylogenies were joined into time-scaled trees of modern Mammalia (section 7).

Table S3.

Final alignment details for the 31 gene fragments used in this study. Comparison is made to the family-level phylogenetic study of Meredith et al. (20) (M11) for the number of aligned sites (with gaps) and mammalian taxa sampled per gene. The per-gene outgroup(s) are noted in parentheses, either as the number of outgroup taxa used in M11, or identifying the outgroup used in gene tree-building for this study (A = *Anolis*, O = *Ornithorhynchus*, M = *Monodelphis*). Note that RAG1a and RAG1b fragments are combined in M11. Site identity is calculated pairwise, matrix completeness (comp.) is the sites-by-taxa percentage of ungapped sites, and mean coverage refers to the mean ungapped sites per matrix column (i.e., mean taxon sampling per site). NC = non-coding.

		M11		This study					
Gene	**Region**	**# sites**	**# taxa**	**# sites**	**# taxa**	**GC content**	**Identical sites**	**Matrix comp.**	**Mean coverage**
A2AB	exon	848	165 (4)	603	290 (A)	61.0%	85.2%	91.9%	284.1
ADORA3	exon	332	163 (3)	369	429 (A)	45.8%	83.0%	86.6%	427.7
ADRB2	exon	803	155 (5)	846	218 (A)	53.3%	86.1%	94.3%	215.1
APOB	exon	2624	168 (5)	2523	587 (A)	41.8%	35.2%	51.7%	334.7
APP	NC	696	152 (0)	636	414 (M)	37.7%	84.1%	94.7%	403.6
ATP7	exon	686	163 (3)	723	469 (A)	40.6%	83.4%	91.5%	459.8
BCHE	exon	995	149 (5)	1020	309 (A)	40.8%	82.0%	94.0%	300.3
BDNF	exon	560	157 (5)	612	508 (A)	55.1%	85.3%	87.8%	489.4
BMI1	NC	336	150 (0)	292	191 (O)	33.5%	92.4%	98.9%	189.9
BRCA1	exon	3092	160 (0)	3264	969 (M)	41.7%	36.1%	47.0%	538.1
BRCA2	exon	5045	163 (0)	4854	306 (O)	34.4%	41.8%	52.5%	183.3
CNR1	exon	1004	162 (5)	1017	356 (A)	54.0%	83.9%	93.8%	342.6
COI	mtDNA	--	--	672	1686 (A)	43.0%	76.6%	96.1%	1657.4
CREM	NC	441	155 (0)	350	331 (O)	44.7%	80.7%	95.8%	322.5
CYTB	mtDNA	--	--	1167	3581 (A)	41.5%	65.8%	90.4%	3318.0
DMP1	exon	1361	161 (0)	1503	415 (M)	51.6%	28.3%	41.1%	205.3
EDG1	exon	959	153 (5)	963	313 (A)	56.3%	84.1%	95.5%	301.8
ENAM	exon	3899	162 (0)	3477	247 (O)	44.5%	58.2%	68.9%	215.5
FBN1	NC	745	150 (0)	669	301 (M)	33.6%	81.8%	93.6%	289.3
GHR	exon	947	165 (4)	1044	978 (A)	49.1%	58.2%	70.1%	794.5
IRBP	exon	1253	161 (5)	1146	1345 (A)	59.4%	69.5%	85.4%	1231.9
ND1	mtDNA	--	--	975	962 (A)	40.6%	71.0%	94.4%	925.5
ND2	mtDNA	--	--	1074	983 (A)	37.2%	57.7%	86.3%	873.3
PLCB4	NC	350	156 (0)	288	478 (M)	40.1%	75.9%	96.2%	469.6
PNOC	exon	320	144 (0)	339	410 (M)	62.5%	79.7%	82.7%	403.5
RAG1a	exon	1799	168 (5)	1050	639 (A)	51.5%	66.2%	84.6%	556.8
RAG1b	exon	--	--	1071	936 (A)	50.6%	61.8%	81.1%	763.6
RAG2	exon	446	163 (5)	450	889 (A)	44.1%	86.9%	97.5%	879.4
TTN	exon	4437	168 (5)	4479	345 (A)	42.0%	41.1%	58.9%	205.4
TYR1	exon	428	151 (5)	429	336 (A)	46.9%	85.4%	98.8%	334.2
VWF	exon	1172	162 (3)	1194	821 (A)	59.0%	64.4%	84.0%	707.5
Total concatenated		35603	164 (5)	39099	4098 (A)	45.3%	13.4%	11.9%	1651.2

4. Global genetic scaffold tree using maximum likelihood

4.1 Supermatrix concatenation

Concatenation of the 31 gene fragments was performed in Geneious v.9.1 (46), resulting in a sites-by-taxon supermatrix of 39,099 base pairs (bp) and 4098 species that was 11.9% complete in terms of ungapped sites. This is a substantial level of missing data (88.1%), but is comparable to other recent large-scale studies (e.g., 81% for squamates in Pyron et al. (47)) and not expected to interfere with accurate phylogeny estimation (48, 49). Simulations instead suggest that specifying relevant nucleotide evolution models and properly partitioning sequence data are more consequential for accurate phylogeny reconstruction than matrix completion (49).

4.2 PartitionFinder

We estimated an optimal partitioning scheme for the supermatrix using PartitionFinder v.1.1.1 (50) to test whether sets of partitions could be combined (e.g., based on similar nucleotide compositions or substitution rates) to yield simpler models of molecular evolution. We tested 3 *a priori* sets of partitions: (i) 83 partitions, 1 for each coding gene by codon position (26 × 3) plus the 5 NC genes; (ii) 31 partitions, 1 for each gene; and (iii) 11 partitions, 1 for each nDNA and mtDNA coding region by codon position (2 × 3) plus the 5 NC genes. Running PartitionFinder using the full concatenated alignment, relaxed cluster searching (top 10% of schemes; (51)), linked branch lengths, and BIC model selection, we found those partition sets could be reduced to 38, 19, and 9 partitions, respectively.

The best BIC score was for the simplest 9-partition model (6,790,459.3; the 38- and 19-partition models had BIC scores of 6,844,238.7 and 6,933,022.3). We subsequently used the 9-partition model for all ensuing phylogenetic analyses, including global, patch, and backbone trees (see below). This model has a combined partition for APP, CREM, and FBN1, and then 1 partition each for BMI1; PLCB4; and first, second and third codon partitions for nDNA exons as well as for mtDNA fragments (Table S4). For all partitions, either general time-reversible plus gamma (GTR+G) or plus gamma and invariant sites (GTR+I+G) was the best model of nucleotide evolution. We chose the simpler GTR+G model for all downstream phylogenetic analyses, since including both I and G types of rate heterogeneity is known to make both model parameters difficult to estimate (37, 52). Our final partitioning scheme usefully captures rate heterogeneity across inheritance types and synonymous versus non-synonymous substitution types, while not being overly complex for large-scale inference on our gappy supermatrix (see (53) for a similar partitioning strategy).

Table S4.

Model parameters optimized during the global RAxML tree search of the 4098-species supermatrix. Summarized per partition are the number of distinct alignment patterns, estimated alpha-shape parameter (α) of the gamma distribution, two-way rates of the GTR (general time-reversible) model of nucleotide evolution, and empirical base frequencies.

			Rates						Frequencies			
Partition	**Patterns**	**α**	**A/C**	**A/G**	**A/T**	**C/G**	**C/T**	**G/T**	**A**	**C**	**G**	**T**
nDNA, pos1	9345	0.40	1.69	4.54	0.86	1.07	4.02	1.00	0.28	0.23	0.28	0.21
nDNA, pos2	8806	0.38	1.27	5.34	0.76	1.50	4.44	1.00	0.29	0.24	0.21	0.26
nDNA, pos3	10685	1.19	1.22	5.42	0.90	1.08	5.88	1.00	0.24	0.26	0.25	0.25
mtDNA, pos1	1253	0.52	1.08	6.67	1.70	0.17	16.01	1.00	0.30	0.25	0.22	0.23
mtDNA, pos2	1213	0.39	3.38	18.08	2.25	3.84	14.26	1.00	0.19	0.27	0.13	0.42
mtDNA, pos3	1292	0.05	0.36	9.53	0.52	0.46	6.04	1.00	0.42	0.32	0.04	0.22
APP, CREM, FBN1	1558	0.34	1.32	3.39	0.39	0.93	3.40	1.00	0.27	0.22	0.22	0.29
BMI1	244	0.24	1.65	4.33	1.04	0.78	5.00	1.00	0.26	0.23	0.22	0.29
PLCB4	287	0.49	1.03	3.67	0.52	0.78	3.08	1.00	0.32	0.24	0.19	0.25

4.3 Global ML tree in RAxML

Phylogenetic analysis of the 4098-species supermatrix was first performed under ML criteria in RAxML with the goal to identify the best-supported topology for global mammals. We ran 5 independent analyses, each specifying 100 bootstrap replicates and using the "-f a" option and GTRCAT model to search for the best-scoring ML tree (with this setting, the ML optimizations start from every fifth bootstrap tree (37)). Each RAxML analysis took ~5.7 days as conducted on 12 nodes of 4 threads each on the XSEDE on-line computing cluster (accessed via the CIPRES Science Gateway (54)). All five runs returned the exact same ML optimization likelihood of -3383607.6 and tree lengths of 255.3, although with slight differences in topology.

We subsequently summarized this single best ML tree by rooting it with *Anolis* and annotating nodes with bipartition values from 100 bootstrap replicates. Note that it is the normal behavior of ML algorithms, including RAxML, to initially estimate all trees as unrooted and then to secondarily root with outgroup(s) for purposes of tree-drawing (37). This global ML tree was re-rooted and plotted using the R package ape (55) with nodal support values annotated using "phyloch" functions. See files and pdf plots of this global RAxML tree in Dataset S3.

5. Patch clade trees and PASTIS completion of missing species

5.1 Delimitation of patch clades

Examination of well-supported nodes (>75% bootstrap support [BS]) in the global ML tree informed inferences of how to best divide the mammalian phylogeny into "patch clade" units, i.e., non-overlapping subclades where hard monophyly was assumed throughout subsequent analyses (2). Delimiting patch clades was an essential step toward accomplishing goals of (i) estimating branch lengths from root-to-tip using the same underlying DNA matrix; (ii) adding DNA-missing species within taxonomic constraints (1); and (iii) propagating

posterior uncertainty in node ages and topology downstream. Bayesian methods implemented in MrBayes v.3.2.6 (3) allowed flexible topological and model constraints that were especially well suited to these goals. However, because MrBayes is computationally intensive, the size of our patch clades was limited to < 800 species to foster analysis completion in less than 1 month. Near this maximum, our largest patch clade (Muridae, 778 species) took 3.7 weeks to finish 33,330,000 generations in parallel on 16 BEAGLE-enabled compute nodes in the XSEDE on-line cluster (1.5-4.5 weeks for clades >200 species; matrix complexity also affected run times).

In total, we delimited 28 patch clades (Table S5). These were selected after considering criteria of clade size, evidence for clade monophyly from the global ML tree, and the structure of inter-clade phylogenetic relationships. This task of balancing between reasonable assumptions of monophyly and the maximum patch clade size was especially challenging in bats and rodents. Here species richness is highest, but so is missing genetic data and topological uncertainty. In the mouse-related clade of rodents (1768 total species, 64% genetic sampling; (56)), we addressed this issue by dividing data into 2 large and likely monophyletic clades (Muridae and Cricetidae) and several smaller Muroidea patch clades for which interrelationships are uncertain (e.g., Dipodidae, Spalacidae, Nesomyidae, Calomyscidae, Platacanthomyidae; (57)). We thus avoided assuming a backbone topology for mouse-related rodents; instead, uncertainty in patch interrelationships was captured on the dated Mammalia backbone (see below). Note that these smaller patches were all well supported in the global ML tree except the Nesomyidae rodents of Madagascar (BS 72), which are well supported as monophyletic in other studies (57, 58)

For bats, major topological uncertainty lies within Yangochiroptera (902 species, 67% genetic sampling), especially among its most basal divergences (59–61). However, the compute time required to run Yangochiroptera as a single patch clade was prohibitive (initial attempts suggested 6-8 weeks), and with no guarantee of convergence (matrix < 10% complete). Rather, we divided this monophyletic unit (94 BS value, Dataset S3) into 3 patch clades:

(i) Noctilionoidea (Phyllostomidae, Mormoopidae, Noctilionidae, Thyropteridae, Furipteridae, Mystacinidae, and Myzopodidae);
(ii) Vespertilionoidea (Vespertilionidae, Molossidae, and Natalidae); and,
(iii) Emballonuroidea (Emballonuridae and Nycteridae).

Most controversial of these delimitations is the placement of Myzopodidae, which we include with Noctilionoidea according to BS 76% in the global ML tree (supported by (20, 61) but (60) instead links this family to emballonurids). Support for the Vespertilionoidea was uncertain in our global ML tree (BS 51 joining Natalidae with Molossidae + Vespertilionidae; BS 48 for Vespertilionidae with Mollosidae), and similarly we recovered Emballonuroidea with BS 52. Nevertheless, our patch clade schema represents the best-supported hypotheses for Yangochiroptera given computational constraints. These bats are a poorly known portion of mammalian diversity that will undoubtedly improve in resolution with further work (see (60)).

The remaining patch clades encompassed major swaths of mammalian diversity (e.g., Marsupialia, Primates), but also very small clades like Monotremata (5 species), Pholidota (8), and Dermoptera (2; Table S5). The structure of the phylogeny and backbone uncertainty necessitated small clades to minimize unsupported monophyly assumptions. Our small patch clades (Dermoptera and Platacanthomyidae) were needed for this reason; yet since phylogeny construction requires a minimum of 4 taxa, we added 2 species to their ingroups for MrBayes runs (*Callithrix jacchus* and *Gorilla gorilla*, and *Rattus norvegicus* and *Spalax ehrenbergi*, respectively). These species were pruned out before rescaling and pasting to the backbone.

Table S5.

Summary of patch clade and matrix composition. Included are per-patch clade values for total species in our master taxonomy, number of species sampled for DNA (one or more genes), bootstrap support value in the global RAxML tree (ML tree BS), outgroup clade and designated representative in MrBayes analyses, matrix percent complete (sites-by-taxa completeness of ungapped sites, with the no-DNA species as missing data), distinct alignment patterns as determined by RAxML, and the full run time (weeks) in MrBayes if > 1 week.

#	Patch name	Total	Samp.	%	ML tree BS	Outgroup species in MrBayes	Matrix % comp.	Patterns	Run time
1	Marsupials	362	279	77	97	*Rattus_norvegicus*	18.0	20617	4.50
2	Afrotheria	92	61	66	99	*Dasypus_novemcinctus*	21.8	14132	< 1
3	Xenarthra	33	21	64	100	*Trichechus_manatus*	33.4	7164	< 1
4	Scandentia	20	13	65	100	*Galeopterus_variegatus*	32.5	3324	< 1
5	Primates	458	333	73	95	*Galeopterus_variegatus*	19.4	16165	4.50
6	Lagomorpha	91	72	79	100	*Rattus_norvegicus*	8.8	3855	< 1
7	Castorimorpha	109	100	92	100	*Rattus_norvegicus*	9.0	5507	< 1
8	Dipodidae	51	33	16	100	*Rattus_norvegicus*	15.4	4166	< 1
9	Spalacidae	21	16	76	37	*Rattus_norvegicus*	16.5	2487	< 1
10	Nesomyidae	63	37	59	72	*Rattus_norvegicus*	10.6	3291	< 1
11	Muridae	779	411	53	88	*Cricetulus_barabensis*	8.8	9480	3.70
12	Cricetidae	726	528	73	93	*Rattus_norvegicus*	7.3	9926	4.50
13	Squirrel-related	320	216	68	95	*Erethizon_dorsatum*	6.7	8050	1.50
14	Guinea pig-related	304	204	67	100	*Ictidomys_tridecemlineatus*	13.3	18949	3.70
15	Eulipotyphla	491	301	61	94	*Pteronotus_parnellii*	8.7	13786	3.70
16	Noctilionoidea	227	190	84	76	*Pteropus_alecto*	11.5	11273	1.50
17	Vespertilionoidea	605	367	61	51	*Pteropus_alecto*	7.0	9694	3.50
18	Emballonuroidea	70	46	66	51	*Pteropus_alecto*	9.7	4013	< 1
19	Yinpterochiroptera	385	250	65	96	*Pteronotus_parnellii*	10.6	11463	2.50
20	Artiodactyla	348	311	89	100	*Felis_catus*	17.3	14488	2.00
21	Perissodactyla	24	22	92	100	*Felis_catus*	28.1	3411	< 1
22	Carnivora	298	267	90	99	*Manis_pentadactyla*	18.0	12978	2.20
23	Monotremata	5	3	60	100	*Rattus_norvegicus*	47.1	802	< 1
24	Pholidota	8	6	75	100	*Felis_catus*	36.6	1132	< 1
25	Dermoptera	2*	2	100	100	*Tupaia_belangeri*	79.9	2094	< 1
26	Anomaluromorpha	9	4	44	100	*Rattus_norvegicus*	46.9	972	< 1
27	Calomyscidae	8	3	38	100	*Rattus_norvegicus*	23.9	185	< 1
28	Platacanthomyidae	2*	1	50	N/A	*Jaculus_jaculus*	61.5	1055	< 1

* Patch clades with fewer than 4 species were supplemented with additional related taxa for the purposes of MrBayes runs, but they were then pruned out before rescaling and pasting the patches to the backbone.

5.2 Genetic missingness, taxonomic constraints, and species completion

We followed Jetz et al. (2) in classifying DNA-sampled species as type 1 (sampled for 1 or more genes) and DNA-missing species as type 2, 3, or 4, as follows:

- Type 2: DNA available for at least 1 congeneric species (constrain to genus)
- Type 3: no DNA in the genus, but available in the same family (constrain to family)
- Type 4: no DNA in the family, but available in the same order (constrain to order)

Along with 4098 type 1 species, we had 1649 species in the type 2 category, meaning that 91% of the 1813 DNA-missing species could be constrained to a DNA-sampled genus. Beyond that, we had 115 genera entirely unsampled for DNA, to which 156 type 3 species belong. Most of these missing genera are rodents (73 genera, 58 of which are muroids) or bats (22 genera), highlighting the large amount of molecular systematics yet to be conducted in those groups. Additionally, there were 3 extinct families in our taxonomy to which no DNA was available (8 species in the type 4 category): Nesophontidae, Prolagidae, and Thylacinidae. Both *Nesophontes* (62) and *Thylacinus* (63) have been sequenced since our data cutoff date; however, *Prolagus* remains unsequenced (but see (64)). Full details of these DNA-missing species are in Dataset S4. Taxon assignments, including subfamily and tribal constraints for the speciose and uncertain Cricetidae and Muridae, are noted in Dataset S4.

Taxonomic constraints for the addition of missing species (also called 'taxonomic imputation') during patch clade estimation in MrBayes were formed with the assistance of the PASTIS package in R (1). Using this package, we generated ready-to-execute MrBayes files for each patch clade from the following inputs: (i) sequences file of aligned DNA in FASTA format; (ii) taxa file of genus membership for all sampled and missing species; (iii) missing clades file (if needed) designating where to constrain missing genera; (iv) guide tree file giving the relationships of DNA-sampled species (global ML tree described in section 4, pruned to patch clade species); and (v) template file specifying other MrBayes settings (e.g., rate priors, data partitions). Pruned portions of the global ML tree were not further altered, so all nodes present in that global tree—even those with low BS support—were enforced as topology constraints for purposes of adding DNA-missing species to posterior phylogenies. This procedure ensured that missing species were added in a phylogenetically informed way. However, it also fixed the topology of DNA-sampled species to the exact topology of the global ML tree. We viewed this trade-off in phylogenetic certainty to be acceptable given that it propagated our most confident inferences of species-level phylogenetic relationships (i.e., those from DNA-only likelihood analyses) into the completed patch phylogenies and to full Mammalia trees downstream, while guaranteeing that DNA-missing species were placed appropriately.

From the input files, PASTIS adds DNA-missing species to the matrix block with "?" as the character datum for all aligned sites. If left unconstrained, those completed species would be placed at random throughout the posterior sample of trees. The flexible system of "hard", "negative", and "partial" constraints in MrBayes, when arranged hierarchically, can restrict taxon additions to inside a given clade and outside other clades (1, 3). Branch lengths for those completed species are drawn from the same underlying birth-death distribution as the rest of the patch clade, tending PASTIS completions conservatively to rate-constant processes (1, 2). Therefore, tests of the null hypothesis of constant rate diversification were expected to be conservative. By using PASTIS to construct our taxon addition constraints, we reduced the potential for human error while automating the recognition of non-monophyletic genera in the global ML tree. Given the tree topology and presumed genus assignment, PASTIS uses the least

inclusive clade containing all DNA-sampled members of a given genus as the partial constraint for placing missing species randomly within that clade. For example, the task of constraining 39 missing species of *Rattus* (of 66 total) is complicated by its paraphyly with respect to *Diplothrix*, *Limnomys*, *Tarsomys*, *Bandicota*, and *Nesokia* (Dataset S3). By using partial constraints, we could constrain those missing *Rattus* species to their paraphyletic grouping across the posterior distribution.

A main advantage of phylogeny-based completion using PASTIS, as compared to other methods of taxonomic imputation (e.g., (65)), is that it preserves the taxonomically expected tree shape for downstream applications (1). However, we note that comparative analyses using these completed trees are especially sensitive to posterior topological uncertainty among the DNA-missing species. Thus, downstream analyses should aim to propagate uncertainty by analyzing a sample of trees, not just the consensus topology. Although we display a maximum clade consensus (MCC) topology in Fig. 1, all comparative analyses were based on 100 trees (except for the BAMM analyses, where 10 trees were examined). See section 7 below on the pitfalls of generating a consensus topology from PASTIS-completed trees.

5.3 Patch clade estimation in MrBayes

The topology and relative branch lengths of each patch clade was estimated using identical modelling frameworks and settings implemented in MrBayes v.3.2.6 (3). Ultrametric branch lengths were initially estimated in units of expected substitutions/site and subsequently re-scaled to absolute time in millions of years (see below, section 7). For each patch clade, parameters of the GTR+G model were estimated independently among the 9 DNA partitions, as described above for the global ML tree. Although simpler partitioning strategies might have been selected for some (especially smaller) patch clades, we decided to maintain consistency in the model parameters across all reconstructions. Molecular rate multipliers were estimated for each partition (ratepr=variable) to account for heterotachy (e.g., mtDNA 2nd vs 3rd positions (66, 67), the latter of which evolved ~30x faster in our analyses, data not shown). We specified a relaxed clock model of each branch having an independent rate drawn from a gamma distribution (68) and length drawn from a birth-death process (brlenspr = clock:birthdeath). Exponential distributions were given to priors for clock rate variance and net diversification (with mean of 0.1) and a beta prior (0-1) on the relative extinction rate. We set the ingroup sampling probability to 1.0 in all cases, since the DNA matrices were taxonomically complete.

For each patch clade, we performed four parallel runs of MrBayes on the XSEDE on-line computing cluster, each run consisting of four chains of Markov chain Monte Carlo (MCMC; 3 heated and 1 cold), and sampled every 10,000 steps for 33,330,000 generations. Here is an example of our command blocks:

```
begin MRBAYES;
<define charsets of 9 partitions>

partition matrices = 9: nDNA_pos1, nDNA_pos2, nDNA_pos3, mtDNA_pos1,
mtDNA_pos2, mtDNA_pos3, APP_CREM_FBN1, BMI1, PLCB4;
set partition = matrices;

lset applyto = (all) nst=6 rates=gamma;          [GTR+G model]
unlink statefreq=(all) revmat=(all) shape=(all); [model unlink by partition]
prset applyto=(all) ratepr=variable;             [partition-specific rates]
```

```
<define topology constraints>
prset topologypr=constraints(<list constraint names>)

prset brlenspr = clock:birthdeath;                [clock trees, no fossils]
prset speciationpr = exp(10);                     [net diversification rate]
prset extinctionpr = beta(1,1);                   [relative extinction rate]
prset sampleprob = 1.0;                           [taxon sampling complete]
prset clockvarpr=igr;                             [independent gamma rates]
prset igrvarpr=exponential(10);                   [prior on IGR variance]
prset clockratepr = Fixed(1.0);                   [default: time unit is number
                                                   of expected
                                                   substitutions/site]
mcmcp ngen= 33330000 nruns=4 nchains=4
samplefreq=10000 printfreq=10000 savebrlens=yes; [mcmc settings]
propset ParsSPRClock(Tau{all},V{all})$warp=0.01; [parsimony-based topology
                                                  proposals to speed up
                                                  searches]
mcmc;                                             [start mcmc]
```

6. Fossil-dated backbone trees

Divergence times and evolutionary relationships among basal lineages of mammals served as the "backbone phylogeny" to which all patch clades were re-scaled to absolute time, and then joined to form full species-level trees of Mammalia (Fig. S1). Fossil information provided the temporal framework for calibrating backbone divergences. We examined 2 types of fossil-calibrated analyses for the backbone: (i) node-dating, where the oldest fossil per living lineage was used to constrain minimum node ages; and (ii) tip-dating, where fossil and living taxa were jointly analyzed and fossil stratigraphy informed node ages without other assumptions.

In both sets of analyses, we focused on a common set of extant taxa to subset the 31-gene supermatrix for molecular characters: 59 mammals, representing each of the 28 patch clades plus select family-level taxa, and 1 outgroup (*Anolis carolinensis*). Taxa were selected as representatives based on their extent of genetic sampling, which for most taxa was >25 of 31 genes (median: 29, range: 3-31). Some taxa were selected so that nodes were present for subsequent age constraint in the node-dating analyses (section 6.1, below). Other taxa were selected by their inclusion in the morphological data set of Zhou et al. (69), which we used in the tip-dating analyses (section 6.2). Dataset S5 provides details of backbone taxon sampling and the constraints employed in each analysis.

6.1 Node-dating backbone analyses

Fossil calibrations for the constraint of mammalian node ages were selected from the compendium of Benton et al. (70), as augmented by Philips (71), and using the following criteria (72): (i) confidence in placement, especially in cladistic analyses; (ii) confidence in the monophyly of the age-constrained node, which was a requirement of MrBayes; and (iii) lack of conflict in age priors, determined both in proximity of node constraints and empirically with trial runs in MrBayes. In total, we decided upon 17 optimal age constraints (also Dataset S5):

1. **Mammalia**: 164.9 Ma minimum age to 201.5 Ma maximum age (set by Jurassic-Triassic boundary). Minimum defined by *Ambondro mahabo*, member of the monotreme clade Australosphenida from the middle Jurassic (Bathonian) of Madagascar (70, 73–75).

2. **Monotremata**: 15.97 to 113.0 Ma (lower Albian, early Cretaceous). *Obdurodon dicksoni*, stem member of Ornithorhynchidae from the early Miocene (Burdigalian) of northwestern Queensland, Australia (71, 76, 77).
3. **Marsupialia**: 47.6 to 131.3 Ma (lower Barremian, early Cretaceous). *Djarthia murgonensis*, crown marsupial from the early Eocene (Ypresian) of Murgon, Australia (70, 78).
4. **Macropodoidea**: 15.97 to 54.65 Ma (earliest Eocene). *Ganguroo bilamina*, stem or crown member of Macropodidae (to the exclusion of Potoroidae from the early Miocene (Burdigalian) of northwestern Queensland, Australia (71, 79).
5. **Theria**: 156.3 to 169.6 Ma (lower Bathonian, middle Jurassic). *Juramaia sinensis*, stem eutherian from the late Jurassic (Oxfordian) of the Northeastern China (70, 75).
6. **Placentalia**: 61.6 to 164.6 Ma (lower Oxfordian, late Jurassic). *Ravenictis krausei*, stem carnivoran from the early Paleocene (Danian) of Saskatchewan, Canada (70, 80).
7. **Afrotheria**: 56.0 to 164.6 Ma (lower Oxfordian, late Jurassic). *Eritherium azzouzorum*, stem proboscidean from the upper Paleocene (early Thanetian) of Morocco (70, 81).
8. **Xenarthra**: 47.6 to 164.6 Ma (lower Oxfordian, late Jurassic). *Riostegotherium yanei*, stem cingulate from the early Eocene (Ypresian) of Itaboraí, Brazil (70, 82).
9. **Chiroptera**: 45.0 to 58.9 Ma (lower Thanetian, Paleocene). *Tanzanycteris mannardi*, stem member of Rhinolophoidea within Yinpterochiroptera from the middle Eocene (Lutetian) of Tanzania (71, 83).
10. **Lagomorpha**: 47.6 to 66.0 Ma (earliest Paleocene). Unnamed stem leporid fossils from the early Eocene (Ypresian) of West-Central India (70, 84).
11. **Rodentia**: 56.0 to 66.0 Ma (earliest Paleocene). *Paramys atavus*, stem member of Sciuromorpha from the late Paleocene (Thanetian) of Montana, USA that is nested well within crown Rodentia (70, 85).
12. **Caviomorpha-Phiomorpha**: 40.94 to 56.0 Ma (upper Thanetian, latest Paleocene). *Cachiyacuy contamanensis*, stem caviomorph rodent from the middle Eocene (Lutetian) of Yahuarango, Peru (71, 86).
13. **Primates**: 56.0 to 66.0 Ma (earliest Paleocene). *Altiatlasius koulchii*, stem anthropoid from the late Paleocene (Thanetian) of Morocco (70, 87).
14. **Strepsirhini**: 33.9 to 56.0 Ma (upper Thanetian, latest Paleocene). *Karanisia clarki*, stem lorisiform or a crown strepsirrhine of uncertain affinities from the late Eocene (Priabonian) of Fayûm, Egypt (70, 88, 89).
15. **Anthropoidea**: 33.9 to 66.0 Ma (earliest Paleocene). *Catopithecus browni*, crown Catarrhini from late Eocene (Priabonian) Fayûm, Egypt (70, 89).
16. **Cetartiodactyla**: 52.4 to 66.0 Ma (earliest Paleocene). *Himalayacetus subathuensis*, stem member of Cetacea from the early Eocene (Ypresian) of India (70, 90, 91).
17. **Carnivora**: 37.3 to 66.0 Ma (earliest Paleocene). *Hesperocyon gregarius*, stem caniform from the middle Eocene (Bartonian) of Saskatchewan, Canada (70, 92).

Monophyly constraints were enforced on each calibrated node plus the root, which we calibrated with a uniform distribution of 318.0-332.9 Ma based on the stem diapsid *Hylonomus lyelli* (divergence between Eureptilia including Diapsida and Synapsida (70)). Three additional calibrations in Benton et al. (70) were ultimately excluded due to conflicts among node age priors during initial MrBayes runs: (i) Eulipotyphla: *Adunator ladae*, 61.6-164.6 Ma; (ii) Euarchontoglires: extinct primate sister taxa such as plesiadapids (e.g., *Paromomys farrandi*), 61.6-164.6 Ma; and (iii) Glires: *Mimotona lii*, 56-164.6 Ma. It appears those calibrations

produced conflict with adjacent calibrations due to their extended maximum ages, which were set to the earliest eutherian *Juramaia* (75) given the associated stratocladistic uncertainty (70).

All 17 calibrations were set either as exponential priors ("NDexp"), offset to minimum ages with soft maxima (93) so that the upper 95% of the distribution equaled maximum ages [formula based on the exponential distribution: exp mean = (-ln(0.05)/(max-min))^-1]; or, as uniform priors ("NDuni") spanning minima to maxima. These strategies of exponential vs. uniform priors were compared to test the sensitivity of dating results to their shape (see Supplementary Results). Similar node ages led us to focus on the more conservative NDexp backbone for comparison to the tip-dated backbone and downstream diversification rate analyses (section 8). Dataset S5 contains the execution files associated with these backbone runs.

Node-dating analyses were run in MrBayes v.3.2.6 similarly as the patch clades, but with the following exceptions: (i) the taxon sampling probability was set to 0.01017 (59 of 5803 extant species in the master taxonomy); (ii) the sampling strategy was set to "diversity" given our maximization of taxonomic diversity along the backbone phylogeny; and (iii) the birth-death clock rate prior was set to a lognormal that assumed each nucleotide site changed 1 time in the ~318 Ma root-to-tip distance [mean = log(1/318), standard deviation = exp(1/318)] (53). The node age prior was set to "calibrated", indicating that the probability distribution on terminal and interior node ages was derived from the calibration settings. Note that the birth-death process with variable rates per molecular partition was also implemented here, the same as with the patch clades. We conducted 4 independent runs of 4 chains each (3 heated and 1 cold), each run for 50,000,000 generations and sampled every 10,000 trees.

6.2 Tip-dating backbone analyses

Tip-dating methods place fossil and living taxa as tips in the same phylogeny according to morphological character data coded for both taxon classes, a procedure that leverages the stratigraphic ranges of fossils to inform the birth-death clock model (94, 95). Extensions to this approach that parameterize fossilization along with birth and death (FBD; (96)), and accommodate diversified sampling of extant and fossil taxa in the FBD process (97), now enable rigorous "total evidence" dating where molecular and morphological data are jointly considered. Applications of FBD with diversified sampling have been shown to increase congruence between node age estimates and the fossil record (e.g., mammals; (98)), so we chose to test the sensitivity of our DNA data set to this divergence-time estimation procedure. A key contrast in tip-dating versus node-dating is that fossils are placed cladistically using morphological characters, impacting node ages via their placement. Thus, different assumptions are involved in tip- than node-dating, and the methods are in greater flux (98–100).

We focused on the morphological data set of Zhou et al. (69), which consists of cladistic characters for extant and fossil mammals relevant to their interrelationships throughout the Mesozoic (66–252 Ma). Previous studies have also re-analyzed this data set (101, 102), and so served as comparisons for our work. Zhou et al. (69) originally had 84 fossil and 26 extant taxa that we trimmed to 76 fossil and 22 extant taxa. We removed 7 fossils allied to crown placentals (*Aspanlestes, Cimolestes, Eoungulatum, Glyptotherium, Gypsonictops, Leptictis,* and *Protungulatum*) and 1 taxon of unknown stratigraphic provenance (*Eleuterodon*). Removing crown fossils avoided complications with the subsequent union of backbone and patch clades (e.g., nesting *Glyptotherium* in the Xenarthra patch clade). However, we did retain *Obdurodon* within the monotreme crown given its uncontroversial placement. We also removed four extant taxa in Dasypodidae (*Chaetophractus, Euphractus*), Didelphidae (*Marmosa*), and

Pseudocheiridae (*Pseudocheirus*) since those families were already sampled by other extant genera. We gathered stratigraphic ranges for sampled fossils from the Paleobiology Database (https://paleobiodb.org/; downloaded on 9 February 2016). This direct download of fossil age information provided a variety of stratigraphic sources and so usually gave wider age intervals than previously used (e.g., *Morganucodon* 190.8–208.5 Ma and *Juramaia* 150.8–167.7 Ma versus 199–203 Ma and fixed at 160 Ma, respectively, in Slater (101)). See Dataset S5 for full details of the age ranges and taxon sampling used in FBD analyses. Note that by following the topology of Zhou et al. (69) exactly, we constrained two shuotheriids (*Shuotherium* and *Pseudotribos*) to be paraphyletic due to an apparent error their matrix.

Tip-dating analyses were run in MrBayes v.3.2.6 in a manner analogous to node-dating, but with the following exceptions: (i) each fossil tip was given a uniform calibration prior between minimum and maximum stratigraphic ages; (ii) the "clock:fossilization" branch length prior was specified, as appropriate for clock trees including fossils (96, 97); and, (iii) no node calibrations were enforced. Whereas ND analyses required topology constraints for each calibration point, none were required in FBD. However, to be sure that our backbone topology matched that recovered in Zhou et al. (69), we used hard constraints on the following nodes: ingroup from *Anolis* outgroup; crowns (extant taxa) and total groups (with stem fossils) for Placentalia, Marsupialia, and Monotremata; and constraints on the crowns of Theria and Mammalia to ensure the placement of haramiyidans in Mammaliformes but outside crown mammals ((69, 103); contra to (104)). To make FBD and ND runs analogous, we similarly conducted 4 independent runs of 4 chains each (3 heated and 1 cold), each run for 50,000,000 generations and sampled every 10,000 trees.

7. Construction of full dated mammalian phylogenies

7.1 Summary of patch clade and backbone posteriors

For all 28 patch clade analyses, we found that discarding the first 25% of samples was sufficient to reach convergent traces in combined log-likelihoods, ESS scores > 200 for most parameters, and PSRF (potential scale reduction factors) of ~1 among the chains. Each of four runs started from 3,333 sampled trees and was reduced to 2,500, yielding posterior distributions of exactly 10,000 trees upon combining the runs per patch clade. All burn-ins were conducted in the bash shell after viewing traces and ESS scores in Tracer v1.5.

For the backbone analyses, running longer MCMC chains and recording four runs of 5000 trees each allowed us to more conservatively burn-in 50% of the trees per run, ensuring proper convergence. The resulting 10,000-tree distributions for each backbone analysis contained fossil-calibrated branch lengths in units of substitutions per site that required translation to time in Ma. We used the "burntrees.pl" perl script (https://github.com/nylander/Burntrees) with the flag for "--myr" to transform the branch length from molecular to absolute time units. Three sets of 10,000 time-calibrated backbones were then ready for use in rescaling the patch clades (in units of expected substitutions/site) and grafting together to form full mammal phylogenies. See Supplementary Results for comparison of backbone consensus topologies.

7.2 Consensus trees and their pitfalls for taxonomically completed trees

We constructed maximum clade credibility (MCC) consensus trees for: (i) patch clades to ensure taxonomic constraints worked as intended across their posteriors; and (ii) backbone

analyses to summarize the results of node ages and support values. We used TreeAnnotator v1.8.2 (105) for both these purposes. MCC trees are not necessarily the majority-rule consensus trees, but rather are the tree within a given posterior sample with the maximum sum of posterior probabilities on its (n – 2) internal nodes (105). The identified MCC tree can either be annotated with its own node ages (specified with height setting of "keep" in the command line; "user target tree" in the graphical interface), or else the node heights can be rescaled and annotated as average ages of the clades in that target tree.

We treated the backbone MCC trees normally, constructing them with median node heights, but used target node heights for the patch clade MCC trees given their high posterior variability from PASTIS-completion of DNA-missing species (Table S5). Failed attempts to use mean or median node heights returned *negative* branch lengths in some cases due to node age uncertainty (i.e., average ages of descendent nodes were younger than their ancestors—a clear impossibility). This issue highlights a broader point about our trees, and "completed" trees in general (e.g., (1, 65)), that summarizing them in 1 consensus tree is inappropriate. Completed trees should instead be sampled from the posterior distribution to meaningfully capture a given phylogenetic hypothesis. While posterior samples of trees have application to all types of phylogenetic uncertainty, it is especially critical for our patch clades, and thus also the full species-level Mammalia phylogenies of which they are components. For display (Fig. 1), we constructed MCC trees for the full distribution of 10,000 Mammalia trees with target heights (increasing the "-Xmx" memory of TreeAnnotator to 40 gigabytes; Dataset S6). However, we performed no analyses on these MCC trees since rate-based questions were our focus (see also section 0).

7.3 Patch-to-backbone grafting for full Mammalia trees

In order to unite the 28 patch clades and the backbone phylogeny (Fig. S1), we first needed to rescale the patch clade distributions of 10,000 trees to absolute time in millions of years (Ma). Because the patch clades were estimated with ultrametric branch lengths in relative units (brlenspr = clock:birthdeath, without age calibrations), this procedure was accomplished with a simple multiplication in R with the ape package. We used the rescale-and-graft procedure of previous studies (2, 53, 106), outlined here as pertains to our mammal phylogenies:

(i) Load in all 10,000 trees for a selected backbone analysis and each of the patch clades;
(ii) Prune all backbones to the overall outgroup (*Anolis carolinensis*) and 28 species representatives, 1 for each of the patch clades;
(iii) Prune the placeholder taxa from the Dermoptera and Platacanthomyidae patch clades;
(iv) For each of the 10,000 samples of backbones and patches (sequentially):
    a. Take 1 pruned backbone tree; get branching times and identify pairwise MRCA nodes that correspond to the outgroup-to-ingroup relationship, recording the node age per patch clade (this root time is used to rescale the patch clade to Ma);
    b. Take 28 trees, 1 from each patch clade; for each, get the relative branching times and divide the age of the ingroup crown by that of the root, obtaining the relative scale of the stem edge from outgroup to ingroup; prune outgroups;
    c. For each patch clade, multiply root time (in Ma) from the backbone by the relative scale of the patch clade to obtain the absolute scale of the stem edge leading to the patch crown; divide all edge lengths by the maximum node height to obtain relative edge lengths of the patch clade, and then multiply those by the absolute scale of the stem to rescale all patch clade branches to time in Ma;

d. Use which.edge() to identify and name the tip edge in the pruned backbone upon which each patch clade is to be grafted; shorten those branches by subtracting the absolute scale of the stem edge per clade;
e. Use bind.tree() to graft each rescaled patch clade to the corresponding shortened edge of the pruned backbone, thereby forming 1 uniformly time-scaled tree of 5911 species of mammals;

(v) Repeat that procedure to construct posterior distributions of 10,000 phylogenies for each of the backbone analyses (NDexp and FBD). Note that some authors call these "pseudo-posterior" trees since the final trees are grafted together.

Uncertainty in the sister relationships of 3 patch clades of bats (Noctilionoidea, Vespertilionoidea, and Emballonuroidea; see section 5.1) required us to use the same distant outgroup (*Pteropus alecto*, a bat belonging to Pteropodidae) for all 3 clades. As a result, the absolute scale of the stem edges in those patches was longer (older) than the backbone tip edge for grafting, an incompatibility that prompted us to use an arbitrary short branch length of 0.000001 to graft those clades onto the backbone. The same solution was used in amphibians (53) and birds (2), where uncertainty of outgroup choice was more common and patch clades more numerous than in mammals (84 and 129 patch clades, respectively). While this solution is not ideal, it is a realistic outcome of backbone taxonomic uncertainty among bats (20, 60, 61). Because confidence in patch clade and sister taxon delimitation requires confidence in the backbone relationships of any major radiation, we expect these limits to our "divide-and-conquer" strategy of tree-building to persist, at least until disputed backbone nodes can be resolved or computational limits on patch clade size lifted.

8. Tests of diversification-rate variation or constancy

8.1 Tip-level diversification rates

The primary means by which diversification rate variation was examined in this study was using per-species estimates of expected pure-birth (PB) diversification rates, calculated for the instantaneous present moment (tips of the tree) using the inverse of the equal splits measure (2, 107). We call this statistic "tip-level diversification rate" (tip DR) because it contains rate information weighted toward recent PB diversification processes occurring among extant species ((108); we feel that "tip DR" is more descriptive than the term "DR statistic" used for this metric in Jetz et al (2)). Redding and Mooers (107) developed equal splits as a phylogenetic metric of per-lineage evolutionary isolation, Steel and Mooers (109) derived expected edge lengths in Yule trees, and Jetz et al (2) applied the reciprocal of equal splits to measure recent rates of species PB diversification. The harmonic mean of tip DR closely approximates the PB diversification rate for clades greater than 10 species (supplementary equations 5 and 6 in Jetz et al (2)). We calculate tip DR on full Mammalia phylogenies from the root to each tip as

$$Tip\ DR_i = 1 \Big/ \sum_{j=1}^{N_i} l_j \frac{1}{2^{j-1}}$$

where N_i is the number of edges on the path from tip i to the root, and l_j is the length of edge j. This equation assumes a fully bifurcating tree (2, 107). Because j=1 is the pendant edge leading to tip i, that branch length carries the greatest weight on the resulting value, with every ensuing rootward edge discounted exponentially as it is shared with other species. Sister species thus

have identical tip DR values. Species with the highest tip DR have many short branches shared with other species toward the present, implying recent branching is abundant, whereas low-tip-DR species are subtended by long unshared branches (i.e., they are evolutionarily distinct (107)).

8.2 Tip DR compared to model-based estimators

Here we use tip DR in 2 ways: (i) at the species level, where tip DR measures recent rates of PB diversification (≈ speciation, if recent extinction is minimal); (ii) at the clade level, using the harmonic mean of tip DR among species (referred to as "tip DR mean") to approximate clade rates of PB diversification. The harmonic, not arithmetic, mean is preferred where rates are averaged (110). Fig. S4 shows that tip DR among species is closely related to tip net diversification rates from the BAMM birth-death model (see section 8.3, below). Tip speciation rates from BAMM are similarly highly correlated with species tip DR, while tip extinction rates are generally low (0–0.2 species/Ma) with a slight positive trend suggesting greater turnover in high-tip-DR species (Fig. S4a; see Quintero and Jetz (108) for similar tip DR-to-BAMM comparisons in birds).

At the clade level, Fig. S4b shows that tip DR harmonic mean best approximates PB diversification rates across time-slice defined clades (see section 8.8). PB rates and tip DR mean show tighter correspondence for 50-Ma versus 10-Ma clades, as is expected since we calculated tip DR values upon full mammal trees but PB values on a per-clade basis (i.e., clades from older time slices are closer to the root, where tip DR mean equals the tree-wide Yule rate (2)). Tip DR mean is thus a clade-level average of species-level branching processes that is meaningfully aligned with clade-level models of diversification rates that ignore extinction. As expected, tip DR mean underestimates birth-death (BD) rates of speciation and net diversification per clade (Fig. S4b), since BD processes are modelling extinct branches (largely unrecorded in our nearly extant-only mammal trees). Similar underestimates of BD rates by tip DR mean were found in named bird clades (supplementary methods Fig. 5d in Jetz et al (2)) and bird elevational assemblages (fig. S6 in Quintero and Jetz (108)). Additionally, we examined the skewness of clade tip DR (called "tip DR skew") as a way to characterize the clade tip DR distribution beyond its central tendency.

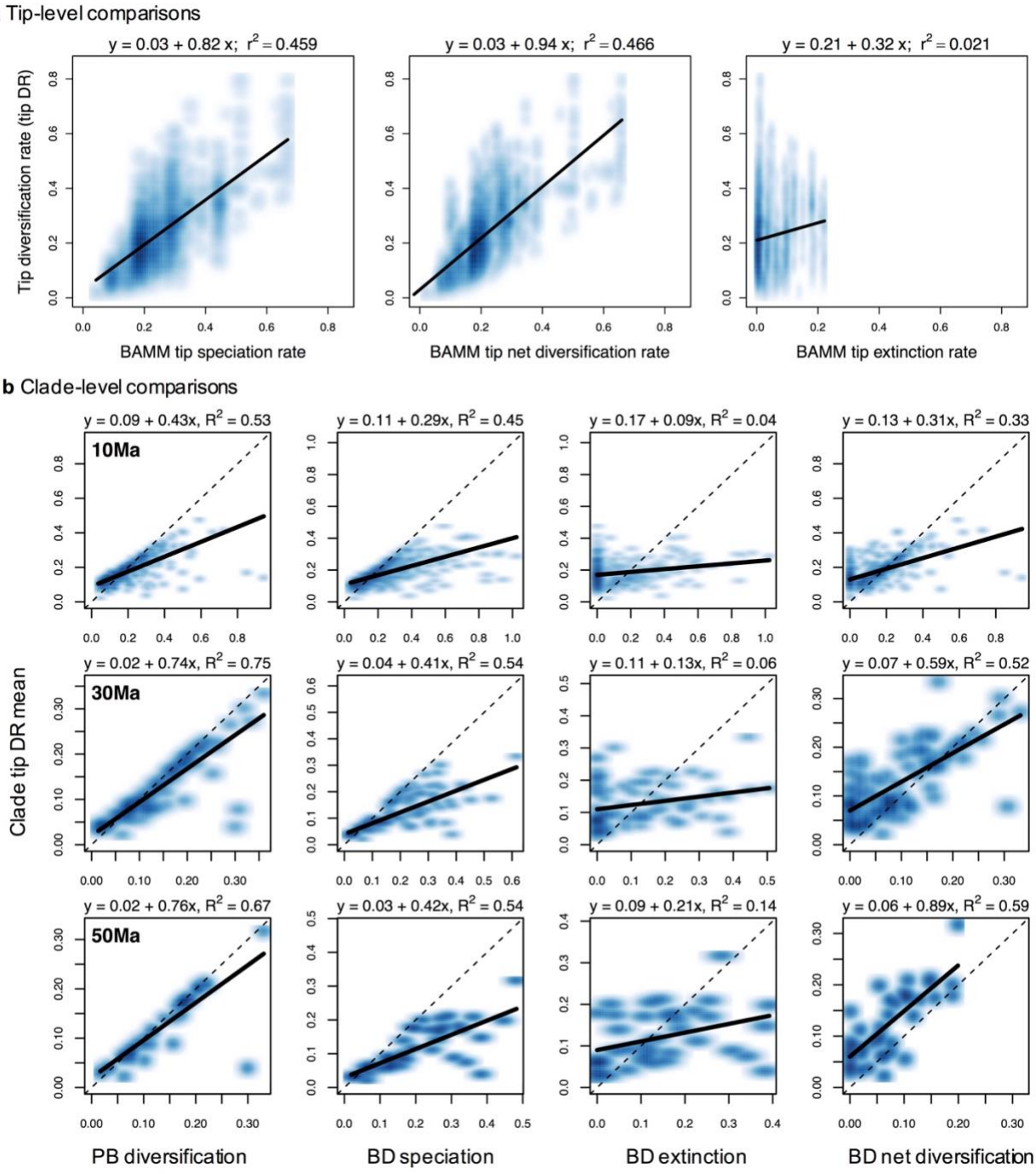

Fig. S4

Comparison of tip-level diversification rates (tip DR) from this study to other rate metrics. (**a**) At the tip-level, species tip DR values are compared to tip-level estimates of speciation, net diversification, and extinction calculated in BAMM v2.5. Shown are the harmonic means of per-species values from 10,000 full Mammalia trees (node-dated backbone) versus BAMM tip rates (summary of runs on 10 trees). Note that BAMM tip rates for net diversification predict tip DR more strongly than does BAMM speciation rate (linear models shown). (**b**) At the clade-level, the harmonic mean of tip DR among species (clade tip DR mean) is compared to model-based estimators for time-sliced clades at 10, 30, and 50 Ma (see main text Fig. 4). Plotted are the data from one mammal tree, with 1:1 reference lines (dotted) and linear model equations (solid) for relationships with pure-birth (PB) and birth-death (BD) rates. Tip DR mean best approximates PB rates (note: the PB outlier among 50-Ma clades is the long branch leading to *Solenodon*).

8.3 Lineage-specific rate shifts in BAMM

To formally test whether per-lineage diversification rates have varied throughout the root-to-tip history of Mammalia, we performed searches for macroevolutionary shifts using BAMM v2.5 (111). This algorithm uses reversible-jump MCMC to sample birth-death scenarios that vary in the number of distinct evolutionary rate regimes without specifying a particular *a priori* hypothesis. For each branch, a Poisson distribution governs the sampling of shift events and a gamma distribution the degree of rate change (i.e., a compound Poisson process (112)). These rate shifts are sampled at any point along a branch, so are not necessarily associated with branching events (for simplicity, we nevertheless plotted rate shift summaries at nodes in Fig. 1). The model thus allows for as few as 1 diversification process (zero rate shifts) or many more, and independently estimates the speciation and extinction parameters within each evolutionary rate regime (111). Those rates can then be summarized on a tree-wide basis to generate rate-through-time plots (see main text Fig. 3c and Supplementary Results).

Recent controversy over BAMM's implementation highlight several ongoing issues in macroevolutionary analysis (113, 114), in particular how undetected extinction events can bias diversification-rate inferences (115). However, these issues are not unique to BAMM (e.g., state-dependent models suffer similarly (114, 116, 117)), nor do they preclude the model's utility for detecting rate shifts. We suggest that, like any comparative method, BAMM should be used in parallel to other methods of inference. We therefore chose to apply it to our mammalian phylogenies for comparison among (i) BAMM tip rates to our tip DR calculations (Fig. S4), and (ii) lineage-specific rate-shifts to the tree-wide rate shifts detected by CoMET and TreePar models (Supplementary Results; see section 8.4).

We evaluated the number and location of rate shifts in Mammalia with independent runs on 10 trees drawn randomly from the node-dated sample. Although most studies run BAMM on a single consensus tree, a justifiable practice when phylogenetic uncertainty is small (118), the high degree of uncertainty in both node ages and taxonomic placement across our trees (including ~30% completed species) prompted us to use a sample of trees. We ran the models on the completed full trees of 5911 species and using globalSamplingFraction = 1.0, because adding missing species using PASTIS (birth-death branch lengths informed by patch clade context) was presumably more realistic than specifying sampling fractions in BAMM. For all models, we used the following settings determined using the Mammalia MCC tree analyzed with the "setBAMMpriors" function in the R package BAMMtools (119): expectedNumberOfShifts = 1.0; lambdaInitPrior = 6.446; lambdaShiftPrior = 0.00447; and muInitPrior = 6.446. We set the model to estimate speciation rates as exponentially varying through time and extinction rates as constant, which is equivalent to an independent SPVAR model within each rate regime (120), yet allowing for exponential decay or growth with a symmetric change function (121).

On each tree, we ran the model targeting 100 million generations, while sampling every 10,000 generations. Two of the 10 trees finished all generations using 168-hours of runtime on 1 node (the analysis is not parallelizable) of the High Performance Computing center at Yale University, and the other 8 runs finished in the same time a mean of 46.1 million generations (range: 29.2-83.1 million). That amount of runtime was sufficient to yield high ESS scores across all 10 runs after a conservative burnin of 33%, including for the log likelihood (ESS mean: 585.4; range: 268.9-1200.0) and the number of shift events (827.0; 328.0-1498.0). The resultant post-burnin events (mean: 3727.4; range: 1949-6667) were then subsampled to yield 1000 even-spaced samples for each of 10 runs with the function "getEventData" in BAMMtools.

The many nearly-equiprobable shift configurations in our 95% credible set of shifts for each of 10 trees prompted us to focus on the most likely shift sets—called maximum shift credibility (MSC) sets—on a per tree basis (see Supplementary Results). MSC sets are analogous to MCC trees derived from Bayesian phylogenetic analyses, and similarly are not necessarily equivalent to the shifts with maximum *a posteriori* likelihood (122). For the rate shifts in each MSC set, we summarized the node and clade contents implicated in the shift, and the mean net diversification rate ($=\lambda - \mu$) of all branches inside the shifted clade (clade rate) and outside that clade (background rate). The ratio of the clade and background rates was taken as the rate shift magnitude and used to identify whether an up-shift or down-shift was inferred. Comparing the contents of the rate-shifted clades allowed us to identify 24 rate shifts that were present in at least 5 of the 10 trees, including non-independent (paired) shifts that occurred on 1 or the other nearby nodes but not both (see Fig. 1). Dataset S7 summarizes details of MSC rate shifts from all 10 trees, including 35 independent shifts present in 2 or more trees and 48 more shifts only inferred in 1 tree.

8.4 Tree-wide rate shifts in CoMET and TreePar

We used the same 10 completed trees as above to assess time-specific, tree-wide shifts in rates, a strategy which differs from lineage-specific analyses by traversing time intervals rather than root-to-tip branches. We compared 2 modelling frameworks designed for this purpose: TreePar (17), which uses ML to best fit a birth-death-shift model to a set of branching times, and CoMET (123), a Bayesian implementation that allows joint inference and probabilistic priors on the same piecewise model as TreePar. Like BAMM, CoMET uses reversible-jump MCMC and a compound Poisson process to model shifts between reconstructed rate models and estimates both speciation and extinction shifts. TreePar estimates tree-wide shifts in net diversification rates.

We implemented these models on our mammalian phylogenies as follows, in both cases considering 7 possible rate-shift points, an arbitrary setting that made our results comparable to the mammalian analyses of Stadler (17). For TreePar, we used the "bd.shifts.optim" function, setting the sampling fraction to 1.0 (completed trees) for each of the 7 possible shift points (0-7 shifts, 8 total models), using a grid size of 1 Ma, and allowing for periods of declining diversity. Mass-extinction events were not separately estimated, only diversification rate shifts (see justification below). Results were parsed to compare the 8 models per tree, and the best model (lowest AICc) was in each case selected for summary across the 10 trees, including tallying of shift events within 1-Ma bins and 5-Ma bins.

For CoMET, we used the R package TESS (124) to set up an analogous model with sampling fraction of 1.0, up to 7 shifts (seven expected rate changes), and no mass extinctions allowed. We ran each tree for up to 100 million generations or until ESS scores of at least 500 were reached, and conducting four independent runs per tree. CoMET runs were summarized by removing a burn-in of 25% and tallying the number of speciation and extinction rate changes within 1-Ma bins (set relative to that tree's root time, so the number of bins differed across trees). Results from the four runs per tree were joined, and then results from each of the 10 trees were combined, each time maintaining the common 1-Ma time bins as needed, and using Gelman-Rubin statistics to assess parameter convergence (see Supplementary Results).

8.5 Lineages-through-time (LTT) plots

To visualize variation in branching times across Mammalia, we randomly selected 100 completed trees of 5911 species and plotted the accumulation of lineages through time from root-

to-tip. These trees were taken as a representative sample of the full 10,000-tree distribution for a range of analyses conducted in this study. We used a modified version of the "ltt95" function in the R package phytools (45) that allowed us to generate 95% confidence intervals around the LTT for those 100 full mammal trees. We could then plot those intervals as LTT polygons for mammalian higher taxa and K-Pg orders of placentals (main text Fig. 3).

8.6 Simulation of rate-constant trees

We simulated 100 phylogenies using birth-death models with constant speciation and extinction through time, for comparison to empirical phylogenies of all mammals (n=5911 species, root ages 165–210 Ma). For each simulation, we did the following: (i) load a single empirical tree (of 100 total); (ii) estimate rates from empirical branching times using the "birthdeath" function in ape; and (iii) simulate 1 tree using the "pbtree" function in phytools to the same extant diversity and root age as the empirical tree (specifying empirical lambda and mu, setting "scale" to the root age, and using the empirical taxa-stop criterion in continuous time). We conducted 3 sets of Mammalia-based simulations, under an extinction fraction matching the empirical mammals (ε=0.65 on average over 100 trees) as well as under low (ε=0.2), and high (ε=0.8) extinction. These simulation sets are compared to empirical mammal trees in Fig 3.

We also simulated separate trees matching the diversity and age of named subclades of mammals, in this case only simulating 1 set of 100 trees matching the empirical extinction fractions of each named clade. These rate-constant (RC) simulations were used to generate the null distribution for ML model fitting tests versus rate-variable (RV) models (see below).

8.7 Likelihood tests of RC and RV models of diversification

The branching times of named mammalian subclades were also tested for their ML fit to models of RC and RV diversification processes. We analyzed 27 subclades in total, 11 mammalian orders and 16 ordinal subclades that contained $\geq$ 25 extant or recently extinct species. For each subclade, we pruned those tips from the same 100 mammal trees used to generate the LTT plots. We focused on models developed by Morlon et al. ((125) for application to whales (Cetacea; implemented in RPANDA (126)):

- Two RC models, constant pure-birth (B) and constant birth-constant death (B_D);
- Eight RV models, four with exponentially time-varying rates (B-Exp, B-Exp_D, B_D-Exp, and B-Exp_D-Exp); and four with linearly time-varying rates (B-Lin, B-Lin_D, B_D-Lin, and B-Lin_D-Lin).

These 10 models were each fit for 100 trees of the 27 empirical subclades and their matching RC-simulated trees (null models). We parsed model outputs by adapting code from Condamine et al. ((127); https://github.com/FabienCondamine/Diversification_analyses) and including AICc per model and tree to generate empirical and null distributions of best model fits.

This procedure was designed following the birth-death likelihood (BDL) tests described in Rabosky (128), where the AICc scores of the best-fitting RC and RV models are subtracted to give the $\Delta AIC_{RC\text{-}RV}$ test statistic per tree and subclade. The 100 values of that empirical test statistic are compared to the null distribution as generated by calculating $\Delta AIC_{RC\text{-}RV}$ for each of the RC-simulated trees. Comparing directly between empirical trees and RC simulations of the same size and age serves to minimize Type I (false positive) error rates (128). We performed BDL tests of the overlap among empirical and simulated $\Delta AIC_{RC\text{-}RV}$ distributions at the alpha-

level of 0.05. See Supplementary Results for the full results of these models on the 27 clades, and main text Fig. 3f for a focus on 13 placental subclades.

8.8 Time-sliced clades

In order to objectively define clades for tests of among clade variation in richness and diversification rates, we arbitrarily drew lines (referred to as "time slices") at 5-Ma intervals and took the resulting *tipward* monophyletic clades as units of analysis. The *rootward* relationships of those clades (the "rootward backbone") was retained for each interval, giving the expected covariance structure among clades when performing phylogenetic generalized least squares (PGLS) analyses. Fig. S5 gives a graphical example upon a subclade of the mammal tree. This procedure was scaled up to the full Mammalia tree—for example, for the 35-Ma slice, a typical tree resulted in 90 clades that varied in species richness from 2–726 species (mean, and standard error: 65.5, 13.0), and had crown ages from 0.4–34.9 Ma (22.5, 1.1). The key criterion uniting these crown clades is that their stem branch was extant at 35 Ma, so their species are living descendants of a lineage at least that age. We contrast this approach to analyses performed on named clades (see section 8.9).

Time-sliced clades were constructed at 14 slices from 5–70 Ma for each of 100 trees for Mammalia and the 3 sets of RC simulations (Fig. S5 shows the distribution of clade richness values across time slices). We used the "treeSlice" function in phytools with orientation set to "tipwards" and "rootwards" for time-slice clades and backbone, respectively, re-naming the backbone tips to match the row names of the tipward clade summaries. We summarized clades for the following values, with rates and ages specific to each tree: species richness; crown age (timing of first split not yet extinct, i.e., the most recent common ancestor [MRCA]); tip DR mean, skew, kurtosis, and coefficient of variation; PB and BD diversification rates, and BD speciation, extinction, and turnover; and percent of species sampled for DNA. By definition, all tipward clades at a time slice had identical stem ages. Singleton branches ("clades" of 1 species) were dropped from clade-level summaries, but retained on time-slice backbones with their species-level values of tip DR and richness for PGLS. Clades with 2 or more species were summarized for MRCA. Clades with four or more species were assessed for tip DR skew and PB and BD rates (n=4 is the minimum tree size for modelling rates).

Note that our use of the term "time slice" to delimit tipward clades and their rootward backbone differs from the usages of some other authors. Most commonly in palaeontology, only the rootward time slices of fossil chronograms are examined (e.g., (129–131)). That approach seeks to compare sets of contemporaneous lineages at past time slices, while considering present-day taxa representatives of the 0-Ma time slice (reviewed in (132)). In contrast, other authors have used time slices to delimit units of analysis *within* time intervals rather than tipward or rootward, summarizing rates or traits of tree-wide branches bounded by time bins (e.g., (17, 133)). Here we use time slices to delimit non-nested, tipward clades and their rootward phylogenetic covariance as an objective means of conducting clade-level PGLS analyses. We compare our results to analyses using traditional taxon-based clades (mammalian genera, families, and orders).

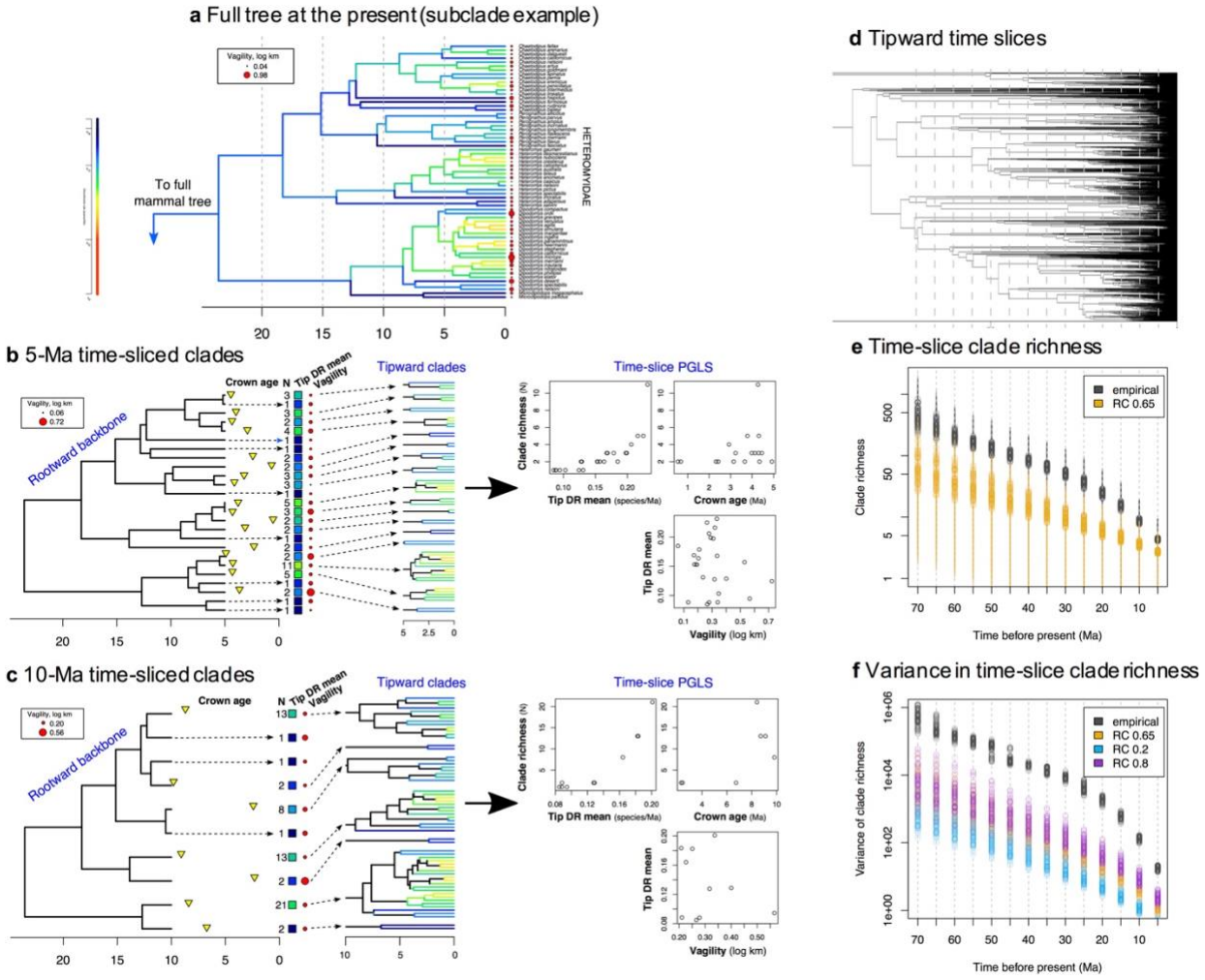

Fig. S5

Explanation of time-sliced clade delimitation and summarization for testing hypotheses. (**a**) An example subclade of 64 species, the rodent family Heteromyidae, is divided into time-sliced clades in the same way as for all Mammalia. Branch colors in the family-level phylogeny correspond to tip-level diversification rates (tip DR) calculated on the full tree, and red symbols are sized according to estimates of species vagility. For time slices at (**b**) 5 Ma and (**c**) 10 Ma, summaries of tipward clades are made for tip DR mean and vagility (harmonic and geometric means) to compare to crown age and richness. Note that PGLS (phylogenetic generalized least squares) regression was performed on log clade richness throughout this study. (**d**) The time-slice procedure was conducted at 5-Ma intervals across 100 full mammal trees (gray) and compared to trees simulated under rate-constant (RC) diversification (colors). Shown is the MCC tree, but 100 trees were sampled. (**e**) Mammalian and RC-simulated richness values (mean and standard error) and (**f**) their variance for clades at each time slice across 100 trees (legend shows extinction fractions for RC simulations). Observed clade richness values were consistently greater than expected, giving further evidence for rate-variable processes in mammals.

8.9 Clade-level PGLS to test RC versus RV diversification

To test what factors best explain variation in species richness among clades, we performed PGLS analyses using Pagel's "lambda" transformation (134), as implemented in either the nlme R package (135) or phylolm (136). The phylolm package implemented the same PGLS models as nlme with numerically identical results in over an order of magnitude less time (results not shown), a finding that surprised us but is expected because phylolm is optimized for large trees (136). As a result, we used phylolm wherever possible. We also used the caper package (137) for PGLS when calculating R^2 values. Lambda was always estimated on a per tree and per comparison basis, so as to only correct for the amount of phylogenetic signal present in the data (lambda=1.0 is full Brownian motion). Extinct taxa were always excluded from PGLS.

We conducted PGLS upon time-slice clades for each of 100 trees as follows: (i) load in tree-specific backbones and tipward clade summaries; (ii) set the natural log of species richness as the response variable; (iii) standardize the predictors as mean centered and scaled by the standard deviation; and then for each slice interval (iv) match the backbone tree tips to the clade summary row names using "treedata" in geiger (138); (v) perform univariate PGLS for each of the predictors to understand their shared effects on log richness; and (vi) select top predictors for multivariate PGLS to understand their unique effects on log richness. See Supplementary Results for results of the full univariate and multivariate analyses including percent sampling.

We repeated these 100-tree PGLS analyses for higher taxa to compare our results to other studies of clade richness in mammals (e.g., (139, 140)). We used taxa having ≥ 4 species:

- Genera: n=385 of 1283 total, 4–192 species, 1.1–27.8 Ma crown age means across 100 trees (grand mean, standard error: 8.2, 0.3)
- Families: n=102 of 162 total, 4–768 species, 4.0–58.0 Ma (19.1, 1.2)
- Orders: n=22 of 27 total, 4–2354 species, 9.6–73.7 Ma (42.3, 4.4)

For the taxon-based clades, we similarly generated per-clade summaries of richness, MRCA, tip DR mean and skew, and PB and BD rates. Those summaries then served as data points united by the backbone structure of phylogenetic covariance between clades. Pruning clades off the backbone results is a non-ultrametric tree (due to their widely different stem ages), in contrast to the time-sliced clades where each slice produces a rootward ultrametric backbone. Our solution was to simply prune full Mammalia trees to per-clade representatives, and do it the same way for time-sliced and taxon-based clades, so that the pendant edges of clade backbones extended to the present day. Long terminal branch lengths do not affect the resulting phylogenetic covariance structure among clades, only internode relationships and distances do (134), so this procedure did not differently impact the PGLS analyses based on different clade delimitations. See Supplementary Results for univariate and multivariate predictions of species richness in taxa.

8.10 Fossil genus diversification

We gathered fossil occurrence data of Mammalia from the Paleobiology Database and Fossilworks, as downloaded on 16 August 2018. Grouping by genus after excluding ichnotaxa and uncertain genera, we recovered 71,928 occurrences of 5300 genera from the earliest basal Mammaliformes (e.g., *Gondwanadon*, late Triassic ~235 Ma) to modern genera with fossil records (e.g., *Pteropus*). We binned these genus-level occurrences in 10-Ma intervals and used shareholder quorum subsampling (SQS (141)) to maximize the uniformity of taxonomic

coverage sampled during a given time bin. This conservative approach differs from classical rarefaction by subsampling for coverage rather than sample size, which makes diversity levels across intervals directly comparable (141). Using "sqs()" (https://bio.mq.edu.au/~jalroy/SQS-3-3.R), we specified a quorum size of 0.5 and performed 1000 trials with singletons. We calculated corresponding origination and extinction rates per stage using the per-capita rate method of Foote (142) (table 1 in that publication), which compares the number of taxa which exist both before and after each interval. We did not calculate rates for the late Pleistocene-Recent.

9. Tests for causes of diversification-rate variation

9.1 Mammalian trait data

Our workflow for gathering trait data for this study (Fig. S6) involved (i) unifying multiple trait taxonomies to our phylogeny's master taxonomy of 5911 species; and (ii) interpolating home range area and vagility to the species level for mammals. We unified data sources via a two-step process of matching binomial names to the same synonym list as used in section 2.1 (C. Meyer, unpublished), and then matching those translated names directly to the master taxonomy. Using *join* and *awk* in the bash shell, we joined four databases: EltonTraits v1.0 (25), IUCN Global Mammal Assessment (23), PanTHERIA (143), and the island rule database of Faurby and Svenning ((144); called "F&S"). Dataset S7 gives our full trait database.

We focused on ten ecological variables (circles and rectangles in Fig. S6): body mass (log kg), home range (log km^2), geographic range (log km^2), vagility (log km), insularity (0/1), trophic level (1/2/3), diurnality (0/1), marine or not (0/1), latitude (centroid, deg), longitude (centroid, deg). Mean body masses were assembled per species from F&S (5351 species) and EltonTraits (46 species, only those coded with certainty level "1" for direct observations). We note that Smith (145) is the citation for ~70% of those body mass values, which in turn gathered species means from the primary literature.

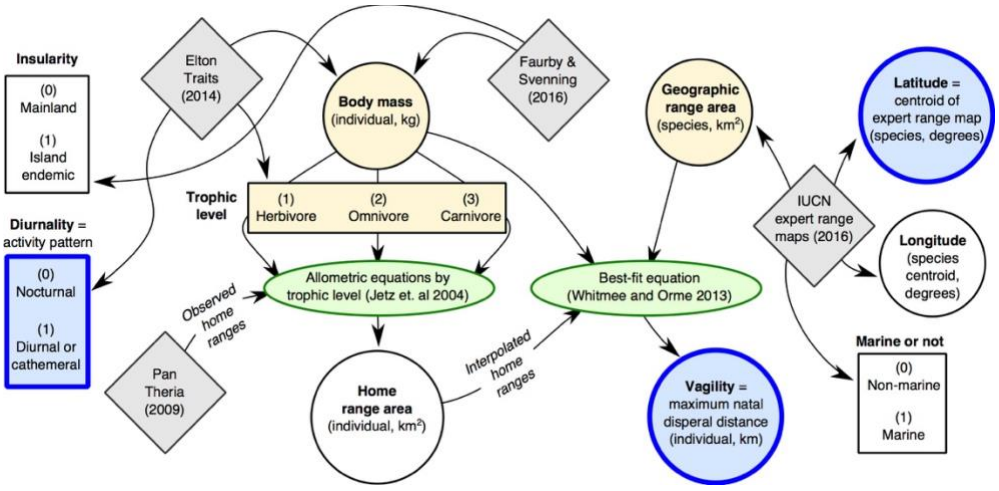

Fig. S6

Workflow for trait data compilation. (a) Schematic for compiling the 3 focal predictors (thick blue circles) of diversification-rate variation in main text Fig. 5. Shapes and colors represent: data sources (gray diamonds), interpolation equations (green ovals), continuous and discrete variables (circles and rectangles), and variables subjected to phylogenetic imputation (yellow fill). Coding categories are shown for discrete variables. Arrows represent input flows proceeding from data sources to taxonomic matching with our phylogeny.

The remaining 514 species without body mass values were imputed using the phylogeny and the R package "Rphylopars" (146). For each of 100 mammal trees, we (i) loaded the named trait data (including missing values); (ii) ran phylopars using models of Brownian motion (BM) and Pagel's lambda (LAM); and (iii) matched the model-imputed values back to the taxonomy. We then summarized the BM and LAM imputations across the 100 trees as medians and 95% CI bounds for each species. While the LAM models generally had better BIC scores than BM models, LAM yielded consistently larger values than BM, which were often unrealistic (e.g., *Acomys ngurui* has median of 573.3 grams [g] with LAM versus 90.9 g with BM, when the empirical range for *Acomys* is 18.5– 71.2 g; in contrast, the BM CI of 22.9–221.0 g is within the 13–38 g range given in the type description for *A. ngurui*, which was withheld (147)). We used the BM-based imputations of body mass for all calculations, including as related to interpolations of home range area and vagility (see below).

The geographic area and centroids of species geographic ranges were derived from expert range maps ((23), 18 August 2016 download). We calculated WGS84 ellipsoid areas of terrestrial and marine mammals in QGIS (148) while excluding the introduced portions of the ranges ("origin": 2, 3, or 4). Latitudinal and longitudinal centroids were taken as absolute values. Marine and non-marine mammals were given a binary coding. Insularity codings were gathered from F&S using the classical definition of island endemicity as pertaining to oceanic or landbridge islands (1122 species on islands of 5420 matched); species unmatched for island codings were manually interpolated (26 species on islands vs. 465 species assumed on the mainland). Missing values of geographic range area for 590 species were imputed based on phylogeny using the same Rphylopars procedure described above. Latitude and longitude centroid values were retained as "NA" for those 590 species without range maps due to concerns that geographic position is not a heritable trait in the same manner as body mass, geographic range, or intrinsic traits like activity pattern.

For trophic level, we modified the original diet classification from EltonTraits (10% intervals of 10 different food categories; (25)) into categories of percent vertebrates, invertebrates, and plants. That re-categorization was then collapsed into an ordinal multistate variable per species: (1) herbivorous if 100% plant diet; (2) omnivorous if mix of plants and (in)vertebrates; and (3) carnivorous if 100% animal diet (vertebrates or not). Those 3 categories contained similar numbers of species (1637 vs. 1852 vs. 1565, respectively).

For activity pattern (diurnality), we similarly modified the overlapping binary codings of "nocturnal", "crepuscular", and "diurnal" in EltonTraits to make a mutually exclusive variable that was binary per species, as follows: (0) nocturnal if nocturnal only, nocturnal + crepuscular only, or crepuscular only; (1) diurnal if any daytime activity is present (i.e., diurnal only, diurnal + crepuscular, or mix of diurnal, crepuscular, and nocturnal). This re-categorization was clumped toward nocturnality (3413 vs. 1614 species, respectively). BM imputations of activity and trophic level were performed in Rphylopars the same as for continuous traits (imputing 857 species), except that median results were rounded to the nearest whole number to match missing species with values of their closest relatives.

Home range area per individual (km^2) was interpolated following the allometric equations of Jetz et al. (149), which we updated using additional empirical data for non-marine home ranges reported in PanTheria ((143); n=603 species). Fig. S7 shows these empirical values best predicted by body masses (kg) with trophic level-specific equations (R^2 = 0.7–0.8 compared to 0.67 for all mammals). These equations can be compared directly to Table 1 in Jetz et al.

(149), although note that they reported slopes in $\log_{10}$ kg units while the intercepts are in non-log hectares (1 ha = 0.1 km^2) not the corresponding $\log_{10}$ km^2 units (see Fig. S7a). Our updated coefficients thus differ as follows: all mammals, 1.08 $\log_{10}$ kg slope (1.07 in Jetz et al. (149)), 7.08 ha intercept (6.69); herbivores, 1.07 (1.02), 2.34 (2.05); omnivores, 1.14 (1.12), 12.02 (15.87); and carnivores, 1.35 (1.20), 29.51 (52.07). We used these updated trophic level equations to interpolate the home ranges of all remaining species (n=5308). We then validated model-predicted values vs. empirical observations (Fig. S7b).

Vagility, also called dispersal ability (e.g., (150)), was measured as the mean per-individual distance of maximum natal dispersal (km), and interpolated for each species following the best-fit equation of Whitmee and Orme (151). That study identified the top 3 predictors of empirically measured maximum dispersal in mammals as adult body mass (g), home range size (km^2), and geographic range (km^2). They used natural log (ln) rather than $\log_{10}$, so we followed suit. We updated their equations using our estimates of the same traits by finding the best-fitting linear model to explain empirical data on maximum dispersal (n=89; (151)). We estimated coefficients for the intercept, and slopes of body mass, home range, and geographic range as -2.496 (-1.153 in Whitmee and Orme (151)), 0.206 (0.315), 0.323 (0.220), and 0.216 (0.252). We used that equation to interpolate estimates of maximum dispersal distance across all remaining species (n=5822), and validate predictions for the same 89 species as the empirical data (Fig. S7b).

Collinearity among the resulting variables was examined in Fig. S7c ("corrplot" package in R (152)). As expected, body mass, home range, and geographic range gave strong correlations with vagility (r=0.5–0.8), indicating that vagility is an "index" variable containing information from the other more classically studied traits in macroevolution (especially body size, e.g., (153–155)). In contrast, diurnality and latitude showed low levels of collinearity with other variables (maximum r=0.34 and 0.13) and were relevant to key hypotheses in mammalian diversification. We thus focused on 3 primary variables—vagility, diurnality, and latitude—for analyses of rate-trait dynamics (main text Fig. 5 and main text).

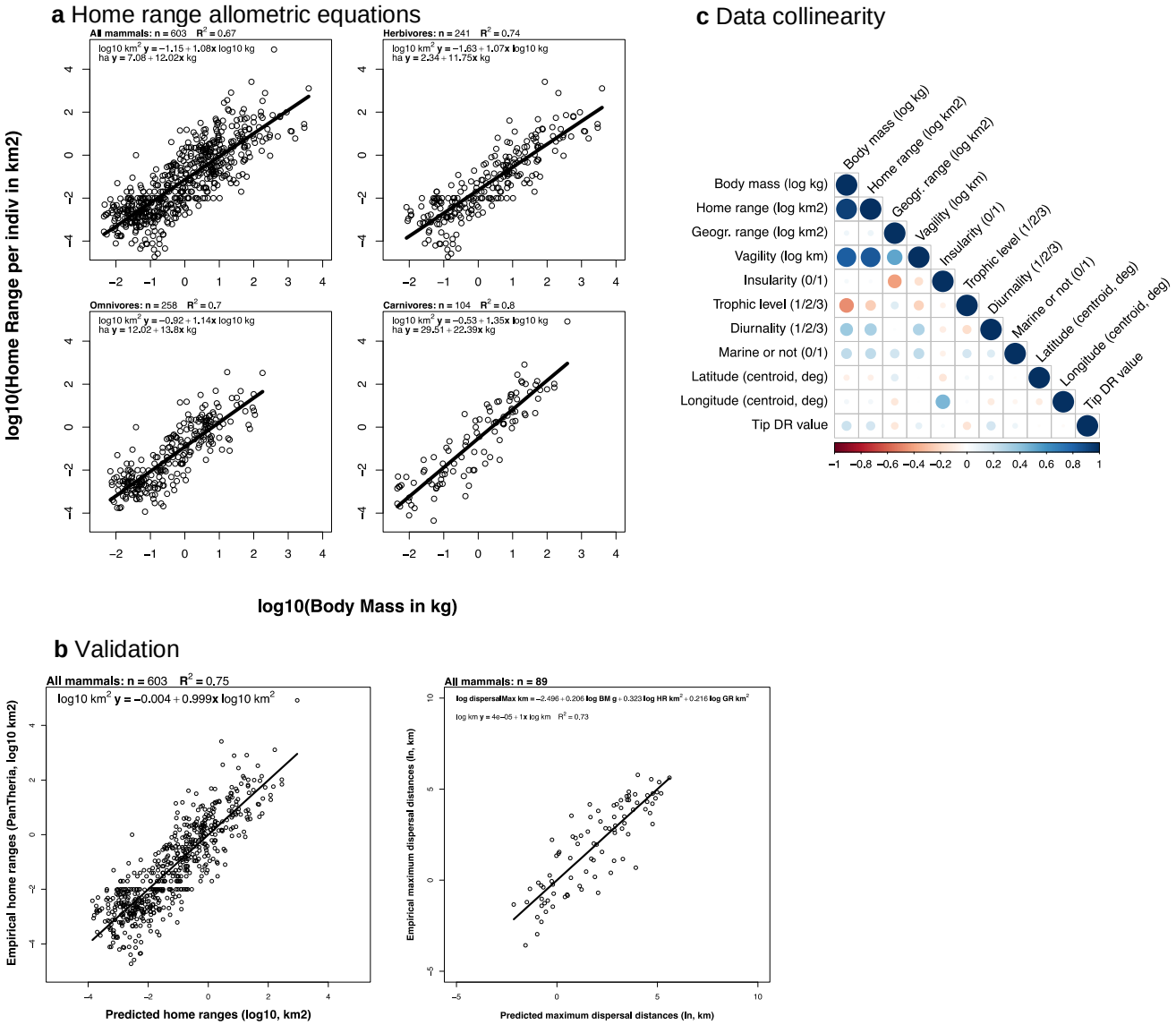

Fig. S7

Data and equations used to predict per-individual estimates of home range and vagility. (**a**) Using the approach of Jetz et al. (2004), we calculated log-log fits of body mass to empirically observed home range areas across all mammals (n=603) and within trophic-level categorizations. These updated per-trophic level equations were then used to expand the calculation of home range area to all species, which was in turn used in the vagility calculations. (**b**) Shown is the resulting fit of our predicted data for those same empirical values (from the PanTheria database). Additionally, we used the top three predictors for maximum natal dispersal distance in the analysis of Whitmee and Orme (2013) to calculate log-log fits to empirically observed data. This updated allometric equation was then used to expand the calculation of maximum dispersal distances to all species. (**c**) Pairwise spearman rank correlations among variables from which we selected independent predictors in analyses of diversification-rate variation. Colors correspond to correlation coefficients in the bottom legend. All extant species were used in these calculations (n=5804). Tip DR values are here compared based on the harmonic mean per species of estimates from 10,000 trees. Note that these are non-phylogenetic correlations, so not interpretable evolutionarily.

9.2 Tip-level correlates of diversification rates

For all PGLS analyses involving ecological traits (including those at the species level and clade level), we focused on a 5675-species data set that excluded (i) the 107 extinct species in our phylogeny due to trait uncertainty; and (ii) all 129 marine mammal species because of their order-of-magnitude trait differences relative to terrestrial species (and disparate selective constraints in marine environments; (155)). Sensitivity tests were additionally conducted for all rate-trait analyses to examine whether our conclusions were affected by the further exclusion of island endemic species (n=4553), DNA-imputed species (n=3941), and the separate analysis of trophic level categories (herbivore: n=1802; omnivore: n=2166; carnivore: n=1707 after excluding marine and extinct species; see Supplementary Results). For each of 100 trees, we used per-tree estimates of (natural) log tip DR, and species-level values for traits. We performed tip-level PGLS using the "phylolm" function in R, which performs well on large trees (136), and plotted results using the "plotrix" (156) and "hexbin" packages in R (157).

To better understand correlative structures underlying the observed rate variation across our mammal trees, we performed tip-level PGLS analyses between species' ecological traits and tip DR values across 100 trees. We followed Freckleton et al. (158) in using trait ~ rate models in our tip-level PGLS analyses. This approach reverses the typical rate ~ trait model, where the rate is dependent on the independent trait (predictor) variable (159), even though the aim is still to draw inference on the effect of the trait upon the rate (158). This is because we sought to avoid identical residuals in the dependent variable — i.e., sister species by definition share all speciation events and have the same pendant branch length, so their tip DR values are always identical, which violates the assumption of within-variable data independence in bivariate normal distributions, and so should be avoided (158). The trait ~ rate approach was originally formulated for use with node depth (number of nodes from the root to each species' tip), but the same logic applies to other species-level rate metrics. Note that while sister species could share identical trait values, their independent evolution since splitting still arguably renders their traits independent (theoretically in this case, if not empirically).

Trait ~ rate PGLS has been applied to a variety of species-level evolutionary questions (e.g., (160–162)), including with tip DR in univariate contexts (163). Multivariate PGLS models (e.g., rate ~ trait1 + trait2) should not suffer the same issue, since the comparative method models the residual variation among trait variables in that case, not the rate ((158); see (163) for an example using 9 traits). Although we did not conduct multivariate PGLS at the species level, we did do so at the clade level as part of phylogenetic path analyses upon time-sliced clades (see below, section 9.4)

9.3 Clade-level correlates of diversification rates

At the clade level, univariate PGLS could be performed typically, using rate ~ trait models, since averaging species' rates to clade tip DR mean resulted in sister clades having independent rate values. We performed univariate PGLS on time-sliced clades at 10-, 30-, and 50-Ma intervals as well as named taxonomic clades. These analyses were conducted by analogy to the previous analyses explaining log clade richness, with exceptions that (i) log tip DR mean was the dependent variable; and (ii) per-clade trait data summaries were the predictors (mean centered and standard deviation scaled to standardize the effect for comparison). Trait data was summarized using geometric means for vagility (to avoid skewing the clade means with large dispersal distances) and arithmetic means for latitudinal centroid (absolute value) and diurnality

(averaging species coded 0–1 gave a clade proportion of diurnal species). Clade-level PGLS analyses were conducted on 100 trees (see Supplementary Results).

We also performed clade-level tests for trait-dependent diversification using rate-shifted clades identified in BAMM runs on each of 10 mammal trees (see section 8.3). Lineage-specific rate shifts delimit "regimes" of independent evolutionary rates, to which we asked what traits are most associated with elevated rate regimes. A method called "structured rate permutations on phylogenies" (STRAPP; (164)) allowed us to randomly shuffle rate values among regimes, each time re-calculating trait-rate correlations to generate null distributions for comparison to empirical rate correlations. This test thus aims to correct for phylogenetic pseudoreplication of traits within rate regimes; i.e., all species in a regime share both evolutionary and rate-shift histories, so are not statistically independent (164, 165). PGLS also corrects for phylogenetic pseudoreplication, but by considering the full tree covariance structure. STRAPP analyses instead reduce the tree to rate regimes because these tree regions are the most independently diversifying. The downside is that the power of STRAPP tests is limited by the number of rate regimes present (164), and their accuracy of identification (113, 114). We performed STRAPP tests using the function "traitDependentBAMM" in BAMMtools, specifying 1000 replicates for relationships between BAMM speciation rates and our 3 focal ecological variables of vagility, diurnality, and latitude, as well as the binary variable insularity (see Supplementary Results).

9.4 Phylogenetic path analyses: clade-level causes of diversification and richness

Path analyses are formal methods for translating between the languages of causality and statistical probability, the latter of which is usually employed in correlational (not causal) contexts. Causality can nonetheless be approached using statistics by completely resolving the correlational structure of a given phenomenon, which implies that all full and partial correlations underlying that phenomenon are known. Of the universe of theoretical correlation sets, only 1 can be causally correct. Sets are expressed as directed acyclic graphs (DAGs; also called structural equation models) and employed in path analyses to test the observed data (166).

Phylogenetic path analyses (PPA; (167)) differ from other path models in their use of PGLS to test the statements of conditional independency that make up the "gaps" or non-paths in a path diagram (168). For example, the model $A \rightarrow B \rightarrow C$ is made up of paths $C \sim B$, $B \sim A$, and $C \sim B + A$ (conditional dependencies), which means that several non-paths are also implied for this DAG to be true (conditional independencies). So if any of the non-paths (e.g., $C \sim A$) have significant PGLS slopes, it means that the null hypothesis of that independency is rejected, and thus the model $A \rightarrow B \rightarrow C$ is not the best fit to the observed data (path $A \rightarrow C$ may improve the model; (169)). Path analyses are generally confirmatory not exploratory (166), so a key step is constructing models to test the most relevant causal hypotheses.

We chose 27 path models for PPA using our observed mammal data, with the goal of connecting hypotheses of species' ecological traits impacting diversification rates and, in turn, patterns of observed clade richness (Fig. S8). All models had 3 levels of vertices consisting of (i) clade traits (log vagility, non-log diurnality and latitude; as described in section 9.3); (ii) clade rates (log tip DR mean and non-log tip DR skew) and log crown age; and (iii) log clade species richness. DAGs varied from having 0-3 paths from clade traits to rates, with each trait only able to affect 1 rate variable (mean or skew) at a time; no paths were drawn from clade traits to crown age (Fig. S8). All 27 models included the 3 paths from clade rates and ages to richness, as we previously showed is best supported (main text Fig. 4, Fig. S8). Time-sliced clades at 10-, 30-,

and 50-Ma intervals were analyzed along with taxon-based clades. Sensitivity tests of path analyses were additionally conducted to examine the impact of excluding island endemic species (n=4553) and DNA-imputed species (n=3941; Supplementary Results).

We used the "phylopath" package in R (169) to specify the PPA models, as well as implement the PGLS analyses (conducted in phylolm) and compare models from the resulting outputs. For each of 1000 trees, we did the following: (i) load the tree and per-clade summaries for traits; (ii) subset to the targeted traits and standardize all model variables (including richness and rates) to establish common scaling; (iii) specify the 27 models; (iv) for each clade, prune the tree to the data using "treedata" in geiger (row names of clade summaries were given correspondences to tree tip labels in advance); and (v) use the "phylo_path" function to calculate model fits using PGLS and lambda transformations.

Our goal in summarizing results from the 27 models was to identify best supported *paths*, rather than 1 specific model over the others. For this reason, we used a model averaging approach focusing on AICc-equivalent scores called "CICc" to quantify model fits per tree and clade set (time-sliced or taxon-based clades). CICc uses Fisher's C-statistic to conduct goodness of fit tests on the conditional independencies of each model (168, 170). A given model passes the "d-sep test" if it has a C-statistic with $P > 0.05$ relative to the chi-square distribution with that degrees of freedom (171). However, for our time-slice analyses we found that only ~2% to 28% of models within 2 CICc units of the best model also satisfied the more conservative d-sep criterion (Supplementary Results). For this reason, we chose to focus only on the 2-CICc unit threshold for deciding which models would go to the next step of model averaging (had we used the d-sep criterion, not all trees and clade sets would have returned supported models). For each tree and clade set, we averaged path coefficients only if they appeared in a given model ("conditional" option in the phylopath function "average"; (167, 169)). We then took those 1000 averaged models and plotted each of their coefficients with standard error intervals, and took median coefficients of all 100 averages to plot in summary path diagrams (main text Fig. 5b, Supplementary Results).

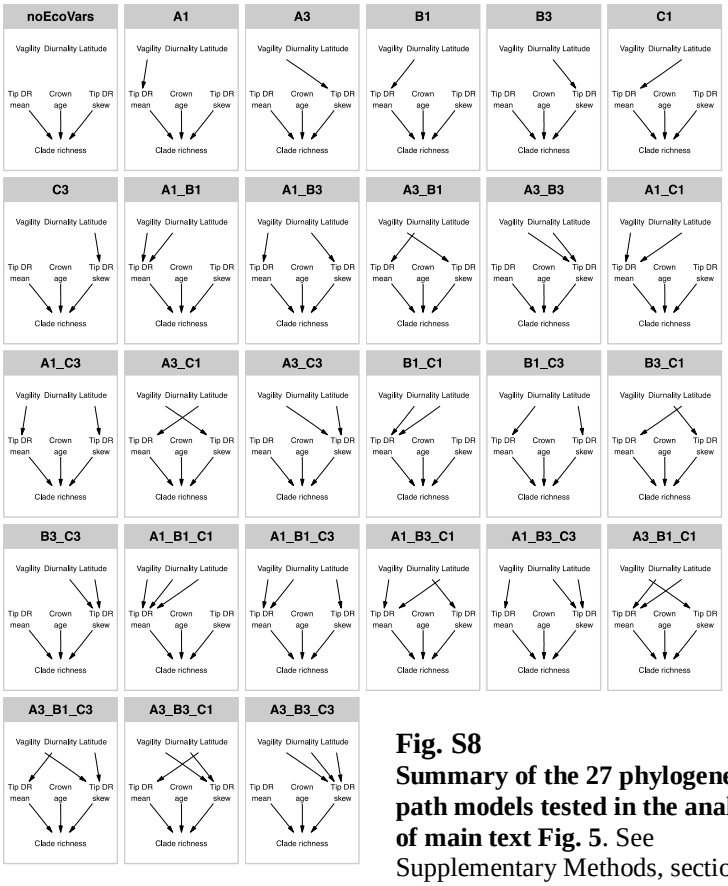

Fig. S8
Summary of the 27 phylogenetic path models tested in the analyses of main text Fig. 5. See Supplementary Methods, section 9.4 for details and Table S11 for

Supplementary Results and Discussion

1. Appropriate use of trees

We emphasize that our Mammalia-wide trees are 'completed' in the sense that we used taxonomic constraints to complete the species sampling (see sections 2, 5), and so the trees are better suited for rate-based than topology-based questions in macroevolution. For rate-based questions, accurately estimating tip-level rates of species diversification depends upon correcting for the non-random sampling of DNA among extant species (172–174). Steps of adding no-DNA species to phylogenies using taxonomic information will necessarily result in substantial uncertainty in the phylogenetic position of those species (e.g., within a genus constraint) across resulting trees. However, the aim is to accurately estimate recent branching processes, and so downstream analyses should always be performed on samples of trees to reflect this goal (1, 2, 65). 'Consensus' completed trees will be misleading because they obscure topological uncertainty (see section 7.2); hence, they should not be relied upon for rate-based comparative methods.

For questions of ancestral states or character evolution that emphasize having the correct topology rather than best rates, it is still best to perform topology-based analyses on a sample of DNA-only trees to capture uncertainty in branching. This issue was raised by Rabosky (175) with respect to the completed bird trees of Jetz et al. (2). The key point is that in order to avoid biasing models of character evolution, the unsampled (no-DNA) species should first be pruned out of PASTIS-completed phylogenies (175, 176). In summary, our completed Mammalia trees of 5911 species (5804 extant) are designed for rate-based questions; for topology-based questions, we recommend either: (i) pruning the time-scaled (ultrametric) distribution of full trees to the 4098 DNA species; or (ii) using the global ML tree estimated from the DNA-only supermatrix (section 4; but note that the ML tree is a point estimate and not ultrametric).

2. Comparisons to previous mammal studies

2.1 Topological relationships

The objective of our study was to provide novel resolution on the rates and timing of mammalian divergence events, but our results are nevertheless relevant to a few longstanding topological issues in the tree (see Fig. S9-11 for detailed comparisons of the backbone consensus trees, and Fig. S12 for a zoom-able view of the full Mammalia tree). We highlight 3 nodes on the placental backbone that are especially controversial:

i. The rooting of Placentalia. We recover support of 0.53 posterior probability (PP) in favor of the Atlantogenata rooting (Xenarthra + Afrotheria) compared to 0.47 PP for the Afrotheria rooting (Exafroplacentalia) in the node-dated analyses (Fig. S1b-c, Fig. S9-11), while the tip-dated backbone recovered the Afrotheria rooting most commonly (0.44 PP; rooting of Atlantogenata and Xenarthra was also recovered). The high uncertainty we recover for this basal divergence event in placentals is typical of other molecular studies (20, 177–181), although the Atlantogenata rooting has received more support in phylogenomic data sets (e.g., (181)). In contrast, studies that filter genes based on their likelihood of incomplete lineage sorting (proxied by AT-content; (178, 182)) generally favour the Afrotheria rooting.

ii. The position of treeshrews (Scandentia) relative to colugos (Dermoptera) and Primates. We find treeshrews allied with colugos (0.78 and 0.84 PP in node- and tip-dated analyses), with

that clade always adjacent to Primates (Fig. S2). By comparison, Scandentia has varied in position considerably depending on analysis methodology in other studies, mostly between the result we recovered and rooting outside all other Euarchontoglires (including rodents and lagomorphs; e.g., (178, 180, 181)).

iii. The position of guinea pig-related rodents (Ctenohystrica) relative to mouse- and squirrel-related clades. We find this controversial node, which was formerly questioned to even be inside Rodentia (183), to be unequivocally recovered as ((guinea pig, squirrel) mouse) in all backbone analyses (Fig. S2). Strong support for this relationship was also recovered in some studies (20, 181), but others have supported squirrels outside other rodents, usually when taxon sampling is smaller (177, 178, 180). Transposon evidence suggests that ancient hybridization may be complicating the early history of rodents (56). Regardless of the order of branching, these basal rodent divergences were very rapid, possibly even simultaneous (i.e., overlapping error bars for nodes 45–47 in Fig. S2d).

2.2 Backbone divergence times

Most node ages are statistically equivalent between our node- and tip-dated backbones, overlapping in their 95% highest posterior density (HPD) intervals (Fig. S9d; Fig. S10 and 11). However, the substantially older root age for crown Mammalia in the tip-dated backbone (245.9 Ma, 222.1–268.3), and implausible overlap of this estimate with the Permian-Triassic extinction event (69), was one of several reasons that we chose to focus on results from the node-dated distribution of trees in our primary analyses. Furthermore, a few nodes are also significantly younger in the tip- than node-dated backbones: in rodents, we find that Muroidea is ~15 Ma younger (e.g., nodes 52, 53, and 54 in Fig. S2d); and in yinpterochiropteran bats, node 39 is similarly young. Although there is an extensive recent literature on tip-dating in mammals (e.g., (184–187), features in Royal Society journals (98, 99, 179)), we note that the indirect use of fossil data as node constraints remains more mainstream (e.g., (180, 188–192)).

Focusing our primary analyses on the node-dating distribution of trees, we found that clade crown ages were broadly similar to previous benchmark studies ((14, 20, 177); Table S6). Our timings implicate the K-Pg event as possibly concurrent with 9 of the 18 crown placental ordinal radiations, which is more than the 3, 5, or 6 orders recovered in previous analyses (gray ages in Table S6). Our study also estimates no placental order radiation as definitively preceding the ~66 Ma K-Pg event, countering previous evidence that Eulipotyphla (14, 20) and possibly Rodentia and Primates (14) began radiating before this event (Table S6).

Our node-dating results correspond well to the fossil record. We synthesized information on the oldest fossil genera per extant mammalian order from the Paleobiology Database(193) (over 70,000 occurrences, see Supplementary Methods section 8.10). Fossil preservation waiting times and other taphonomic biases (e.g., figure 1 in Brown et al. (194)), led us to expect phylogeny-based stem ages to be consistently older than the oldest fossil assigned to each extant order. We found broad agreement with this expectation, with maximum fossil ages overlapping the 95% HPD interval of stem age in all but one case (Fig. S13 and Table S7). For Didelphimorphia, the stem age was ~18 Ma younger than the fossil *Pariadens* (93.5–105.3 Ma). However, that fossil was assigned to "Family? Stagodontidae" by Cifelli (195) with no reference to Didelphimorphia, and subsequently Stagodontidae was added to Didelphimorphia by Davis

(196) without reference to *Pariadens*, suggesting that it more likely attaches to stem Marsupialia. Instead, *Eodelphis* is the oldest confirmed Stagodontidae (66–72.1 Ma (196)) and in line with our expectations of being younger than our estimated stem age of 63.2–87.1 Ma.

2.3 Tip-level rates in mammal supertrees

We compared the tip DR values estimated from our supermatrix-based study to estimates for the same species in existing mammal-wide supertrees to understand how different tree-building methods influence rates. We selected 3 supertrees for comparison: (i) Kuhn et al. ((16); "KEA11"; 5,020 species, sample of 1,000 trees), which has an updated taxonomy (15, 24) and randomly resolves the polytomies from the supertree of Bininda-Emonds et al. (14); (ii) Faurby and Svenning ((18); "F&S15"; 5,747 species, sample of 1,000 trees), which merges genus- and family-level DNA trees using supertree methods; and (iii) the Mammalia portion of the Hedges et al. (19) eukaryote timetree compilation ("HEA15"; 5,364 species, 1 consensus tree), which merges and smooths average divergence times from a range of compiled studies. We calculated tip DR values across all samples of each tree, and then directly matched binomial names across the 4 trees (including ours) to yield 4,403 species with identical names for pairwise comparison.

We find limited concordance between our tree and the earlier supertrees of mammals (Fig. S4), illustrated by tip DR correlations of r = 0.57–0.62. The highest 1% of tip DR species from each study differs substantially, illustrated visually (Fig. S4a, reddest branches) as well as quantitatively, with only 12%, 21%, and 17% of the same 221 species identified with highest tip DR in our study similarly identified by KEA11, F&S15, and HEA15, respectively. Reducing that comparison to the genus level, those 221 species with top 1% of tip DR belong to 46 different genera, of which 22%, 28%, and 41% are similarly recovered with at least one species by those studies (same order). Thus, tip DR estimates from our study best match F&S15 at the species level and HEA15 at the genus level, although neither are close matches. Relative to each other, KEA11 and HEA15 have the most similar pairwise rates (r = 0.78) and F&S15 has a similar level of difference to those studies as to our study (r = 0.57–0.59; Fig. S4b). Comparing the top 1% of tip DR species at the genus level, KEA11 is most similar to HEA15 (68% vs. 25% with F&S15), F&S15 is most similar to HEA15 (58% vs. 27% with KEA11), and HEA15 is most similar to KEA11 (36% vs. 28% with F&S15).

Overall, these pairwise tip DR analyses show that rate estimates in our mammal tree are *substantially different* from previous trees. However, given the known biases of supertree methods for rate-based evolutionary questions—including the addition of short branches (= rapid rates) to nodes where source trees disagree (= high uncertainty)—this discrepancy is not surprising. Indeed, the rate biases in supertrees were a key motivation for our study (section 0), including that only 46.7% of nodes in the widely used Bininda-Emonds et al. (14) tree were originally bifurcating. The signature of resolving the other 53.3% of nodes in KEA11 is still visually apparent as blocky tree shapes at ~30 Ma (Fig. S4a). These branching artifacts were nevertheless interpreted biologically in several rate-based studies (e.g., (17, 197)). The other supertree shapes are qualitatively similar to KEA11, but appear to contain more tipward branching (especially the Rodentia portion of F&S15, lower half; Fig. S4a). We use these tree-wide comparisons to highlight how our Mammalia backbone-and-patch supermatrix phylogeny departs from past studies, and in so doing is more appropriate for testing rate-based evolutionary questions in mammals.

3. Measuring birth and death in the mammal tree

The ability to detect extinction in extant-only trees is not expected in all cases (198, 199), but our trees are apparently large enough to infer consistent signals of extinction at multiple time scales, consistent with earlier suggestions (200). Part of the difference in our mammal trees is that all subclades and backbones are estimated using birth-death branching models (see sections 5 and 6) as compared to previous uses of pure birth models in large trees (2, 53, 106). Using birth-death models is more computationally intensive, but has clear benefits of biological realism in the resulting branch lengths. For example, all else being equal, a 5% overall sequence divergence between two species may be reconstructed to a 10-Ma common ancestor using pure birth, while a birth-death model allows for extinction on the stem branch and so may reconstruct moderate turnover leading to a 5-Ma common ancestor.

Distinguishing between *rate shift scenarios*, where net diversification rates change due to increased speciation relative to extinction, and *high turnover scenarios*, where speciation and extinction are constantly elevated, is an ongoing phylogenetic issue (e.g., (17, 113, 114, 123, 201)) that also affects our analyses of the mammal tree. For instance, our BAMM reconstructions of speciation and extinction rates through time (main text Fig. 3c, Fig. S6) show considerable "coupling" of rate changes, where inferred shifts in rate magnitude usually occur in tandem for speciation and extinction across trees. Similarly, the weak positive relationship between BD extinction rates and clade tip DR mean (Fig. S4) could be from greater turnover in high-tip-DR clades, or else non-independence among rate estimates causing extinction to be "pulled" along with higher speciation. In this study, we therefore attempt to identify dynamics of "rate change or high turnover" in mammal evolution, recognizing that to separate speciation and extinction components of these patterns will most likely require models that fully consider fossil durations.

3.1 Mass extinction dynamics

It is within the stated capabilities of both CoMET and TreePar to model mass-extinction (ME) events parallel to rate shifts (17, 123). However, our initial runs suggest that the results differ considerably when CoMET is parameterized with ME and rate shifts versus when estimating ME events alone (sensitivity tests in Fig. S16; "minor" extinction event (202) with probability of survival p=0.3 seeded at 66 Ma when a bolide impacted Mexico's Yucatán Peninsula (203)). This sensitivity of CoMET to model priors suggests that tree-wide rate variation is being dispatched alternatively to ME or rate-shift categories. This is not surprising, nor a serious criticism of the CoMET model; rather, it simply demonstrates a limit of the uses of extant-only molecular phylogenies to differentiate these past events. Fossils are needed (17, 123). Without direct palaeontological data, it may be impossible to distinguish a mass extinction event from constant rates interrupted by a period of stasis (i.e., no speciation or extinction; (201)).

Overall, our results show apparent anomalies in tree-wide rates at ~66 Ma (main text Fig. 3c), as inferred with 3 methods: (i) BAMM finds that speciation and extinction rates both increase near the K-Pg, indicating higher turnover (Fig. S6); (ii) TreePar finds up-shifts in diversification within 5 Ma of the K-Pg event in 7 of 10 trees (Fig. S6); and, (iii) CoMET recovers an increase in net diversification rates peaking near the K-Pg (Fig. S6). We note that this signature of K-Pg-related environmental upheaval upon dynamics of mammalian lineage turnover is the first such report from a species-level phylogeny of extant mammals, complementing well-established dynamics from fossil mammals (204–207). However, the result

is somewhat qualitative and should be viewed provisionally given the above-stated concerns requiring unified fossil and molecular data to resolve.

We nevertheless, note that the ~66 Ma K-Pg signature was unexpected since no information of the event was seeded in BAMM, TreePar, or CoMET directly (ME priors absent). The lack of Cretaceous fossil evidence for crown placentals (70, 71) led us to use soft maximum age priors set to 66.0 Ma in node-dated divergence time analyses (NDexp) in 6 cases: Lagomorpha, Rodentia, Primates, Anthropoidea, Cetartiodactyla, and Carnivora. But we find similar divergence times without those node constraints in our tip-dated backbone analysis (Fig. S2, overlapping error bars), suggesting the K-Pg diversification rate signals are robust to our backbone analysis methodology. Improving current spatiotemporal biases in the fossil record may yield Cretaceous crown placentals, in which case the timing of ordinal diversifications in mammals is subject to revision.

3.2 Lineage-specific rate shifts in BAMM

Across all branches in Mammalia we find a mean speciation rate of 0.206 (95% CI for 10 runs: 0.188-0.223) and mean extinction rate of 0.068 (0.053-0.088), all in units of species/lineage/Ma. The mean number of post-burnin shifts detected across Mammalia was 36.7 (95% CI for 10 runs: 27.9-43.4), with the most likely number of shifts ranging from 26 to 41 (mean: 35.2) and detected in 4.1–8.5% of event samples (mean: 7.1%).

Important to note is that the reported BAMM rate-shift magnitudes are relative to the non-clade background rate, which differs by clade membership for each rate shift from the Mammalia-wide median rate of 0.138 species/lineages/Ma (Table S8). Rates from all branches across any trees (of 10 tested) that detected a given MSC rate shift are used in the rate magnitude calculations. Some rate-shifts are detected on multiple neighboring branches, but not both together, across the sample of 10 trees, in which case the non-clade rate was calculated on different trees for each portion of the shift. For example, node C has similar clade rates whether it occurred on the branch leading to Placentalia or one node tipward (Boreoeutheria), but the background rate differs from 0.136 (1.1x lower) to 0.088 species/lineage/Ma (1.6x), respectively, depending on which tree is examined (Fig. 1; Table S8). In that particular case, the location of the shift appears to depend on the Atlantogenata or Exafroplacentalia rooting of the trees (see Fig. S2). Alternative placements of 9 other shifts across the 10 trees similarly show differences in the background rate calculations (Table S8 and Data 7), supporting the relevance of considering a sample of phylogenies when performing tests for diversification rate shifts.

3.3 Birth-death likelihood model tests

We find that 20 of the 27 named clades show stronger fits to temporally rate-variable (RV) models of diversification than expected by chance (Table S9), with at least 5 of the 100 trees tested having $\Delta AIC_{RC\text{-}RV}$ test statistics significantly different than the 95% critical values of the same models fit to rate-constant (RC) birth-death tree simulations. For 13 of those 20 named clades, >50 of the 100 trees are significantly more rate-variable than expected, with the RV models B-Exp and B-Lin_D-Lin most commonly best (Table S9).

Of the 7 clades that favoured time-invariant RC processes of diversification more often than expected by chance (Table S9), 2 are species poor (Xenarthra and Talpidae) while the other 5 contain >100 species and so warrant further attention. These clades are: (i) Chiroptera; (ii) the bat subclade Yinpterochiroptera (the other subclade Yangochiroptera also favored RV models in

only 8 trees); (iii) Didelphimorphia opossums; (iv) the lemur and loris clade of Strepsirrhini primates; and (v) the guinea pig-related clade of rodents. Bats are a particular anomaly in our analyses since they overall match RC birth-death processes despite containing rate shifts on 6 lineages (Fig. 1, 2d and e). As the second-most speciose order of mammals, we expected to infer greater RV signatures within Chiroptera, but instead our results match prior suggestions that time predicts bat species richness (family crown age; (59)). Given that bats are the only flying mammals and have other unique features (e.g., (61, 208)), they may in fact depart from the RV diversification modes that predominate in most mammal clades; however, we highlight that bats appear to harbour considerably more undescribed biodiversity than other groups (27, 209), so our RC results could be artifactual. Similarly, species diversity may be reasonably considered as under-described in guinea pig-related rodents (especially Echimyidae; (210–212)) and in Didelphimorphia where 23 new species have been recognized since 2004 (27, 213–215). On the other hand, much taxonomic attention upon the lemur and loris clade of Madagascar (e.g., (216)) has caused some authors to argue they are over-described (217, 218), so finding RC diversification in this primate clade may instead be linked to their high rates of Pleistocene-Recent extinction (219) and their decrease in diversification rates (node O, Fig. 1).

Alternatively, in the absence of undiscovered biodiversity or recent lineage extinction, RC diversification may be a real phenomenon in these mammal clades requiring a biological explanation. Our study suggests that biological factors causing low lineage turnover may be responsible for why some clades diversify under RC while others are robustly RV, including histories of stabile tropical habitats, high species vagility, or niche adaptations promoting persistence such as diurnality (main text Fig. 5). The subjective nature of named clades also makes separating ecological traits that define clades (e.g., flight in bats) from the causality of that trait influencing diversification rate heterogeneity. The more objective approach of time-sliced clades developed here and applied to among-clade rate variation (main text Fig. 4–5), rather than these time-varying rate models (main text Fig. 3e, Table S9), may be profitably extended to examine time-varying rates and the covariates of those processes.

3.4 Tip DR skew for measuring clade rate unevenness

Clade tip DR skew was measured as a way to characterize the distribution of tip DR beyond its central tendency. We hypothesized that tip DR mean and skew would together explain different aspects of diversification rate variation, particularly for older clades where species-level rate variation is averaged out (tip DR mean) or accentuated (tip DR skew). Positive skew implies a long right tail of high tip DR values relative to the distribution median. We found that tip DR skew captures "long tails" of low- or high-tip-DR species relative to the central tendency of given clades, and thus contain information somewhat analogous to lineage-specific rate shifts, although without a formal process-based model (Table S10).

3.5 Testing for trait-dependent diversification in rate-shifted clades

We conducted STRAPP tests of trait-dependent speciation on each of 10 mammal trees, relative to diurnality, vagility, latitude, and insularity. Results corroborate the positive association of diurnality with speciation (Fig. S17a), which we previously uncovered at the tip-level, in 10-Ma clades (main text Fig. 5), and in genera (Fig. S19). No significant associations are found in the other comparisons, although vagility surprisingly shows a positive trend with speciation rate (Fig. S17b), differing from the direction at the tip-level and young clades (main text Fig. 5), but nevertheless non-significant. We interpret diurnality as an example of increased

lineage persistence driving the inference of rate shifts, whereas the other traits may drive species turnover and not be detected in lineage-specific rate shifts.

We additionally plotted the distribution of ecological traits among the 18 rate-shifted clades (Fig. S17e), which are the non-nested subset of the 24 total shifts in Fig. 1 and Table S8. We calculated Mann-Whitney U-tests for difference in trait medians between each clade and the rest of mammals (Fig. S17e; open circles denote non-significant; bars denote 95% CIs on the difference in medians). Compared to the ecological traits expected in the rest of mammals, we find: nine clades are less vagile than expected while seven clades are more vagile (Cetacea, Pecora, and Carnivora are extremely more vagile than the mammal median); four clades are more diurnal than expected (multi-state coding of 1=nocturnal, 2=cathemeral, 3=diurnal); clades are distributed in northern and southern hemispheres; and, four clades are more insular than expected. Further investigation of these rate-shifted clades is warranted to characterize their clade-specific causes for entering a new rate regime.

3.6 Comparing time-sliced clades and taxa in trait diversification

We similarly conducted trait diversification analyses across traditional taxon-defined clades for comparison to our time-sliced clades. For univariate PGLS (Fig. S18), we found genera, families, and orders to have inconsistent positive or negative effects as regards the ecological traits on tip DR mean, and those effects mirrored on tip DR skew. Genera may show opposite vagility trends as compared to 10-Ma clades, although the effects are small.

For the multivariate phylogenetic path analyses (Fig. S20 and Table S11), we found that the vagility effects disappeared on tip DR mean for genera, families, and orders, but instead manifested on tip DR skew. The positive effects of diurnality on tip DR mean persist on genera and families, while those of latitude manifest only on order-level tip DR mean.

4. Sensitivity tests of trait diversification

We conducted re-analyses of tip- and clade-level trait diversification on 1000 trees from both the node- and tip-dated backbone distributions, in each case using data subsets to test for the following types of bias:

(i) *Excluding island endemic species* (n=4553 non-marine species remaining): if islands have smaller geographic-range species (220) and stronger selective regimes on body size (221), then we may expect them to bias our allometric calculations of vagility (151), perhaps driving inverse vagility ~ tip DR in 10 Ma clades;

(ii) *Excluding DNA-missing species* (n=3941 non-marine species remaining): if the birth-death polytomy resolver (PASTIS (1)) that we used to impute DNA-missing species to our phylogeny creates a bias for trait evolution studies (222), then excluding imputed species should change our tip- and clade-level results.

(iii) *Use of an alternative tip rates metric, node density (ND)*: if the reliance on tip DR is driving our results, then we expect key findings to change using another tip rate metric.

The concerns raised in Rabosky (222) regarding the analysis of trait diversification on trees imputed for DNA-missing species prompted us to test their influence. The paper of Harvey and Rabosky (223) similarly motivated our comparison of results using ND (i.e., a simple count of nodes from the root to each species' tip (158)); they show that PGLS using ND can in some cases have higher power than tip DR-based PGLS, although with a higher false discovery rate

(0.06 vs. 0.02 doing PGLS with tip DR). Note that we did not conduct the 'sim' tests described in Harvey and Rabosky (223) over concern that their use of rate ~ trait models violates the assumption of data point independence in bivariate normal distributions (sister species have identical tip rates (158); see Supplementary Methods section 9.2). Instead, we employed trait ~ rate PGLS models throughout our sensitivity tests that are nevertheless interpretable in the context of assessing trait-dependent diversification (see (158, 160, 163)). Overall, these sensitivity tests were broadly self-consistent and produced limited differences in the number of significant trees across backbone samples and data subsets.

4.1 Tip-level PGLS

The inverse effect of vagility ~ rate in 10-Ma clades is recovered similarly using the ND-based approach as using tip DR in both island and DNA-missing exclusions, as well as the trophic level subsets (Fig. S21). Similarly, the mostly null tip-level effects of diurnality and latitude are consistent across subsets. The major difference is that the ND approach is less sensitive to the exclusion of DNA-imputed species – e.g., the 1000 trees with significant vagility effects on ND for all mammals was reduced to 993 (and 992 tip-dated) versus being reduced from 998 to 60 (and 112) using tip DR. The ND approach thus usefully corroborates our tip DR-based findings and suggests that including the traits of DNA-missing species does not bias the conclusions of our tip DR analyses. DNA-missing species are in fact a non-random group of species – so excluding them may instead be a greater bias. Nevertheless, we agree that by testing for the sensitivity of our results to these imputed species we have confirmed the robustness of our trait diversification analyses.

4.2 Clade-level path analyses

Our results similarly hold at the level of time-sliced clades. Repeating these sensitivity analyses for path models finds qualitatively identical results, with minor differences in the number of trees for which a given path coefficient was non-zero (Fig. S22). For ease of interpretation, we summarize these data in Table S12.

For the inverse relationship of vagility ~ rate in 10-Ma clades, we found consistently strong evidence that excluding island and imputed species has no major influence (marginal relationships in the tip-dated backbone using tip DR mean; Table S12). Similarly, the positive diurnality ~ rate relationships in 10-Ma clades are consistently strong or marginal across nearly all comparisons. For latitude ~ rate, the tip DR-based comparisons reveal consistently strong or marginal results across the 10-, 30-, and 50-Ma clades, while the ND-based comparisons only have a consistent signal for the 50-Ma clades. All together, we highlight that the directionality and magnitude of results is visually consistent throughout (Fig. S22), an impressive finding given the extensive data and complex relationships explored. These sensitivity tests add rigor to our primary conclusions regarding ecological causes underlying the uneven recent diversification and species richness in mammals.

5. Limitations

This study was motivated by the clear need for phylogenetic trees that contain comparably time-scaled branch lengths from root to tip. Until the computational challenges of running a data matrix of >6000 taxa in one partitioned and time-scaled analysis can be overcome,

and greater DNA sampling can be obtained, we suggest that the following sources of bias will continue to limit the certainty of resulting inferences.

5.1 Patch clade delimitations and rate shifts

Our backbone-and-subclade analysis framework led us to assume hard monophyly for each of 28 patches from the global ML tree, which are subjective delimitations based on bootstrap support and our maximum clade size of ~800 species (see section 5). Arguably, a different set of break points might have produced somewhat different branch lengths and among-clade rate variation in the full mammal tree, in ways that we did not explore directly (run times on patch clades were up to 5 weeks in MrBayes, so sensitivity tests were not feasible; Table S5).

Each patch phylogeny was estimated with a separate DNA matrix in MrBayes (pruned from the global 31-gene matrix), so their resulting branch and rate parameters are free to differ from the same prior settings. From one perspective, this procedure benefited our results by best-fitting molecular evolutionary processes to local genetic information, balancing a desirable amount of realism with the goal to reduce hard monophyly assumptions by keeping patch clades as speciose as possible. In contrast, dividing mammals into patch clades could be viewed as over-fitting local processes that are more generally "noise" from the mammal-wide perspective. Those disparate philosophical stances require further empirical study, possibly with the use of DNA-simulation approaches that target fluctuating molecular evolutionary rates at different magnitudes and scales, and then build phylogenetic trees from the resulting data. Covariation between empirical molecular evolutionary patterns and life history traits such as generation time, reproductive rate, and fecundity may prove especially useful in understanding how frequent such molecular-rate fluctuation is in nature. Completing DNA matrices with additional genome-scale sequencing is additionally essential, since the gappy-ness of our DNA supermatrix is non-random by taxon and geography, and thus provides unknown biases. For now, simulation studies based on random missing data in supermatrices support our estimates and conclusions (48, 49).

Regardless of those concerns, the location of 24 lineage-specific rate shifts inferred in our BAMM analyses are not dependent on our 28 patch delimitations (Fig. S23). Of the 18 rate shifts that are non-overlapping and tipward (B-X; Fig. 1, Table S8), we find that only 4 are located along the stem branch for a patch clade (shifts P, Lagomorpha; T, Cricetidae; G, Vespertilionoidea; and D, Carnivora), while the remaining 14 shifts are concentrated to 9 patch clades, so that 4 patches contain 2-3 tipward rate shifts (Fig. S23). Fifteen of the 28 patch clades thus contain zero rate shifts, including the fairly speciose squirrel-related clade (320 species). Our contention that rate shift locations are independent from patch decisions is also supported by the bird tree (2), which delimited 129 patch clades and estimated 25 rate shifts.

5.2 PASTIS completion and tip DR

Two take-home messages from our analyses are that (i) tip DR is an informative metric of among-lineage rate processes at multiple phylogenetic scales; and (ii) taxonomic completion methods are required to accurately estimate tip DR if some species are unsampled for DNA. Until full species-level DNA sampling can be obtained for mammals, then taxon completion approaches like ours using PASTIS-generated constraints in MrBayes (1) are useful options for obtaining taxonomically realistic tree shapes (i.e., branches for no-DNA species are drawn from the same prior distribution as DNA species, which is estimated from the local DNA matrix, see section 5). We find up to 2x-higher variance in the tip DR estimates for the completed species (Fig. S24a), which is an expected outcome since their taxonomic placement is random within the

specified MrBayes constraints across the 10,000 trees. Tip DR medians for the same completed species are importantly no different than expected based on the range of tip DRs for DNA-sampled species (Fig. S24b). We thus find no bias in tip DR estimates regarding whether a species was sampled for no genes or all 31 genes. Similarly, including the percent of DNA-sampled species per clade as a covariate of time-sliced clade richness (Fig. S8) shows that our results are insensitive to taxonomic completion.

5.3 Uneven taxonomic descriptions and tip DR

Another possible bias in tip DR estimates is the disparate amounts of revisionary taxonomic attention that different clades of mammals have historically received. Taxonomic descriptions are arguably more narrow in larger- versus smaller-bodied mammals (217, 218), but the many low-tip-DR species among large and well-studied lemurs and carnivorans (Fig. 1) suggest that taxonomy alone is not driving the signal of faster recent diversification in simian primates than in other groups (clades 42 and 43; Fig. 1, 2e). Many small-bodied mammals also continue to be described, especially in the Neotropics and Australasia (e.g., (224, 225)), apparently without inflating rates. We include in our trees most of the 148 new species of Primates described in the last dozen or so years (28.6% of the extant total; (27)), which compares to 371 (14.5%), 304 (21.9%), 86 (16.3%) new species of rodents, bats, and shrews, respectively, in that interval (27).

Importantly, we did not include most of the 227 new species of Artiodactyla described recently (41.1% of the total; (27)) since they nearly all derive from the monograph of Groves and Grubb (226) and are unvetted genetically (217, 218, 227). We conservatively include 348 species in Artiodactlya rather than 551 (27, 28), but still find two major rate shifts and elevated tip DRs in whale- and cow-related clades (Fig. 1–2), suggesting that those shift magnitudes may be underestimates. Overall, we suspect that varied taxonomic efforts should be less biasing in our mammal trees than in groups like amphibians (e.g., due to microendemism and tropical distributions; (228)), but future efforts to harmonize the definition of species-level lineages on a group-wide basis may be fruitful.

6. Coda

The value of continued DNA sequencing of mammal species, genes, and genomes, and further discovery of fossils cannot be overstated. Nevertheless, the 10+ years elapsed since the landmark publication of Bininda-Emonds et al. (14) highlight the clear need for improved rate-based approaches to species-level mammal phylogeny that this study advances toward. The insights gained demonstrate mechanistic links between ecological factors acting on levels of individuals and populations (e.g., vagility), their effects on lineage-level processes of speciation and species turnover, and the resulting patterns of unevenness in species richness among mammal clades. Continued improvements to the tree of life will be the test of those insights.

Table S6.

Divergence times relative to prior studies. Crown divergence mean estimates (Est) and 95% confidence intervals (CI, lower and upper) for each taxon listed, with the 27 extant mammal orders in capital letters. Ages in gray are order-level divergences estimated near the Cretaceous-Paleogene (K-Pg) extinction, with "near" defined as having 95% CI < 3 Ma of 66 Ma, while black ages have CIs >3 before 66 Ma. Our node-dated estimates are compared to global amino acid and DNA dates (20), best estimate dates (14), and combined 14K+Mit dates (177). Dates are missing if a node was not recovered or lacked taxon sampling.

		This study			Meredith et al. (2011)			Bininda-Emonds et al. (2007)			Dos Reis et al. (2012)		
Taxon	**N**	**Est**	**Low**	**Up**	**Est**	**Low**	**Up**	**Est**	**Low**	**Up**	**Est**	**Low**	**Up**
Mammalia	5911	188.4	166.7	210.9	217.8	203.3	238.2	166.2	Fixed	Fixed	184.7	174.6	191.9
MONOTREMATA	5	38.2	13.5	79.4	36.7	22.4	103.1	63.6	52.2	75	56.4	30.6	84.7
Theria	5906	159.6	156.3	166.2	190	167.2	215.3	147.4	141.8	153.1	172.8	168.5	177.9
Marsupialia (Metatheria)	362	79.4	67.9	92.8	81.8	67.9	97.2	82.5	71.4	93.7	76.0	64.3	83.6
PAUCITUBERCULATA	7	16.4	12.3	20.3	11.7	7.2	16.2	33.2	26.3	40.1	27.8	11.0	47.0
DIDELPHIMORPHIA	106	38.3	31.3	45.2	31.4	23	38.4	56.2	45.9	67.7	50.5	39.4	60.4
Australidelphia	249	63.4	54.1	74.8	64.2	53.7	75.5	66.8	63.8	74.2	70.2	58.7	76.6
DASYUROMORPHIA	78	34.1	27.7	40.9	30	22.1	41.7	31.3	16.2	55.8	46.0	35.6	54.9
DIPROTODONTIA	146	48.7	41.1	57.5	52.8	42.4	64	54.1	52.4	55.8	57.5	46.5	64.9
MICROBIOTHERIA	1	.	.	.	.	.	.	.	.	.	.	.	.
NOTORYCTEMORPHIA	2	6.1	3.6	9.0	.	.	.	9.3	8.3	10.2	.	.	.
PERAMELEMORPHIA	22	29.5	24.1	35.2	28	21.1	37.1	36.2	30.6	41.8	40.9	30.8	51.4
Placentalia (Eutheria)	5544	91.8	77.4	105.0	101.3	92.1	116.8	98.5	93.2	108.1	89.2	87.9	90.4
Xenarthra	33	67.4	53.0	83.9	65.4	58.4	71.5	72.5	67.4	77.6	69.4	66.5	71.8
CINGULATA	21	37.6	27.7	47.9	.	.	.	.	.	.	.	.	.
PILOSA	12	59.8	46.8	75.3	56.4	49.2	62.9	.	.	.	62.7	57.5	66.9
Afrotheria	92	80.0	64.0	94.5	80.9	74.4	96.5	93.4	90.4	96.4	70.4	68.7	72.1
Afroinsectiphilia	75	77.5	62.4	92.3	78.6	71.8	95.2	93.2	90.2	96.2	64.7	61.2	67.9
AFROSORICIDA	55	70.4	56.5	85.8	68.2	56.8	88	85.2	81	89.3	.	.	.
MACROSCELIDEA	19	59.0	44.8	71.7	49.1	37.7	57.2	50.7	43.1	58.3	32.4	19.4	43.9
TUBULIDENTATA	1	.	.	.	.	.	.	.	.	.	.	.	.
Paenungulata	17	54.0	41.5	67.4	64.3	56	70.6	75.9	72.0	79.8	60.3	58.3	62.2
HYRACOIDEA	5	10.0	4.3	15.4	6.1	3.9	8.3	19.1	18.4	20	16.0	76	27.0
PROBOSCIDEA	7	10.1	4.8	16.2	5.3	1.8	8	19.5	7.6	31.4	8.4	3.4	15.9
SIRENIA	5	14.3	7.0	22.6	31.4	25	34.4	52.2	37.9	66.5	27.2	12.6	38.7
Boreoeutheria	5419	83.5	73.1	94.8	92	82.9	107.6	96.1	92.9	98.4	83.8	82.8	84.9
Laurasiatheria	2456	75.1	66.3	84.1	84.6	78.5	93	87.8	85	90.5	76.0	74.9	77.0
ARTIODACTYLA	348	58.4	50.3	67.1	65.4	62.3	68.5	70.7	67.6	73.7	61.4	60.7	62.3
Camelidae	7	9.6	7.1	12.2	.	.	.	30.3	10.4	50.3	28.5	20.1	37.4
Ruminantia	225	34.0	29.1	41.3	40.3	35.1	46.4	30.2	26.5	34.5	38.7	34.3	42.9
Suina	21	26.2	21.3	31.1	28.8	20.3	36.9	49.7	35.9	63.5	35.2	27.2	43.7
Whippomorpha	95	39.3	32.7	46.4	53.7	51.1	58.2	52.2	41.9	62.6	48.1	45.9	50.1

Cetacea	91	25.9	15.2	38.6	29.4	13.4	35.1	30.2	26.5	34.5	34.4	33.7	36
CARNIVORA	298	40.2	33.9	47.9	54.7	47.4	60.6	63.4	59.8	67.1	54.2	52.3	56.0
Caniformes	172	34.5	28.6	40.4	46.5	39.6	52.1	59.2	55.8	62.6	41.8	34.6	47.8
Feliformes	126	27.2	22.3	32.2	39.7	33.4	45.9	42.5	37.2	47.9	48.5	45.5	51.5
CHIROPTERA	1287	57.1	48.7	66.0	66.5	62.3	71.3	71.2	68	74.3	59.2	57.7	60.7
Yangochiroptera	902	51.9	45.3	58.8	56.3	52.2	61.3	.	.	.	50.7	46.1	54.6
Yinpterochiroptera	385	50.5	41.4	60.3	62.9	58.6	66.8	.	.	.	53.4	49.2	56.5
EULIPOTYPHLA	491	74.3	65.4	83.6	77.3	70.7	85.8	82.5	79.8	85.3	61.5	60.9	62.0
Erinaceidae	24	46.7	39.1	53.7	38.9	29.0	48.9	65.5	60.9	70.1	48.2	43.1	52.7
Solenodontidae	3	10.9	0.2	39.6	.	.	.	40.8	40.8	40.8	.	.	.
Soricidae	420	47.2	39.5	55.2	.	.	.	49.0	40.3	58	33.2	26.5	39.6
Talpidae	44	40.6	32.8	47.7	.	.	.	61.8	52.3	71.3	34.5	29.5	39.4
PERISSODACTYLA	24	38.7	32.6	45.0	56.8	55.1	61	55.8	51.1	61	52.6	41.8	61.0
PHOLIDOTA	8	27.1	17.9	38.2	25.3	16.9	35.7	19.1	7.3	46.9	.	.	.
Euarchontoglires	2963	77.0	67.8	87.4	83.3	74.1	97.8	91.8	90	93.8	75.7	74.8	76.7
Primatomorpha	480	70.4	61.7	79.8	82	73.7	97.4	88.5	85.9	91	74.1	73.2	75.1
SCANDENTIA	20	52.8	38.1	68.4	55.9	45	63.9	31.7	29.9	34.7	.	.	.
DERMOPTERA	2	9.6	3.3	16.5	7.4	4.5	13.2	15	10.2	19.9	.	.	.
PRIMATES	458	67.1	57.6	76.9	71.5	64.3	78.4	84.5	81.9	87.1	68.2	67.3	69.2
Catarrhini	152	20.7	17.0	24.6	20.6	17.0	22.7	36.6	33.8	39.5	26.3	25.3	27.4
Platyrrhini	161	17.0	14.2	20.1	14.6	11.2	18.4	24.5	21.4	28.3	16.2	10.3	22.1
Tarsiiformes	10	15.7	11.4	19.7	.	.	.	9.7	3.4	15.9	25.3	10.8	41.2
Strepsirrhini	135	49.6	42.2	57.0	55.1	50.2	58.7	75.5	71.3	79.6	55.1	53.4	56.8
Glires	2483	72.5	64.4	81.1	79.5	71.5	94.1	88.9	87.8	90.1	70.8	69.9	71.8
LAGOMORPHA	91	36.2	30.5	42.1	50.2	47.4	56.9	64.3	60	68.7	47.9	45.9	49.3
RODENTIA	2392	67.9	60.5	75.2	69	64.1	74.8	82.8	80.2	85.4	64.4	63.5	65.3
Guinea_pig-related	304	61.7	53.0	69.3	61.1	56.1	68.3	56.5	52.0	68.5	32.3	19.5	43.2
Mouse-related	1768	65.0	58.4	71.6	65.1	60.7	70.0	81.0	78.4	84.5	60.0	55.1	56.7
Squirrel-related	320	49.8	42.1	57.4	60.5	55.5	64.2	80.1	78.2	81.1	52.8	42.7	58.4

Placental orders … near K-Pg (< 3 Ma)				9			6			5			3
… at K-Pg (overlapping)				9			5			3			1
… before K-Pg (preceding)				0			1			4			0

Table S7.

Fossil maximum stratigraphic ages per order relative to stem ages from our node-dated phylogeny (95% HPD age of 10,000 trees). Fossil occurrences (occs.) per extant mammalian order were gathered from the Paleobiology Database as described in Supplementary Methods section 8.10. Plotted in Fig. S13.

Order	Fossil occs. per order	Oldest fossil genus	Fossil max age	Phylogeny stem ages			Diff (tree max - fossil max)
				Mean	Min	Max	
MONOTREMATA	31	*Kryoryctes*	122.5	188.4	166.7	210.9	88.5
Marsupialia							
PAUCITUBERCULATA	70	*Bardalestes*	59.0	79.4	67.9	92.8	33.8
DIDELPHIMORPHIA	281	*Pariadens*	105.3	74.4	63.2	87.1	**-18.2**
MICROBIOTHERIA	36	*Khasia*	66.0	63.4	54.1	74.8	8.8
DIPROTODONTIA	1011	*Cercartetus*	33.9	61.1	51.7	71.9	38.0
NOTORYCTEMORPHIA	2	*Naraboryctes*	23.0	60.0	50.6	70.6	47.5
DASYUROMORPHIA	202	*Gaylordia*	58.7	58.6	49.4	68.9	10.2
PERAMELEMORPHIA	79	*Galadi*	28.4	58.6	49.4	68.9	40.5
Placentalia							
Xenarthra							
PILOSA (=Xenarthra)	1184	*Asiabradypus*	58.7	67.4	53.0	83.8	25.1
CINGULATA	608	*Proeuphractus*	66.0	67.4	53.0	83.8	17.8
Afrotheria							
AFROSORICIDA	192	*Eudaemonema*	63.3	74.8	61.0	90.8	27.5
MACROSCELIDEA	695	*Cingulodon*	66.0	74.8	61.0	90.8	24.8
TUBULIDENTATA	93	*Orycteropus*	28.1	77.5	62.4	92.3	64.2
SIRENIA	438	*Prorastomus*	56.0	54.0	41.5	67.3	11.3
PROBOSCIDEA	2665	*Eritherium*	59.2	50.2	38.5	63.8	4.6
HYRACOIDEA	176	*Megalohyrax*	56.0	50.2	38.5	63.8	7.8
Laurasiatheria							
EULIPOTYPHLA	1442	*Litolestes*	61.7	75.1	66.3	84.1	22.4
CHIROPTERA	770	*Ageina*	56.0	70.0	61.7	79.3	23.3
ARTIODACTYLA	16374	*Basilosaurus*	66.0	61.9	53.1	69.6	3.6
PERISSODACTYLA	8948	*Paschatherium*	59.2	61.9	53.1	69.6	10.4
CARNIVORA	8877	*Pappictidops*	66.0	60.6	52.6	69.6	3.6
PHOLIDOTA	16	*Cryptomanis*	48.6	60.6	52.6	69.6	21.0
Euarchontoglires							
PRIMATES	3181	*Pandemonium*	66.0	70.4	61.7	79.8	13.8
DERMOPTERA	29	*Elpidophorus*	63.3	60.9	50.1	72.4	9.1
SCANDENTIA	7	*Eodendrogale*	48.6	60.9	50.1	72.4	23.8
LAGOMORPHA	1971	*Aktashmys*	56.0	72.4	64.4	81.1	25.1
RODENTIA	15928	*Asiaparamys*	58.7	72.4	64.4	81.1	22.4

Table S8.

Summary of diversification rate shift recovered using BAMM on 10 mammal trees. For all maximum shift credibility (MSC) shifts present in at least 5 of the 10 trees, the average net diversification rates are summarized across all branches in the rate-shift (clade rate) and all branches outside that clade in Mammalia (background rate). Their ratio gave the rate shift factor. Independent shifts are given letters A-X, while related shifts have the same letter (even when in < 5 trees). The mean and 95% HPD divergences are given for each rate-shift location.

		Divergence times								
ID	**Clade**	**Mean**	**Low**	**Up**	**Richness**	**Clade rate**	**Background rate**	**Factor**	**Direction**	**# Trees**
A	Marsupialia	79.4	67.9	92.8	362	0.158	0.140	1.1	up	7
A	Marsup (minus Caenolestidae)	74.4	63.2	87.1	355	0.167	0.137	1.2	up	2
	DIPROTODONTIA								up	
B	Macropodidae-Potoridae	18.1	14.7	21.4	78	0.320	0.139	2.3	up	3
B	Macropodidae	15.1	12.2	18.0	66	0.375	0.141	2.7	up	5
C	Placentalia	91.8	77.4	105.0	5544	0.143	0.136	1.1	up	5
C	Boreoeutheria	83.5	73.1	94.8	5419	0.144	0.088	1.6	up	5
D	CARNIVORA	40.2	33.9	47.9	298	0.178	0.142	1.3	up	5
	ARTIODACTYLA								up	
E	Pecora	18.2	15.0	21.4	215	0.229	0.127	1.8	up	3
E	Cervidae-Moschidae-Bovidae	17.0	14.1	20.2	212	0.250	0.141	1.8	up	5
F	Cetacea	25.9	15.2	38.6	91	0.191	0.143	1.3	up	5
	CHIROPTERA								up	
G	Vespertilionid-related	42.0	35.5	49.3	605	0.160	0.128	1.3	up	3
G	Molossidae-Vespertilionidae	40.2	34.0	47.4	593	0.147	0.141	1.1	up/ down	6
H	Phyllostomidae	27.6	23.2	32.5	205	0.155	0.148	1.1	up/ down	2
H	Stenodermatinae	15.5	12.5	18.4	93	0.208	0.138	1.5	up	6
I	Pteropodidae	24.9	19.7	30.3	194	0.168	0.135	1.2	up	5
I	*Dobsonia-Rousettus*	22.3	18.0	26.5	161	0.177	0.147	1.2	up	2
J	*Pteropus*	10.1	7.8	12.7	69	0.431	0.138	3.2	up	10
K	Rhinolophidae-Hipposideridae	30.0	24.8	36.1	180	0.164	0.139	1.2	up	7
L	Rhinolophidae	14.2	10.4	18.8	87	0.225	0.139	1.6	up	6
	EULIPOTYPHLA									
M	Crocidurinae	17.9	17.1	18.7	213	0.259	0.136	1.9	up	9
N	PRIMATES	31.5	26.4	36.9	313	0.227	0.136	1.7	up	10
O	Strepsirrhini	49.6	42.2	57.0	135	0.083	0.144	1.7	down	6
P	LAGOMORPHA	36.2	30.5	42.1	91	0.140	0.141	1.1	up/ down	5
	RODENTIA									
Q	Ctenomyidae	6.8	3.6	13.3	65	0.548	0.138	4.0	up	10

R	Geomyoidea	25.6	21.3	30.0	107	0.169	0.140	1.2	up	5
S	Cricetidae-Muridae	47.7	43.5	52.3	1505	0.190	0.129	1.5	up	5
T	Cricetidae	35.7	31.4	40.5	726	0.195	0.128	1.5	up	6
	Muridae									
U	Murinae	32.9	28.1	37.8	632	0.189	0.130	1.5	up	5
V	*Apomys-Melomys*	20.9	NA	NA	206	0.228	0.138	1.7	up	5
V	*Anisomys-Melomys*	15.2	14.9	15.6	133	0.231	0.136	1.7	up	3
W	*Rattus-Srilankamys*	11.0	9.2	12.7	109	0.321	0.138	2.3	up	9
X	Gerbillinae	17.3	14.5	19.9	80	0.212	0.142	1.5	up	2
X	*Gerbillus*	12.9	10.5	15.5	50	0.243	0.136	1.8	up	3

Table S9.

Results of birth-death likelihood (BDL) tests on 27 named clades. For each clade, the extant species richness (N) is given adjacent to the number of 100 trees where the ΔAIC_{RC-RV} test statistic of empirical trees is greater than the critical values from the null distribution of tests on simulated rate-constant (RC) trees of the same age and richness. Medians and 95% confidence intervals are given (Med., Low, Up). Positive values of ΔAIC_{RC-RV} indicate that rate-variable (RV) models are favoured. The number of 100 trees that find a particular model with lowest AIC is given for two RC models (B, pure birth; B_D, birth-death) and 8 RV models (Exp., exponentially varying rates; Lin., linearly varying rates; see Supplementary Methods section 8.7).

			Observed mammal trees			Simulated RC trees			Diversification models									
Clade	N	# Sig.	Med.	Low	Up	Med.	Low	Up	B	B_D	B-Exp	B-Exp_D	B_D-Exp	B-Exp_D-Exp	B-Lin	B-Lin_D	B_D-Lin	B-Lin_D-Lin
RODENTIA	2354	100	43.7	31.2	55.9	-1.2	-2.0	3.4	.	.	65	.	.	.	1	.	.	34
Mouse-rel.	1768	100	39.7	29.4	56.1	-1.4	-2.0	5.7	.	.	45	.	.	.	2	.	1	52
Squirrel-rel.	320	27	4.3	0.5	7.9	-1.1	-2.0	5.5	.	.	51	.	5	1	42	.	.	1
Guinea pig-rel.	304	1	0.5	-1.3	3.4	-1.5	-2.0	4.2	.	34	7	21	38	.	.	.	.	.
LAGOMOR.	90	93	8.8	4.1	12.6	-0.6	-2.1	4.9	.	.	17	.	64	.	14	.	5	.
CHIROPTER.	1282	2	-0.3	-1.6	4.0	-1.2	-2.0	4.8	.	58	4	37	.	.	.	.	1	.
Yinptero.	385	0	-0.7	-1.7	1.0	-1.0	-2.0	4.9	.	79	2	3	14	.	.	.	2	.
Yangochiro.	902	8	1.7	-1.3	5.9	-0.8	-2.0	4.9	.	24	76	.	.	.	.	.	.	.
EULIPOTYP.	484	98	14.5	6.0	21.3	-1.2	-2.0	5.6	.	.	85	5	.	.	.	.	.	10
Soricidae	420	96	16.4	3.4	24.3	-1.5	-2.0	4.8	.	.	86	1	2	.	11	.	.	.
Talpidae	44	0	-0.2	-1.5	1.4	-0.4	-2.2	4.4	51	10	5	.	4	.	30	.	.	.
PRIMATES	450	100	22.4	14.2	29.1	-1.4	-2.0	5.5	.	.	94	.	.	.	.	4	.	2
Catarrhini	152	100	12.9	5.9	21.7	-1.1	-2.0	3.3	.	.	.	.	2	.	.	.	.	98
Platyrrhini	161	7	0.3	-2.1	8.5	-0.4	-2.1	6.7	.	45	25	.	.	.	6	4	.	20
Strepsirr.	135	1	0.2	-1.2	4.3	-1.4	-2.1	4.4	.	41	49	.	8	.	.	.	1	1
ARTIODACT.	338	100	24.5	19.0	32.3	-1.0	-2.0	5.1	.	.	40	.	.	.	40	2	.	18
Ruminantia	225	94	7.2	3.0	10.5	-0.9	-2.0	3.8	.	.	.	.	44	.	49	.	.	7
Whippom.	95	93	9.5	6.7	17.3	-0.4	-2.1	7.2	.	.	6	.	11	.	52	.	.	31
CARNIVORA	286	100	15.0	8.2	23.5	-0.6	-2.0	6.6	.	.	14	.	.	.	1	.	.	85
Caniformes	164	40	5.4	3.7	11.5	-0.6	-1.9	5.7	.	.	40	.	.	.	19	.	.	41
Feliformes	122	65	5.4	2.6	13.3	-0.7	-2.0	4.3	.	.	6	.	.	.	27	.	.	67
Afrotheria	92	18	1.2	-2.0	7.9	-0.8	-2.1	4.7	.	37	8	.	.	4	36	11	.	4
AFROSORIC.	55	6	1.4	-1.3	4.4	-0.4	-2.2	3.9	1	10	23	.	.	.	63	.	2	1
Xenarthra	33	0	-0.7	-2.2	1.1	-0.7	-2.3	6.0	66	8	14	.	.	.	12	.	.	.
DASYUROM.	77	100	11.1	5.5	18.3	-1.5	-2.1	3.1	.	.	.	.	.	.	1	.	.	99
DIDELPHIM.	105	0	-1.2	-2.0	0.1	-0.9	-2.1	5.5	91	5	2	.	.	.	.	.	.	2
DIPROTOD.	139	5	1.9	-1.1	7.5	-1.0	-2.1	4.5	.	8	71	.	.	.	.	.	.	21

Table S10.

Per clade summary of tip-level diversification rate (tip DR). Tip DR median, 95% confidence interval, and the skew in a given clade across 10,000 node-dated trees. Tests of the clade tip DR versus the (non-clade) background rate used the Mann-Whitney U statistic: greater (>, grayed), lesser (<), or not significant (NS).

Taxon	Richness	Median	Low (2.5%)	High (97.5%)	Skew	Mann-Whitney U-test	
Mammalia	5804	0.211	0.056	0.480	0.145	.	
MONOTREMATA	5	0.022	0.015	0.022	-1.200	***	<
RODENTIA	2354	0.208	0.061	0.482	1.193	NS	
Mouse-related	1742	0.203	0.060	0.430	0.726	*	<
Squirrel-related	320	0.213	0.076	0.501	0.835	NS	
Guinea pig-related	292	0.233	0.057	0.684	1.090	**	>
LAGOMORPHA	90	0.265	0.113	0.543	0.595	***	>
CHIROPTERA	1282	0.180	0.062	0.442	1.585	***	<
Yinpterochiroptera	381	0.225	0.072	0.647	1.216	**	>
Yangochiroptera	901	0.162	0.059	0.351	0.720	***	<
EULIPOTYPHLA	484	0.229	0.053	0.486	0.753	NS	
Soricidae	414	0.243	0.086	0.491	0.847	***	>
Talpidae	44	0.128	0.043	0.221	-0.003	***	<
Erinaceidae	24	0.113	0.033	0.133	-0.797	***	<
SCANDENTIA	20	0.110	0.022	0.137	-1.163	***	<
DERMOPTERA	2	.	.	.	.	.	
PRIMATES	450	0.326	0.093	0.480	-0.431	***	>
Simiiformes	309	0.345	0.183	0.500	-0.127	***	>
Catarrhini	149	0.346	0.174	0.511	-0.013	***	>
Platyrrhini	160	0.344	0.221	0.487	-0.211	***	>
Strepsirrhini	131	0.259	0.084	0.397	-0.194	**	>
PERISSODACTYLA	18	0.106	0.062	0.171	0.074	***	<
ARTIODACTYLA	338	0.248	0.079	0.537	0.432	***	>
Ruminantia	217	0.260	0.090	0.502	0.163	***	>
Whippomorpha	93	0.247	0.075	0.602	0.599	***	>
PHOLIDOTA	8	0.057	0.054	0.072	0.983	***	<
CARNIVORA	286	0.238	0.084	0.458	0.305	***	>
Feliformes	122	0.259	0.089	0.473	0.153	***	>
Caniformes	164	0.232	0.084	0.426	0.398	*	>
CINGULATA	21	0.068	0.047	0.092	-0.034	***	<
PILOSA	10	0.047	0.024	0.058	-0.742	***	<
AFROSORICIDA	55	0.082	0.032	0.149	0.189	***	<
MACROSCELIDEA	19	0.061	0.044	0.068	-0.630	***	<
TUBULIDENTATA	1	.	.	.	.	.	
PROBOSCIDEA	2	.	.	.	.	.	

HYRACOIDEA	5	0.063	0.056	0.063	-0.408	***	<
SIRENIA	4	.	.	.	.	.	
Marsupialia	350	0.207	0.055	0.414	0.752	NS	
DIPROTODONTIA	139	0.262	0.055	0.530	0.325	***	>
DIDELPHIMORPHIA	105	0.207	0.075	0.336	0.008	NS	
DASYUROMORPHIA	77	0.183	0.104	0.270	0.058	**	<
PERAMELEMORPHIA	19	0.189	0.102	0.215	-1.031	NS	
NOTORYCTEMORPHIA	2	.	.	.	.	.	
PAUCITUBERCULATA	7	0.084	0.070	0.099	-0.155	***	<
MICROBIOTHERIA	1	.	.	.	.	.	

*** P < 0.001; ** P < 0.01; * P < 0.05

Table S11.

Phylogenetic path model results comparing clades defined by time slices vs. taxa. Shown are counts of 100 trees where each of 27 models was within 2 CICc units of the best model (and counts passing the d-sep test). The top 3 models are highlighted in gray for each clade delimitation. All models within 2 CICc units are model averaged within each tree; the median of those model averages is in main text Fig. 5 and Fig. S20 for 100 trees.

	Time slices			Taxa		
Model name	**10 Ma**	**30 Ma**	**50 Ma**	**Gen**	**Fam**	**Ord**
A1	0 (0)	9 (0)	25 (1)	0 (0)	0 (0)	0 (0)
A1_B1	46 (16)	6 (0)	0 (0)	2 (0)	0 (0)	0 (0)
A1_B1_C1	76 (22)	5 (0)	0 (0)	0 (0)	0 (0)	0 (0)
A1_B1_C3	43 (13)	3 (0)	0 (0)	1 (0)	0 (0)	0 (0)
A1_B3	4 (1)	4 (0)	59 (2)	0 (0)	0 (0)	0 (0)
A1_B3_C1	12 (4)	5 (1)	14 (0)	0 (0)	0 (0)	0 (0)
A1_B3_C3	4 (0)	2 (0)	8 (0)	0 (0)	0 (0)	0 (0)
A1_C1	6 (2)	16 (1)	2 (0)	0 (0)	0 (0)	0 (0)
A1_C3	4 (0)	4 (0)	5 (0)	0 (0)	0 (0)	0 (0)
A3	0 (0)	25 (0)	52 (0)	7 (0)	0 (0)	0 (0)
A3_B1	7 (2)	9 (0)	0 (0)	75 (0)	96 (0)	0 (0)
A3_B1_C1	20 (3)	45 (2)	3 (0)	84 (0)	68 (0)	0 (0)
A3_B1_C3	8 (3)	5 (0)	0 (0)	80 (0)	22 (0)	0 (0)
A3_B3	8 (1)	6 (0)	45 (0)	5 (0)	0 (0)	0 (0)
A3_B3_C1	15 (3)	58 (3)	23 (0)	4 (0)	0 (0)	0 (0)
A3_B3_C3	7 (0)	4 (0)	2 (0)	7 (0)	0 (0)	0 (0)
A3_C1	2 (1)	94 (5)	35 (1)	6 (0)	0 (0)	3 (2)
A3_C3	1 (0)	14 (0)	7 (0)	6 (0)	0 (0)	0 (0)
B1	26 (9)	5 (1)	1 (0)	3 (0)	59 (0)	0 (0)
B1_C1	40 (12)	10 (1)	0 (0)	3 (0)	50 (0)	0 (0)
B1_C3	21 (6)	3 (0)	0 (0)	2 (0)	14 (0)	0 (0)
B3	9 (2)	1 (0)	53 (1)	0 (0)	0 (0)	0 (0)
B3_C1	16 (4)	13 (1)	35 (1)	1 (0)	0 (0)	0 (0)
B3_C3	5 (1)	2 (0)	9 (0)	0 (0)	0 (0)	0 (0)
C1	5 (2)	36 (2)	11 (1)	0 (0)	0 (0)	88 (63)
C3	4 (1)	7 (0)	3 (0)	0 (0)	0 (0)	50 (30)
noEcoVars	1 (1)	11 (1)	20 (0)	0 (0)	0 (0)	0 (0)
Percent of models P > 0.05 (d-sep test)	27.9%	4.5%	1.7%	0.0%	0.0%	67.4%

Table S12.

Summary of path analysis sensitivity tests (Fig. S22). The number of trees is given (of 1000 tested) where the median path coefficient ± SE did not overlap zero. Having >500 trees with non-zero estimates was viewed as strong evidence (bolded results), ~250-500 trees as marginal, and < 250 trees as zero. Tip-level diversification rates (tip DR) were compared with the node density metric (ND) on the node- and tip-dated full Mammalia trees. Trees were based on all extant non-marine mammals (5675 species), excluding island endemics (4553 species), and excluding DNA-lacking and imputed (3941 species).

Test	all mammals	w/o islands	w/o imputed
Inverse vagility ~ tip rate mean, 10 Ma			
tip DR, node-dated	**854**	**701**	**555**
tip DR, tip-dated	457	442	271
ND, node-dated	**959**	**929**	**998**
ND, tip-dated	**862**	**675**	**979**
Positive diurnality ~ tip rate mean, 10 Ma			
tip DR, node-dated	**746**	497	**740**
tip DR, tip-dated	**573**	417	**548**
ND, node-dated	**886**	**762**	**714**
ND, tip-dated	316	146	133
Positive latitude ~ tip rate mean, all slices			
tip DR, node-dated	**591, 722, 572**	**756, 930**, 471	475, **644**, 255
tip DR, tip-dated	459, 423, **698**	**603, 626, 703**	264, 228, 366
ND, node-dated	47, 2, 151	69, 45, 187	454, 0, 146
ND, tip-dated	20, 2, **525**	74, 65, **608**	79, 4, **521**

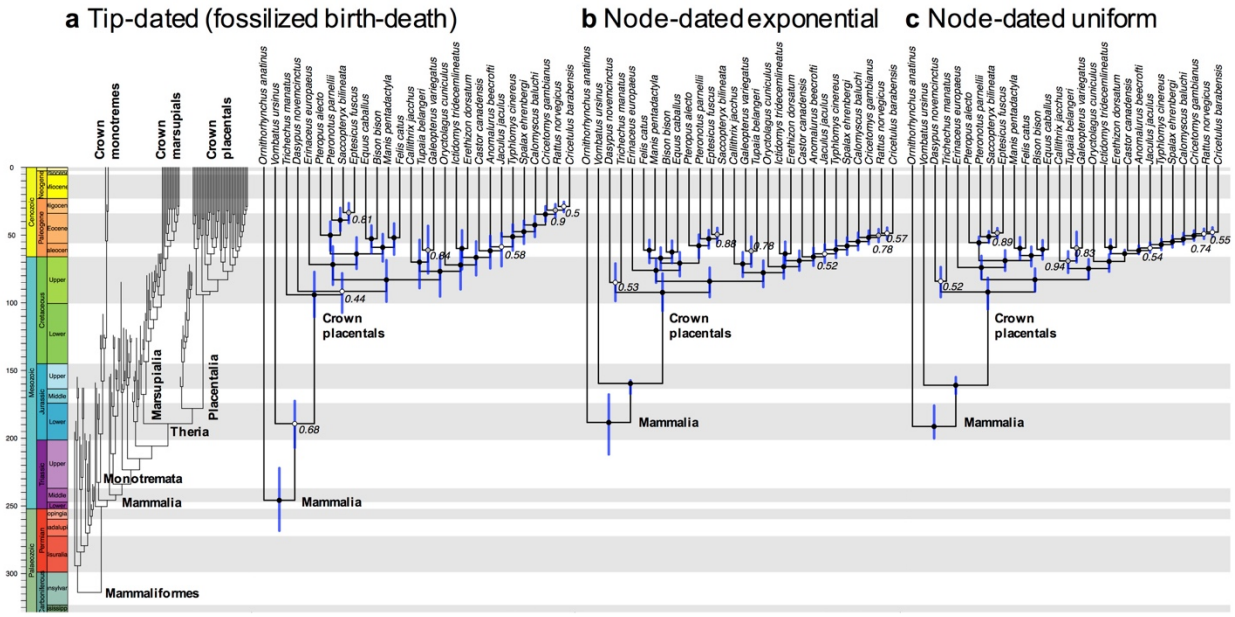

d Node age comparisons across the backbones pruned to 28 patch clade representatives

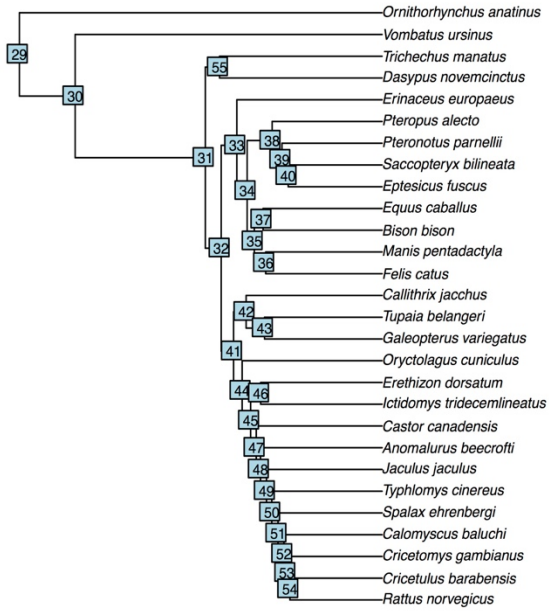

	Node-dated exponential				Node-dated uniform				Tip-dated (FBD)			
Node	Median	Low	Up	Width	Median	Low	Up	Width	Median	Low	Up	Width
29	187.3	166.7	210.9	44.2	192.7	177.3	201.5	24.2	246.1	222.1	268.3	46.3
30	158.5	156.3	166.2	9.9	162.3	156.3	168.7	12.4	189.0	172.5	207.0	34.5
31	91.3	77.4	105.0	27.6	93.4	83.0	106.2	23.2	93.5	77.2	110.5	33.3
32	83.1	73.1	94.7	21.7	84.3	76.1	92.9	16.8	81.4	68.5	99.2	30.6
33	75.0	66.3	84.1	17.8	75.3	66.7	83.9	17.2	71.7	58.4	86.7	28.3
34	69.7	61.7	79.3	17.7	70.2	62.7	77.7	15.0	63.2	51.7	74.9	23.3
35	66.0	58.2	74.5	16.3	66.5	60.0	74.4	14.5	58.6	49.2	69.5	20.2
36	60.1	52.6	69.6	17.0	61.1	53.0	69.2	16.2	51.8	41.4	64.5	23.1
37	61.5	53.1	69.6	16.4	62.0	55.2	69.3	14.1	52.7	42.9	63.2	20.3
38	56.8	48.7	66.0	17.4	57.0	52.6	58.9	6.3	49.2	40.1	61.6	21.5
39	51.7	45.3	58.8	13.5	52.5	48.6	56.9	8.4	39.3	29.9	46.9	17.0
40	48.5	43.7	54.9	11.2	49.8	46.3	53.7	7.5	33.0	26.4	41.1	14.7
41	76.7	67.8	87.3	19.5	76.1	69.2	83.7	14.5	74.1	64.8	95.3	30.6
42	70.2	61.7	79.8	18.2	70.5	63.4	79.3	15.9	68.7	53.6	89.2	35.6
43	60.7	50.1	72.4	22.3	60.9	49.0	71.5	22.5	60.9	43.2	78.3	35.1
44	72.3	64.4	81.1	16.6	70.8	65.7	78.4	12.7	69.7	59.9	90.1	30.1
45	67.9	60.5	75.1	14.6	65.1	62.4	66.0	3.6	65.2	54.7	79.7	25.0
46	62.7	53.9	70.5	16.6	60.5	54.7	65.1	10.4	58.4	46.5	75.3	28.8
47	65.0	58.4	71.6	13.3	62.8	59.1	65.4	6.3	60.8	50.6	74.6	24.0
48	62.8	55.8	69.4	13.6	60.9	56.8	64.3	7.5	58.6	48.4	73.0	24.6
49	59.7	52.8	65.8	13.0	58.4	54.3	62.4	8.1	50.6	42.2	61.4	19.3
50	57.0	50.7	63.5	12.8	56.3	51.8	60.5	8.7	46.8	39.3	56.5	17.1
51	53.7	47.2	60.0	12.9	54.3	49.8	58.3	8.5	41.6	35.8	51.3	15.5
52	50.7	45.7	55.7	10.0	51.8	48.0	55.5	7.4	34.5	28.7	40.0	11.3
53	49.2	44.6	54.1	9.5	50.4	46.8	54.2	7.4	31.2	27.2	36.8	9.6
54	47.6	43.5	52.3	8.9	49.2	45.7	52.6	6.9	28.5	25.5	33.0	7.5
55	84.0	70.0	97.6	27.7	85.5	75.0	97.2	22.2	---	---	---	---
Mean width of 95% HPD				17.0				12.5				24.1

Fig. S9

Comparison of results from three methods used to time-calibrate the backbone. Each method is pruned to the 28 patch clade representatives: (**a**) fossilized birth-death (FBD) where fossil taxa are placed as extinct tips in the tree (left side) and then pruned (right side); and node-dating (ND) approaches setting priors as (**b**) exponential priors from minimum to soft-max ages, and (**c**) uniform priors spanning minimum to maximum ages. Trees are maximum clade credibility summaries of 10,000 trees. Circles at nodes indicate posterior probability (PP) values of ≥ 0.95 (black), 0.94-0.75 (gray), < 0.75 (white), with the values < 0.95 given. (**d**) Inferred ages for backbone nodes are compared across methods, as based on the ND tree. Note that the FBD trees did not recover node 55 (see part **a** & Fig. S11).

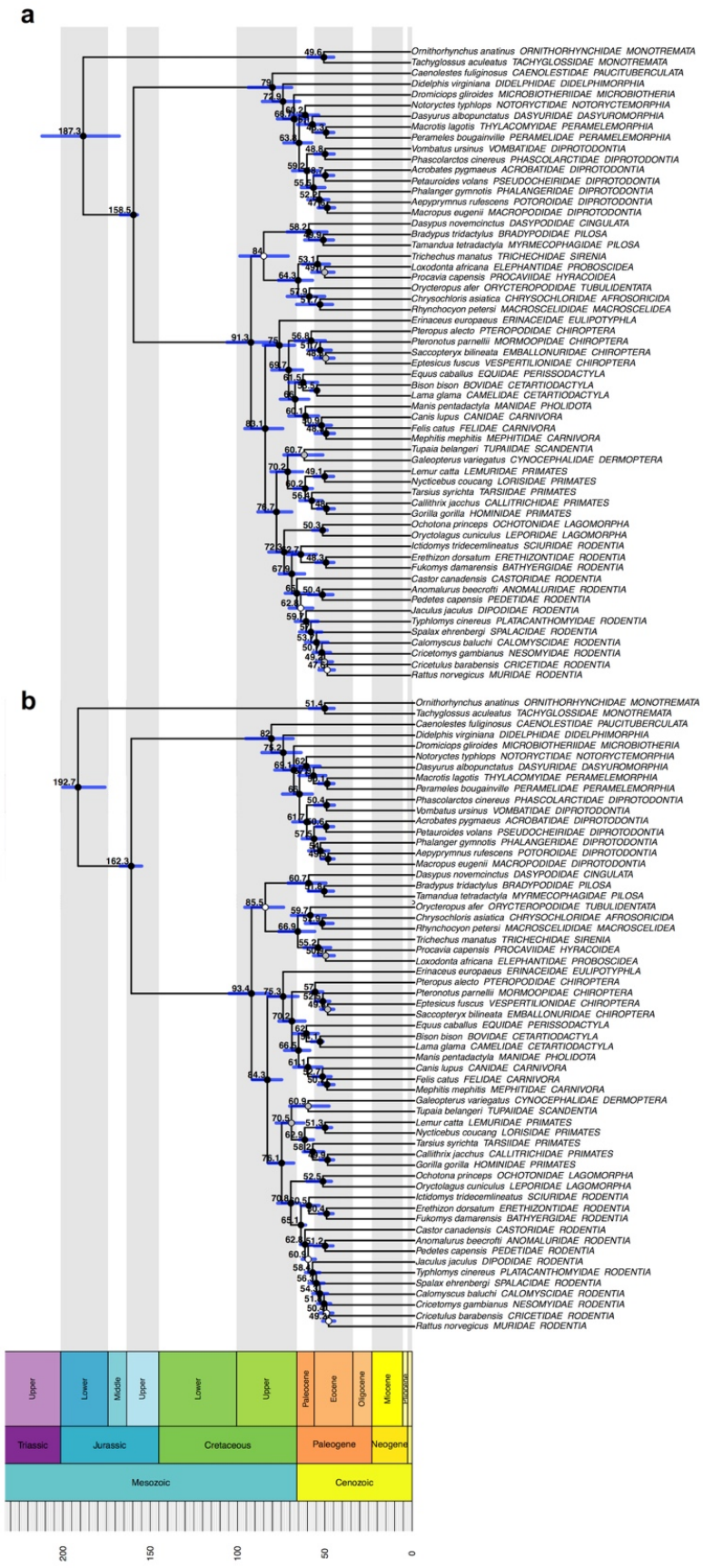

Fig. S10
Full node-dated backbone phylogenies. These were constructed using (**a**) exponential node priors (NDexp) or (**b**) uniform priors (NDuni) in MrBayes based on 17 fossil calibrations and molecular data from our 31-gene supermatrix. Topology is the maximum clade credibility tree of 10,000 phylogenies. Median ages and 95% highest posterior density intervals are displayed at nodes. Node circles indicate posterior probability (PP) values of ≥ 0.95 (black), 0.94-0.75 (gray), < 0.75 (white).

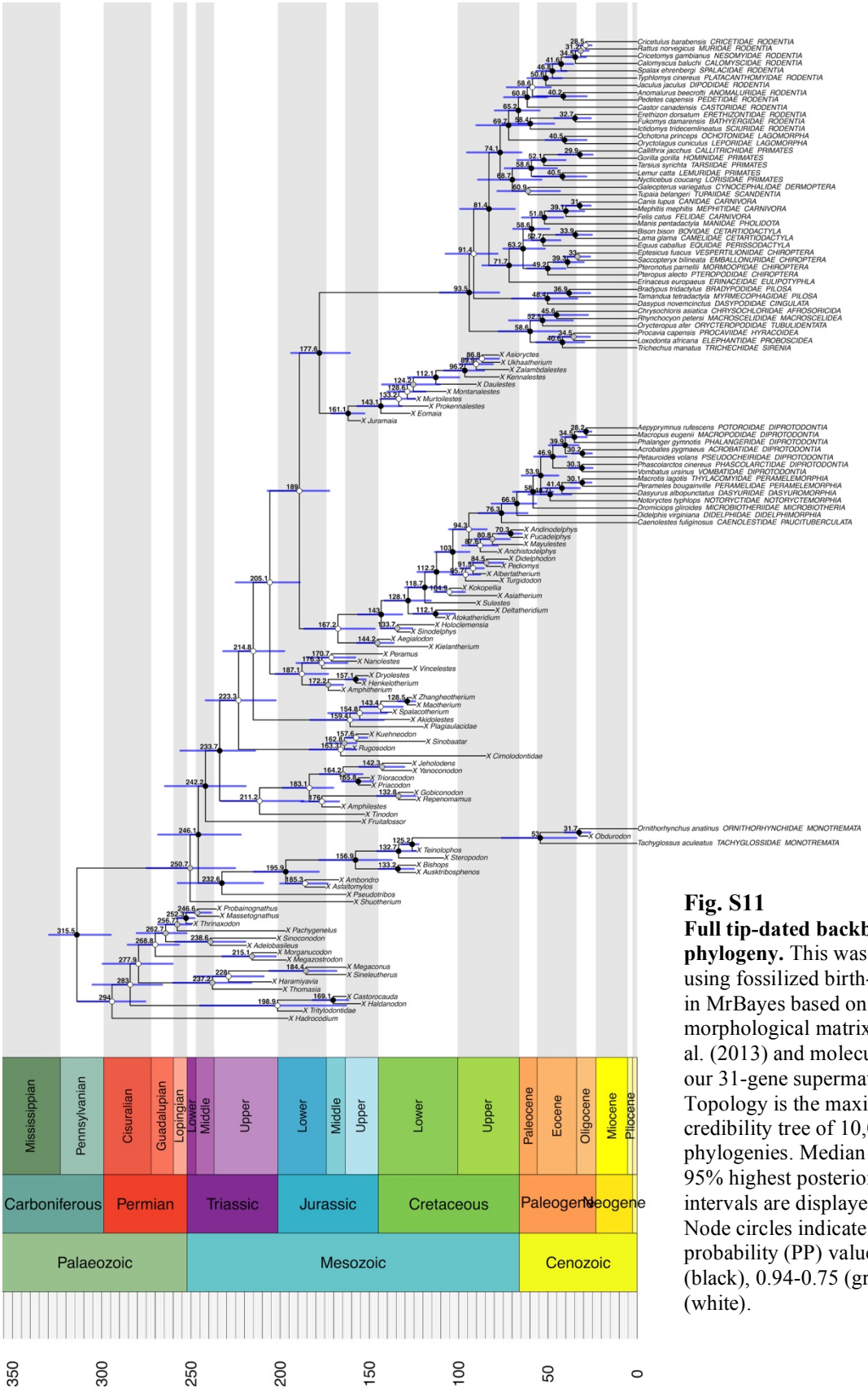

Fig. S11
Full tip-dated backbone phylogeny. This was constructed using fossilized birth-death (FBD) in MrBayes based on the morphological matrix of Zhou et al. (2013) and molecular data from our 31-gene supermatrix. Topology is the maximum clade credibility tree of 10,000 phylogenies. Median ages and 95% highest posterior density intervals are displayed at nodes. Node circles indicate posterior probability (PP) values of ≥ 0.95 (black), 0.94-0.75 (gray), < 0.75 (white).

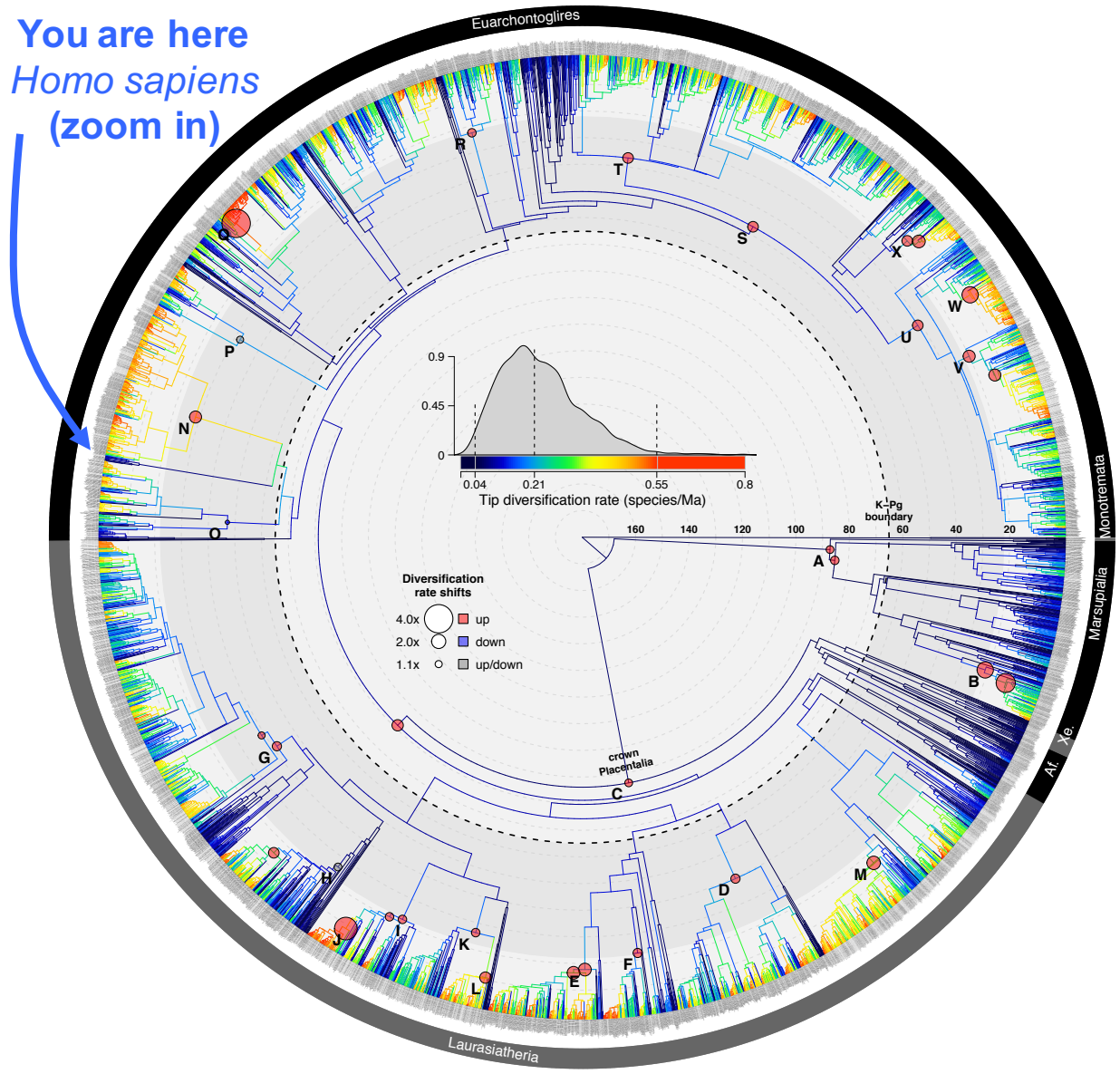

Fig. S12

Detailed full 5911-species phylogeny of Mammalia labeled and zoom-able to the species level. Zoom in to see tree tips named by genus, species, family, and order, with lighter gray text denoting those species without DNA sequences (30% are missing data and were imputed based on taxonomic constraints and a birth-death model for branch lengths). BAMM rate shifts are displayed on nodes following Fig. 1 and Table S8. The time scale follows Fig. 1 with the Cretaceous-Paleogene boundary denoted with a black dotted line and the Neogene (most recent ~23 Ma) denoted as the light gray band near the tips. Higher-level clades are labeled at the edges, including Afrotheria (Af.) and Xenarthra (Xe.). Species-level branches are colored with tip-level diversification rates (tip DR) and reconstructed using simple Brownian motion for the internal branches. Tip DR values < 0.04 are dark blue and > 0.55 are bright red.

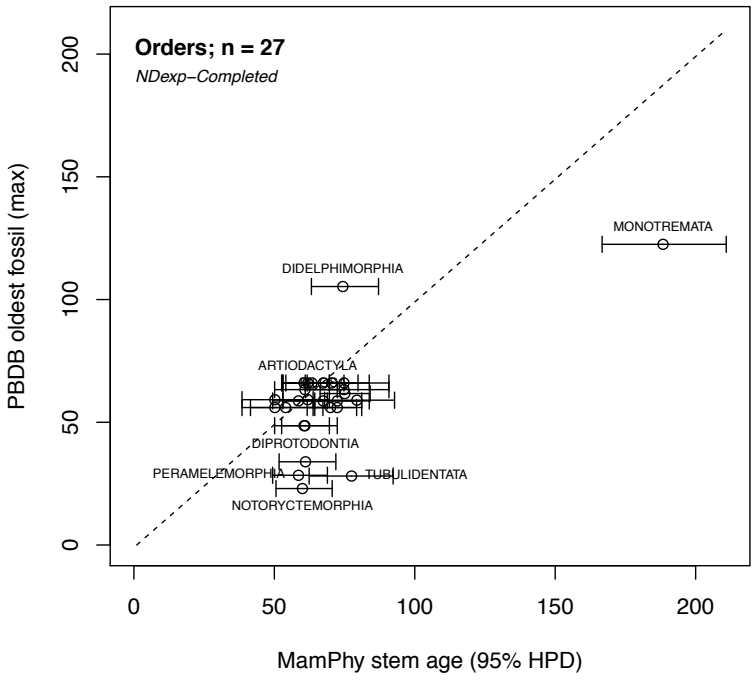

Fig. S13
Oldest fossil occurrences per extant mammalian order vs. phylogeny stem ages. Results from our node-dated phylogeny (95% HPD age of 10,000 trees) compared to fossil maximum stratigraphic ages per order listed in Table S7. Most phylogeny stem age estimates overlap the 1:1 line (dotted), but are somewhat older as expected from biased preservation and waiting times to fossilization. See above as regards the older fossil than phylogeny age for Didelphimorphia.

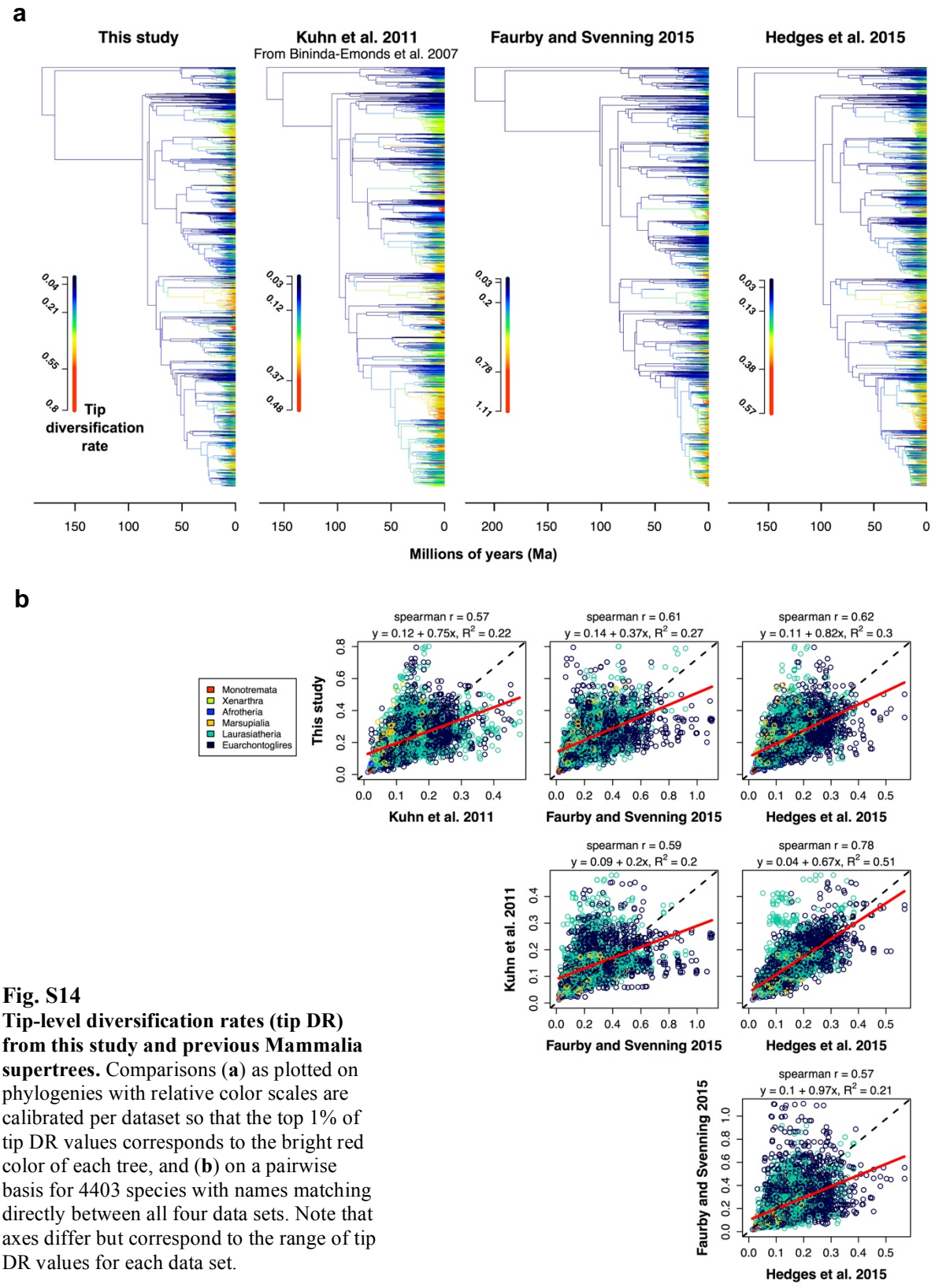

Fig. S14
Tip-level diversification rates (tip DR) from this study and previous Mammalia supertrees. Comparisons (**a**) as plotted on phylogenies with relative color scales are calibrated per dataset so that the top 1% of tip DR values corresponds to the bright red color of each tree, and (**b**) on a pairwise basis for 4403 species with names matching directly between all four data sets. Note that axes differ but correspond to the range of tip DR values for each data set.

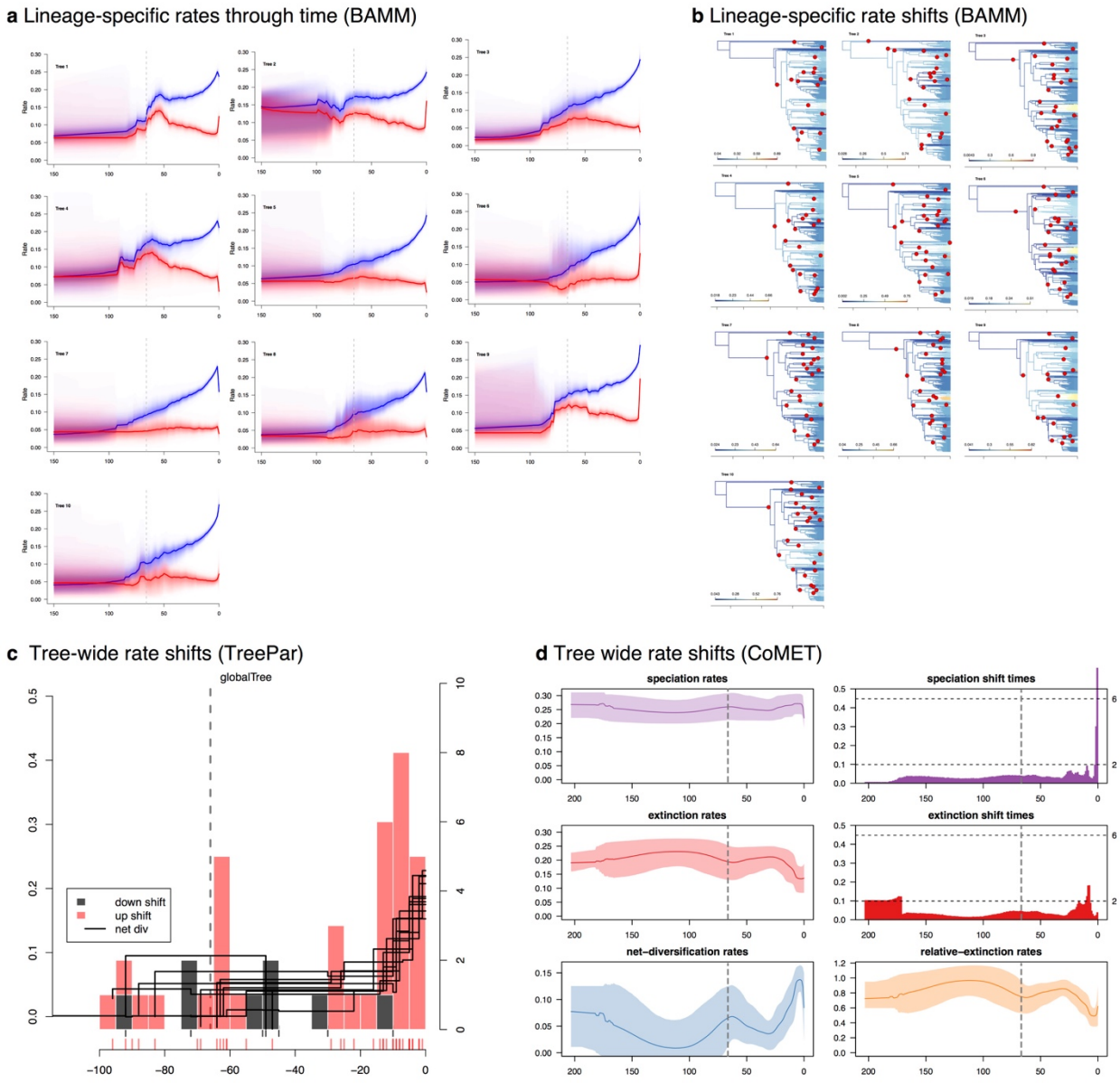

Fig. S15

Tests of lineage-specific and time-specific (tree-wide) rate shifts in Mammalia. Results from analyses on 10 trees relative to the Cretaceous-Paleogene mass extinction event (K-Pg, ~66 Ma; vertical dotted lines): (**a**) BAMM models showing reconstructed speciation (blue) and extinction (red) rates through time (medians and 95% confidence intervals of the rates from 1000 event data samples; Fig. 2c shows the same data group across 10 trees); (**b**) placement of BAMM maximum shift credibility rate-shift sets from each tree (red dots) on the background of different rate regimes (branch colors, hotter colors are faster rates; time scale in intervals of 50 Ma; trees differ in root age but are ladderized for comparison to Fig. 1); (**c**) TreePar models, showing (left axis) reconstructed net diversification rates and (right axis) the number of inferred rate shifts summarized to 5 Ma time bins across the 10 trees (rug underneath the histogram shows the timing and frequency of the individual shifts); (**d**) CoMET models, showing (left axes) reconstructed rates and (right axes) Bayes factors for shift times (see Fig. S16 for results including mass-extinction parameters).

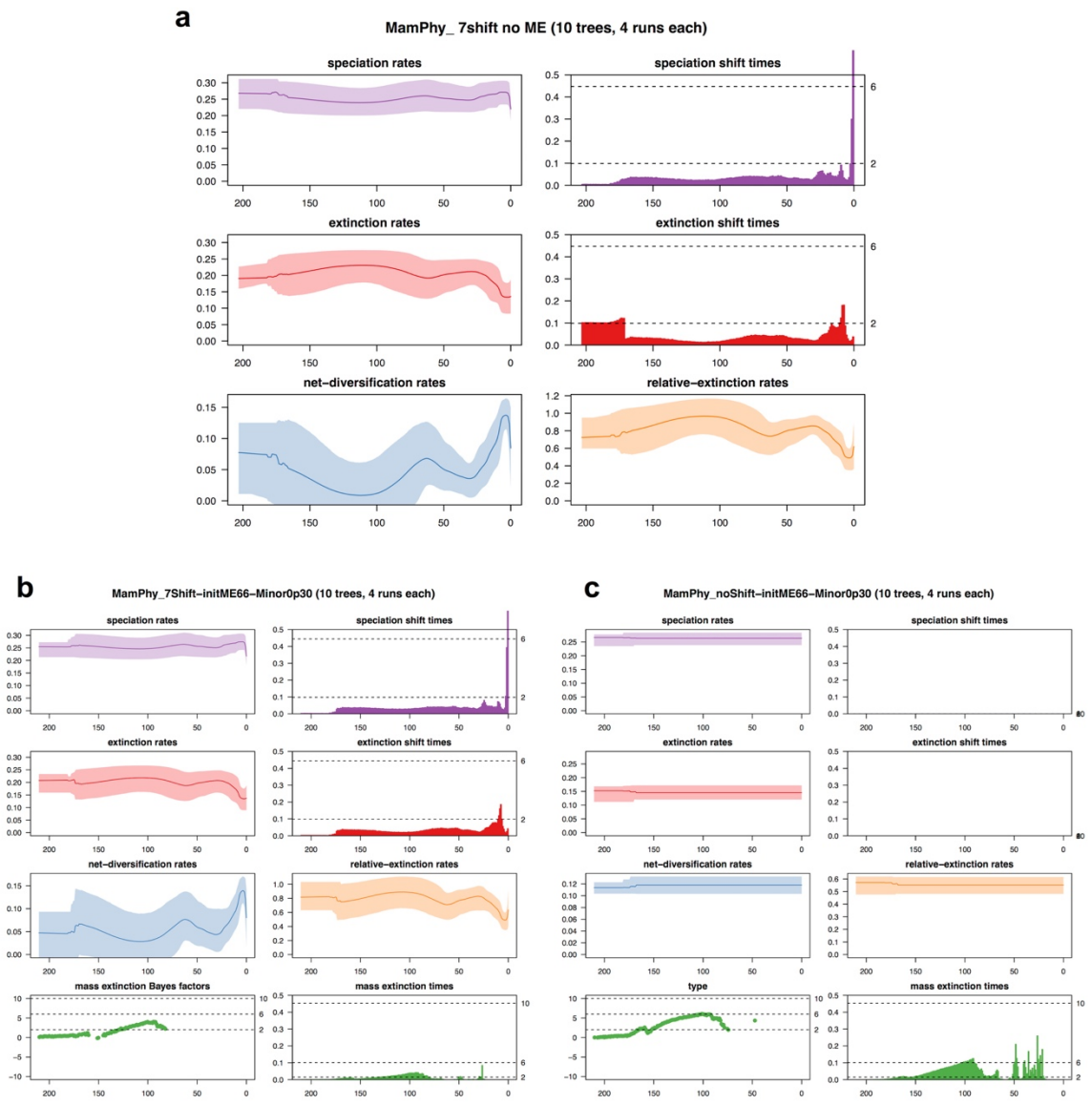

Fig. S16

Results of sensitivity tests for tree-wide rate shifts using CoMET. These models were run on 10 mammal trees parameterized with (**a**) seven expected rate shifts and no mass-extinction events ME; (**b**) seven rate shifts and one minor ME (probability of surviving p=0.3), as seeded at 66 Ma to correspond with the K-Pg event; and (**b**) no rate shifts and the same minor ME at 66 Ma. Note that Fig. S6d also displays the part **a** model. Substantially greater signals of ME events are recovered when rate shifts are not allowed (part **c** model), which questions the validity of this modeling framework.

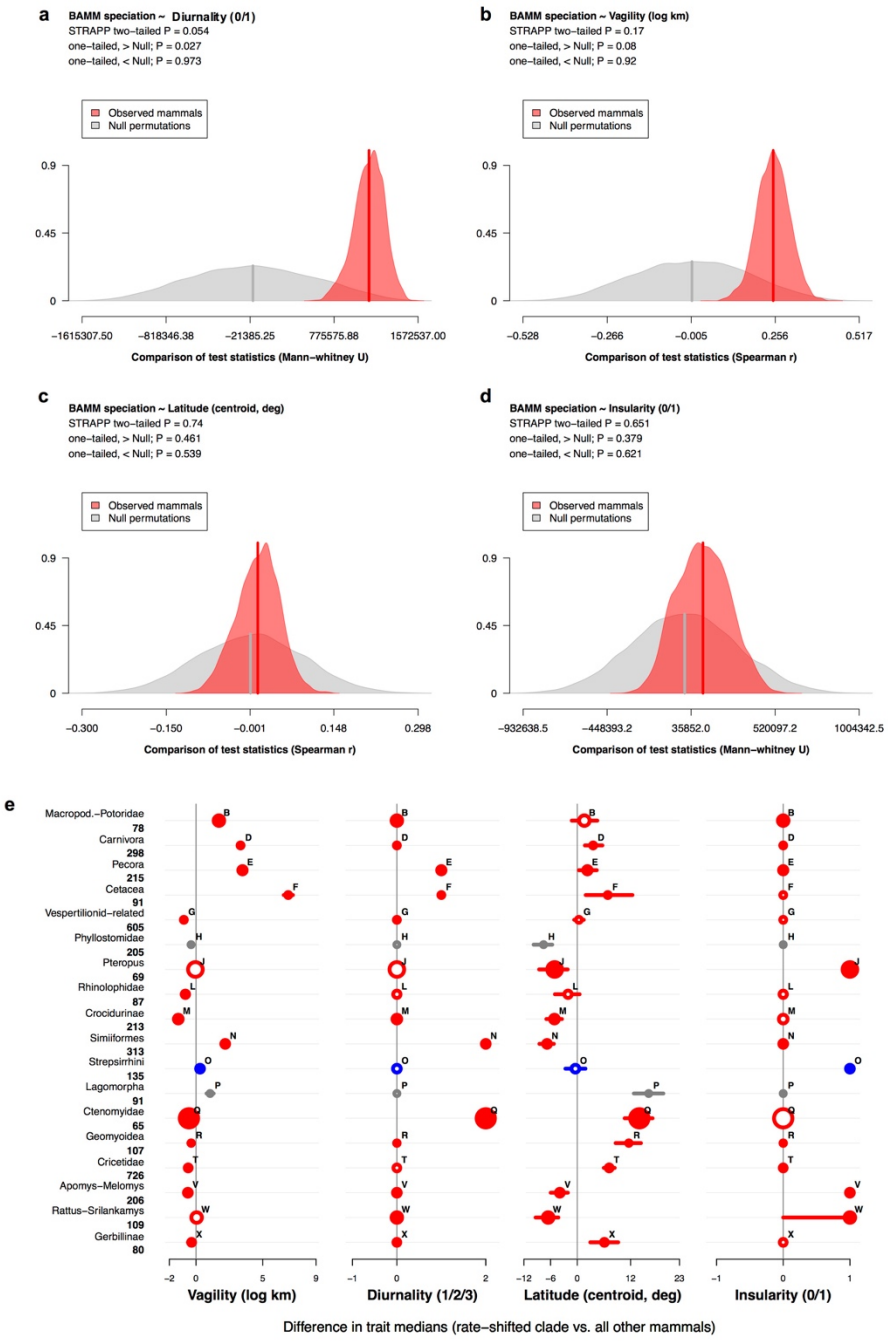

Fig. S17

Ecological characterization of the BAMM rate-shifted clades. Tests of trait-dependent speciation conducted with the STRAPP test for each of 10 mammal trees: (**a**) binary analyses of diurnality, showing positive association with higher rates of speciation (corroborated in 10-Ma clades, Fig. 4; genera, Fig. S19); (**b**) vagility, showing non-significant positive association with speciation rate; and (**c**) latitude and (**d**) insularity showing no associations. We interpret diurnality as an example of increased lineage persistence driving the inference of rate shifts, whereas the other traits may drive species turnover and not be detected in rate shifts. (**e**) Distribution of ecological traits within the 18 rate-shifted clades that are independent from each other (non-nested of 24 total shifts in Fig. 1; Table S8). Mann-Whitney U-tests for difference in trait medians between each clade and the rest of mammals (symbols follow Fig. 1; open circles denote no significant difference, bars denote 95% CIs on the difference in medians).

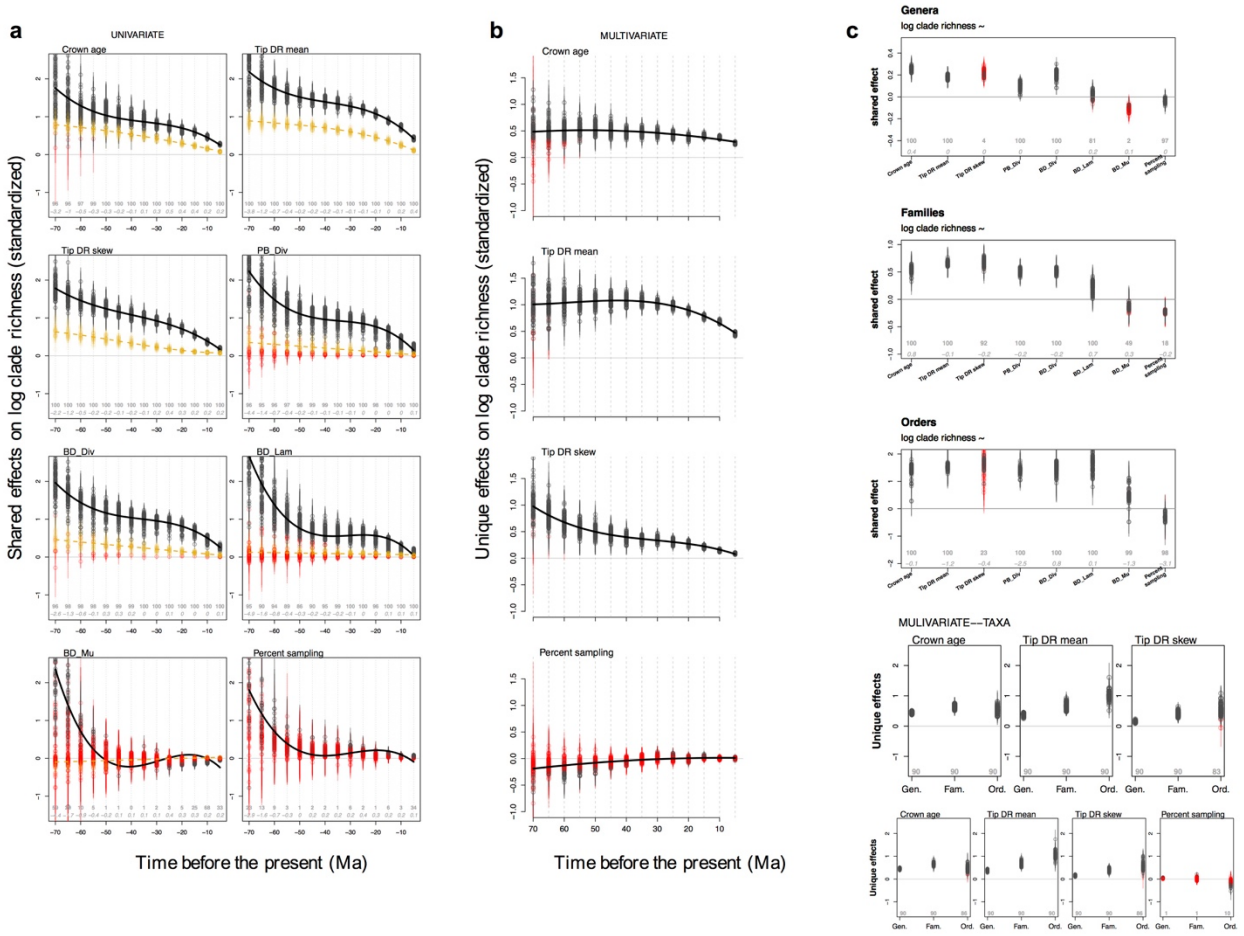

Fig. S18

Tests of factors explaining log clade species richness. Full results from time-sliced clades in (**a**) univariate and (**b**) multivariate contexts for 100 trees (shared vs. unique effects, respectively, on clade richness; standardized data is mean centered and standard deviation scaled). Clades were delimited tipward of 5-Ma intervals in empirical mammal trees (gray symbols, black lines) and rate-constant simulations of trees the same size and age (yellow symbols, extinction fraction=0.65). Red symbols are non-significant effects where the 95% confidence interval overlaps zero. In part **a**, bold numbers per time slice are the percentage of significant results, and italic numbers are the mean values of Pagel's lambda estimated during PGLS for each time slice. In part **b**, simultaneous inference is performed as in Fig. 3, but adding percent of DNA-sampled species per clade to show our results are unaffected by imputing DNA-missing species (simulations lack missing species, so are not shown for comparison). (**c**) Analogous taxon-based analyses in (top) univariate and (bottom) multivariate contexts for 100 trees. Gray circles represent significant terms in the model, while red triangles have $P > 0.05$. Only clades with ≥4 species were examined for genera (n=385), families (n=102), and orders (n=22).

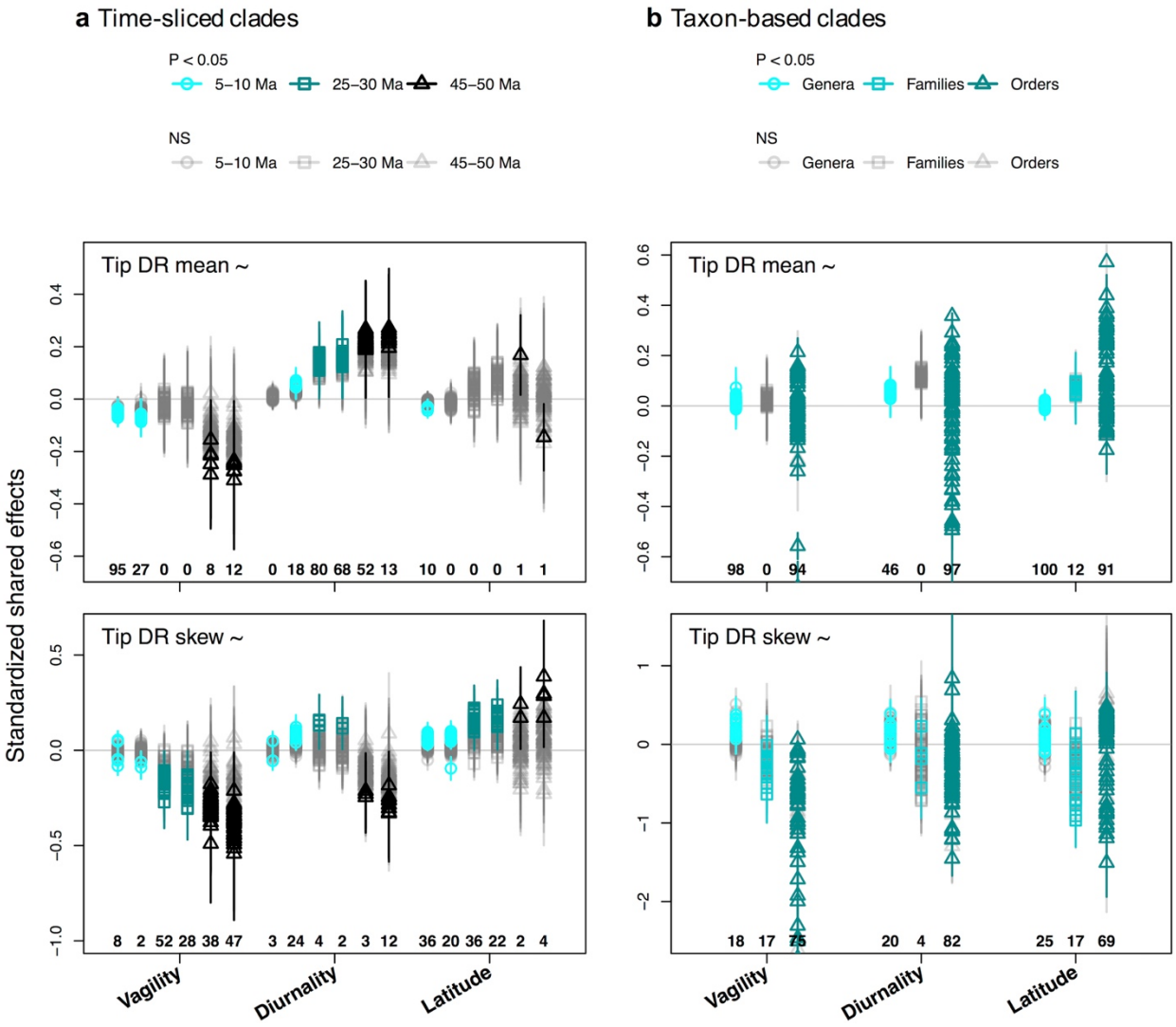

Fig. S19

Clade-level univariate PGLS analyses of ecological factors on tip DR mean and skew. Results across 100 trees are compared using (**a**) time slice-defined clades at five-million-year intervals, showing representative slices (symbols as in legend at top); and (**b**) taxon-defined clades. The number of trees for which a given univariate comparison was significant is displayed below each set of standardized coefficients.

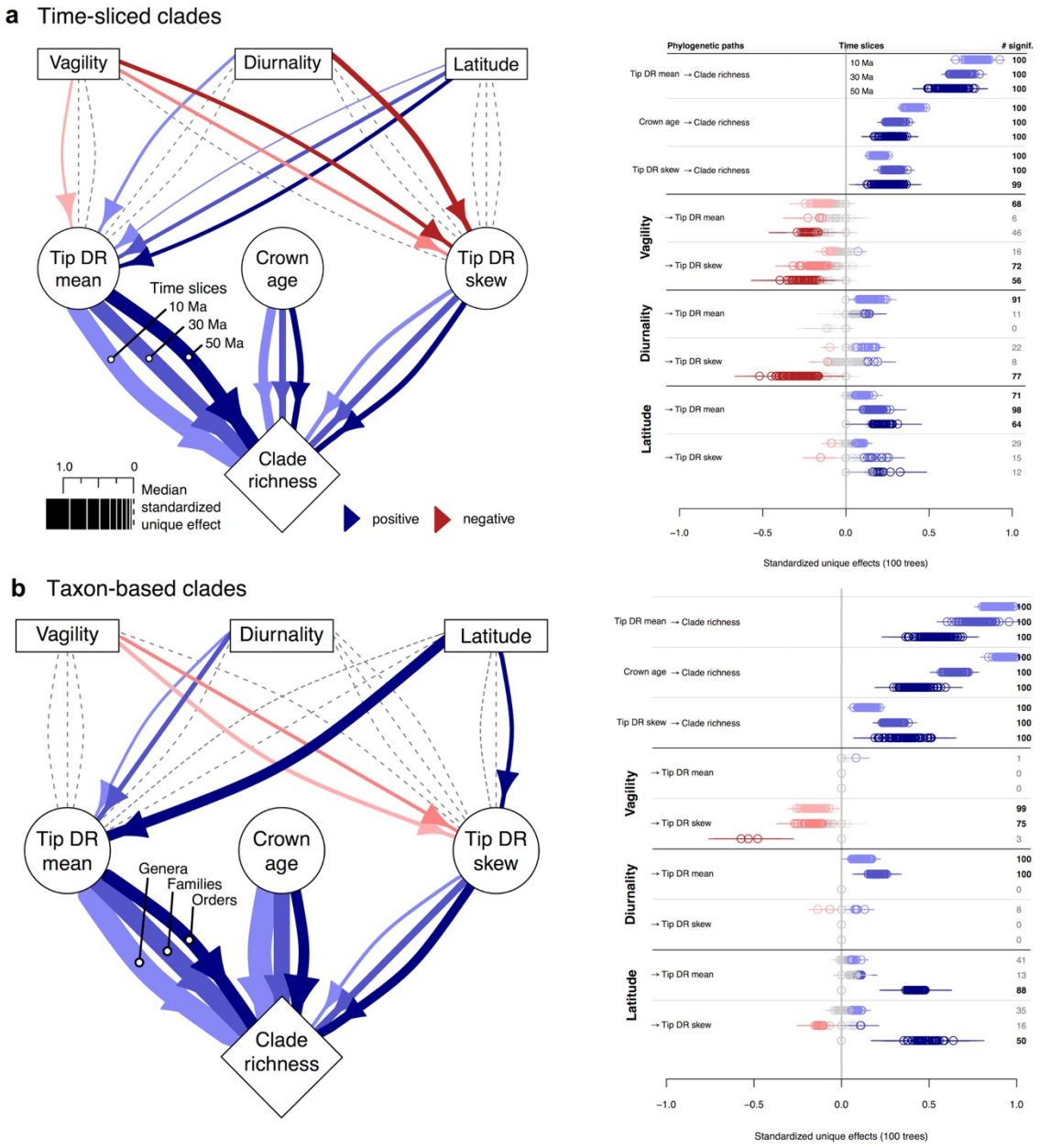

Fig. S20

Expanded display of Fig. 4 path analyses comparing time-sliced clades vs. taxa. (**a**) Clades defined by time slices at 10-, 30-, and 50-Ma intervals (light to dark colors). (left) Path thickness and directionality denotes median coefficients of model-averaged analyses on standardized data and 100 trees. (right) Per-estimate uncertainty across analyses and taxa (slope ± SE, 100 trees). (**b**) The same models run upon clades delimited as genera, families, and orders (light to dark colors). The right-side margin shows totals of non-zero estimates, either positive (blue shades) or negative (red shades), and bolds the totals of paths present in >50 trees (gray denotes majority overlap with zero, which are dashed-line paths on the left-side).

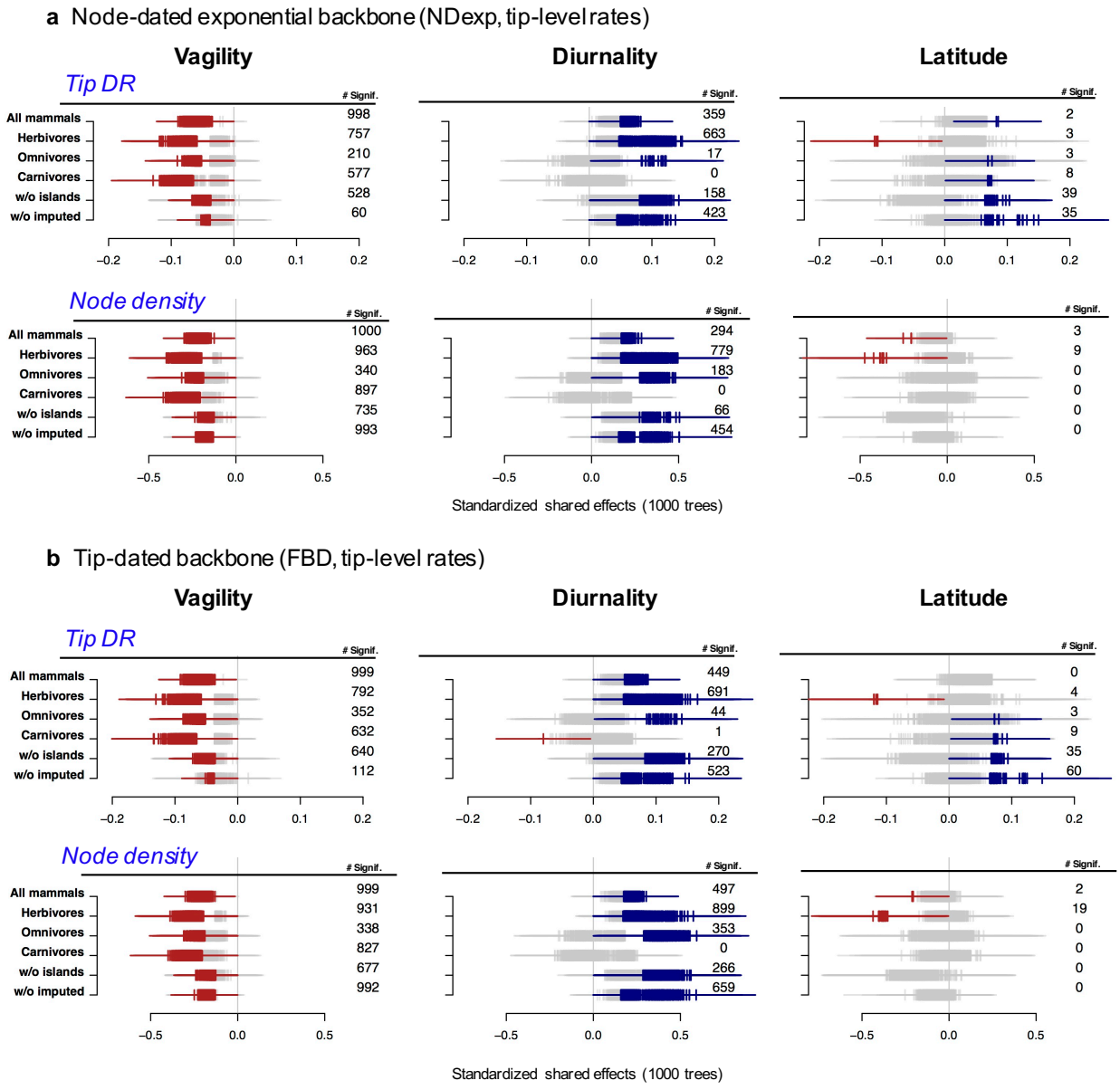

Fig. S21

Tip-level sensitivity analyses of univariate PGLS models (see Fig. 4a). Analyses of trait ~ rate models are repeated across 1000 trees from the Completed TopoCons distributions for (**a**) the node-dated backbone, and (**b**) the tip-dated backbone, in each case comparing standardized shared effects from species-level tip DR and node density statistics. The following data subsets were examined: all mammals (extant and non-marine for all trait analyses; n=5675), herbivores only (n=1802), omnivores only (n=2166), carnivores only (n=1707), excluding island endemics (n=4553), and excluding imputed species unsampled for DNA (n=3941). The right-side margin shows totals of non-zero estimates with $P < 0.05$, either positive (blue shades) or negative (red shades) out of the 1000 trees analyzed (gray denotes majority overlap with zero).

a Node-dated exponential backbone (NDexp, time-slice clade rates)

Tip DR mean and skew

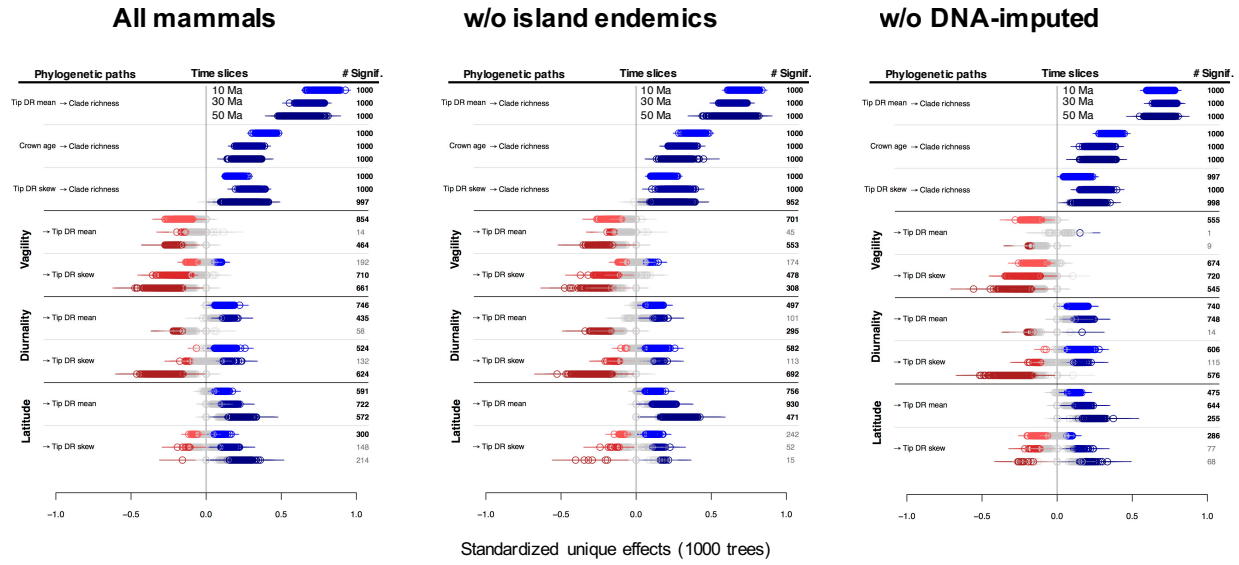

Node density mean and skew

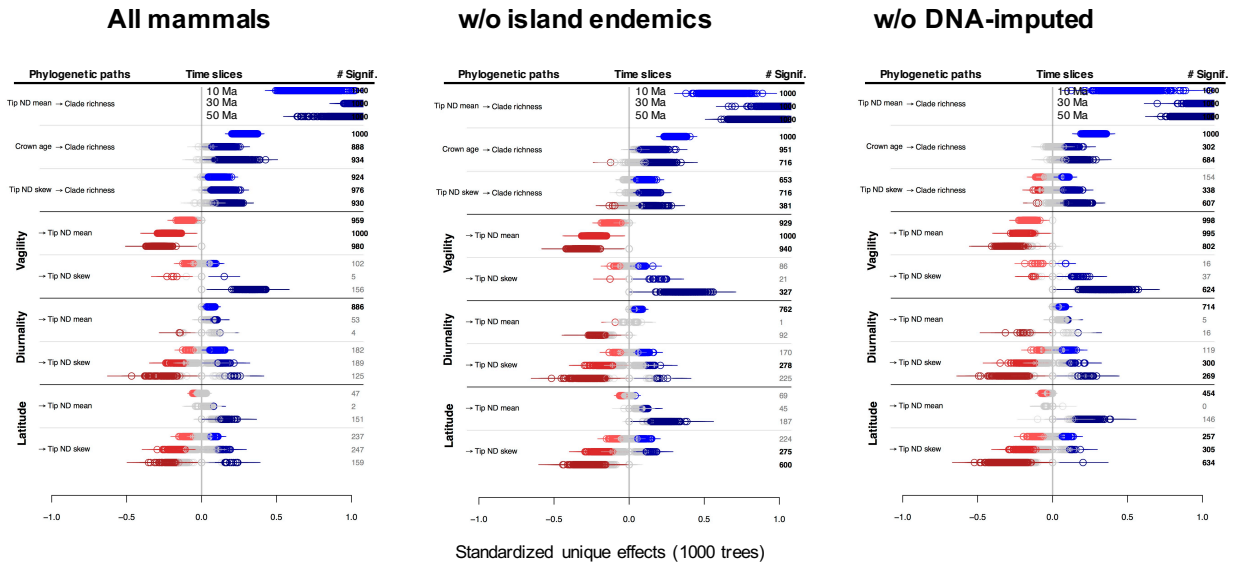

Fig. S22

Clade-level sensitivity analyses of multivariate phylogenetic path models (see Fig. 4b). Comparison of path coefficients on time-sliced clades at 10, 30, and 50 Ma delimited across 1000 trees from the Completed TopoCons distributions for (**a**) the node-dated backbone, and (**b**) the tip-dated backbone. Path models were run on the following data subsets : all mammals (extant and non-marine for all trait analyses; n=5675), excluding island endemics (n=4553), and excluding imputed species unsampled for DNA (n=3941). Median coefficients ± SE are shown for model-averaged runs on 1000 trees using standardized data. The right-side margin shows totals of non-zero estimates with $P < 0.05$, either positive (blue shades) or negative (red shades), and bold totals of paths present in >500 of the 1000 trees analyzed (gray denotes majority overlap with zero).

b Tip-dated backbone (FBD, time-slice clade rates)

Tip DR mean and skew

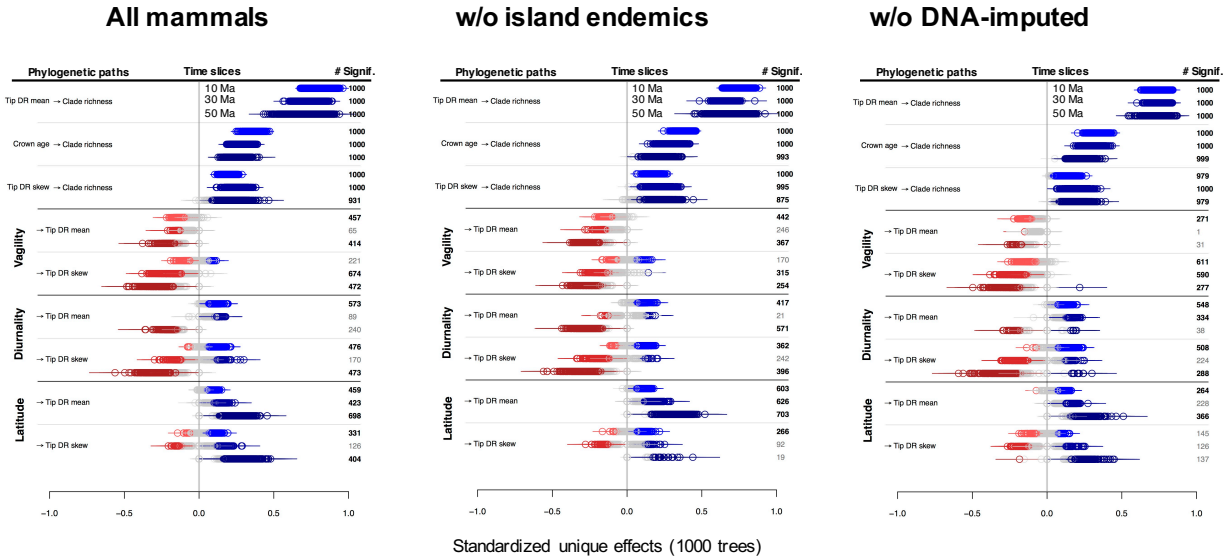

Node density mean and skew

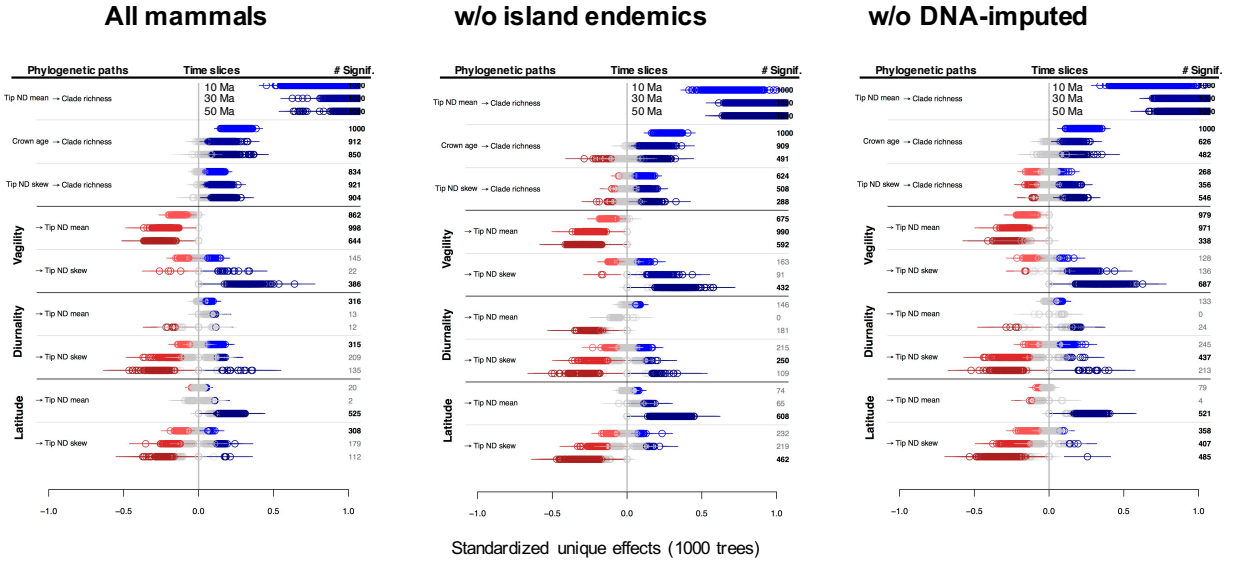

Fig. S22 (continued)
Clade-level sensitivity analyses of multivariate phylogenetic path models. See previous legend.

a

		Clade richness	B	D	E	F	G	H	J	L	M	N	O	P	Q	R	T	V	W	X	Unshifted species		# Shifts
PC1	Marsupialia	362	78	.	.	.	.	.	.	.	.	.	.	.	.	.	.	.	.	.	284	78%	1
PC2	Afrotheria	92	.	.	.	.	.	.	.	.	.	.	.	.	.	.	.	.	.	.	92	100%	0
PC3	Xenarthra	33	.	.	.	.	.	.	.	.	.	.	.	.	.	.	.	.	.	.	33	100%	0
PC4	Scandentia	20	.	.	.	.	.	.	.	.	.	.	.	.	.	.	.	.	.	.	20	100%	0
PC5	Primates	458	.	.	.	.	.	.	.	.	.	313	135	.	.	.	.	.	.	.	10	2%	2
PC6	Lagomorpha	91	.	.	.	.	.	.	.	.	.	.	.	91	.	.	.	.	.	.	0	0%	1
PC7	Castorimorpha	109	.	.	.	.	.	.	.	.	.	.	.	.	.	107	.	.	.	.	2	2%	1
PC8	Dipodidae	51	.	.	.	.	.	.	.	.	.	.	.	.	.	.	.	.	.	.	51	100%	0
PC9	Spalacidae	21	.	.	.	.	.	.	.	.	.	.	.	.	.	.	.	.	.	.	21	100%	0
PC10	Nesomyidae	63	.	.	.	.	.	.	.	.	.	.	.	.	.	.	.	.	.	.	63	100%	0
PC11	Muridae	779	.	.	.	.	.	.	.	.	.	.	.	.	.	.	.	196	104	80	399	51%	3
PC12	Cricetidae	726	.	.	.	.	.	.	.	.	.	.	.	.	.	.	726	.	.	.	0	0%	1
PC13	Squirrel-related	320	.	.	.	.	.	.	.	.	.	.	.	.	.	.	.	.	.	.	320	100%	0
PC14	Guinea pig-related	304	.	.	.	.	.	.	.	.	.	.	.	.	65	.	.	.	.	.	239	79%	1
PC15	Eulipotyphla	491	.	.	.	.	.	.	.	.	213	.	.	.	.	.	.	.	.	.	278	57%	1
PC16	Noctilionoidea	227	.	.	.	.	.	205	.	.	.	.	.	.	.	.	.	.	.	.	22	10%	1
PC17	Vespertilionoidea	605	.	.	.	.	605	.	.	.	.	.	.	.	.	.	.	.	.	.	0	0%	1
PC18	Emballonuroidea	70	.	.	.	.	.	.	.	.	.	.	.	.	.	.	.	.	.	.	70	100%	0
PC19	Yinpterochiroptera	385	.	.	.	.	.	.	69	87	.	.	.	.	.	.	.	.	.	.	229	59%	2
PC20	Artiodactyla	348	.	.	215	91	.	.	.	.	.	.	.	.	.	.	.	.	.	.	42	12%	2
PC21	Perissodactyla	24	.	.	.	.	.	.	.	.	.	.	.	.	.	.	.	.	.	.	24	100%	0
PC22	Carnivora	298	.	298	.	.	.	.	.	.	.	.	.	.	.	.	.	.	.	.	0	0%	1
PC23	Monotremata	5	.	.	.	.	.	.	.	.	.	.	.	.	.	.	.	.	.	.	5	100%	0
PC24	Pholidota	8	.	.	.	.	.	.	.	.	.	.	.	.	.	.	.	.	.	.	8	100%	0
PC25	Dermoptera	2	.	.	.	.	.	.	.	.	.	.	.	.	.	.	.	.	.	.	2	100%	0
PC26	Anomaluromorpha	9	.	.	.	.	.	.	.	.	.	.	.	.	.	.	.	.	.	.	9	100%	0
PC27	Calomyscidae	8	.	.	.	.	.	.	.	.	.	.	.	.	.	.	.	.	.	.	8	100%	0
PC28	Platacanthomyidae	2	.	.	.	.	.	.	.	.	.	.	.	.	.	.	.	.	.	.	2	100%	0

b

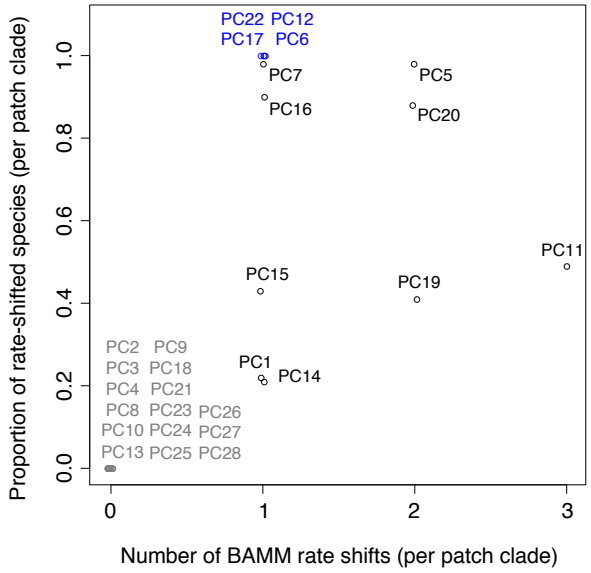

Fig. S23

Membership in phylogenetic patch clades vs. BAMM rate-shifted clades. The overall location of rate shifts present in ≥ 5 of 10 trees analyzed appears unrelated to patch clade delimitations. (**a**) Summary of patch clades PC1-28 relative to the contained species in rate-shifted clades B-X (letters correspond to Fig. 1 and Table S8). Out of 28 patch clades, we find that 15 do not contain any tipward rate shift (gray), 9 contain one or more shift for a subset of patch clade species (white), and 4 have all species contained in a rate shift (blue). (**b**) Plot of the 18 shifts most tipward in a given lineage (e.g., shift C is Placentalia and not shown) shows substantial variation in number of shifts per patch clade.

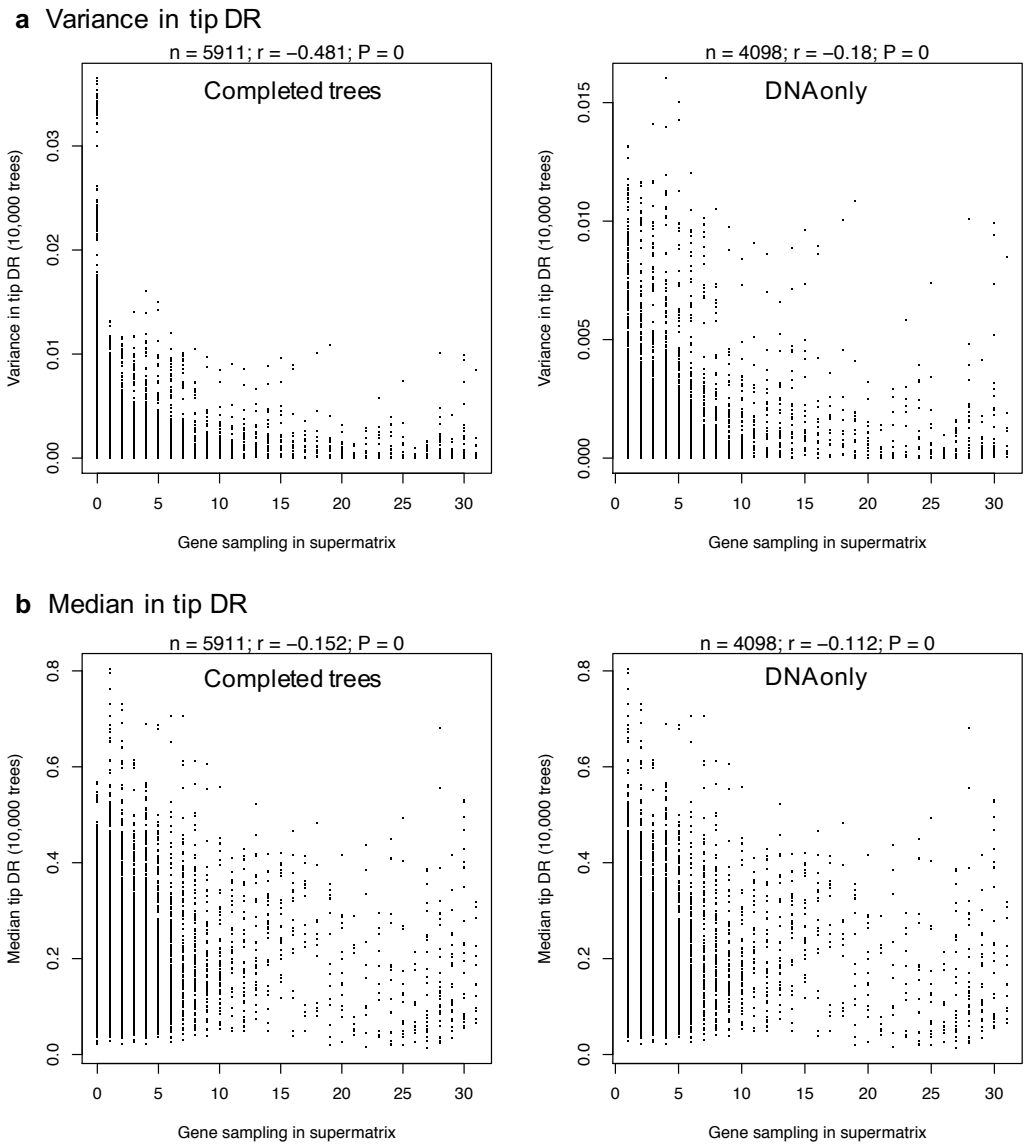

Fig. S24

Effect of gene sampling per species upon tip DR estimates. Compared are the per-species (a) variances and (b) medians in tip DR across 10,000 node-dated trees vs. the number of genes (0–31) sampled in the global DNA supermatrix. Completed trees are those where no-DNA species (0 genes) were added using PASTIS during MrBayes runs (see Supplementary Methods, section 5). As expected, variance in tip DR estimates is higher for completed species (note the different y-axes in part a). However, median tip DR estimates are similar between completed and DNA-only trees. Spearman's correlation coefficients, r, are shown for each plot as an indication of general trends in the data (slight negative trends do not account for phylogenetic covariance).

Supplementary Datasets

Dataset S1. (zipped file)
Details of the DNA error-checking steps and updated master taxonomy of mammals.

Dataset S2. (zipped file)
Final DNA alignments for 31 genes and gene tree outputs from RAxML.

Dataset S3. (zipped file)
Global ML tree for 4098 species of mammals built from the 31-gene supermatrix.

Dataset S4. (zipped file)
Results of 28 patch clade phylogenies delimited across Mammalia.

Dataset S5. (zipped file)
Results and run files for backbone divergence-time analyses in MrBayes.

Dataset S6. (zipped file)
Full 5911-species trees of Mammalia using node-dating and tip-dating.

Dataset S7. (zipped file)
Species ecological trait data, results from BAMM, TreePar, and CoMET, and code for analyses.

Supplementary References

1. Thomas GH, et al. (2013) PASTIS: an R package to facilitate phylogenetic assembly with soft taxonomic inferences. *Methods Ecol Evol* 4(11):1011–1017.

2. Jetz W, Thomas GH, Joy JB, Hartmann K, Mooers AO (2012) The global diversity of birds in space and time. *Nature* 491(7424):444–448.

3. Ronquist F, et al. (2012) MrBayes 3.2: Efficient Bayesian Phylogenetic Inference and Model Choice across a Large Model Space. *Syst Biol*:sys029.

4. Huelsenbeck JP, Rannala B, Masly JP (2000) Accommodating Phylogenetic Uncertainty in Evolutionary Studies. *Science* 288(5475):2349–2350.

5. Huelsenbeck JP, B. Larget, R. E. Miller, F. Ronquist (2002) Potential applications and pitfalls of Bayesian inference of phylogeny. *Syst Biol* 51:673–688.

6. Douady CJ, Delsuc F, Boucher Y, Doolittle WF, Douzery EJP (2003) Comparison of Bayesian and maximum likelihood bootstrap measures of phylogenetic reliability. *Mol Biol Evol* 20:248–254.

7. Yang Z, Rannala B (1997) Bayesian phylogenetic inference using DNA sequences: a Markov Chain Monte Carlo Method. *Mol Biol Evol* 14(7):717–724.

8. Degnan JH, Rosenberg NA (2009) Gene tree discordance, phylogenetic inference and the multispecies coalescent. *Trends Ecol Evol* 24(6):332–340.

9. Heled J, Drummond AJ (2010) Bayesian Inference of Species Trees from Multilocus Data. *Mol Biol Evol* 27(3):570–580.

10. Zimmermann T, Mirarab S, Warnow T (2014) BBCA: Improving the scalability of *BEAST using random binning. *BMC Genomics* 15(6):S11.

11. Mirarab S, Warnow T (2015) ASTRAL-II: coalescent-based species tree estimation with many hundreds of taxa and thousands of genes. *Bioinformatics* 31(12):i44–i52.

12. de Queiroz A, Gatesy J (2007) The supermatrix approach to systematics. *Trends Ecol Evol* 22:34–41.

13. Bininda-Emonds ORP (2004) The evolution of supertrees. *Trends Ecol Evol* 19(6):315–322.

14. Bininda-Emonds ORP, et al. (2007) The delayed rise of present-day mammals. *Nature* 446(7135):507–512.

15. Fritz SA, Bininda-Emonds ORP, Purvis A (2009) Geographical variation in predictors of mammalian extinction risk: big is bad, but only in the tropics. *Ecol Lett* 12(6):538–549.

16. Kuhn TS, Mooers AØ, Thomas GH (2011) A simple polytomy resolver for dated phylogenies. *Methods Ecol Evol* 2(5):427–436.

17. Stadler T (2011) Mammalian phylogeny reveals recent diversification rate shifts. *Proc Natl Acad Sci* 108(15):6187–6192.

18. Faurby S, Svenning J-C (2015) A species-level phylogeny of all extant and late Quaternary extinct mammals using a novel heuristic-hierarchical Bayesian approach. *Mol Phylogenet Evol* 84:14–26.

19. Hedges SB, Marin J, Suleski M, Paymer M, Kumar S (2015) Tree of life reveals clock-like speciation and diversification. *Mol Biol Evol*:msv037.

20. Meredith RW, et al. (2011) Impacts of the Cretaceous Terrestrial Revolution and KPg Extinction on Mammal Diversification. *Science* 334(6055):521–524.

21. Pyle RL (2016) Towards a Global Names Architecture: The future of indexing scientific names. *ZooKeys* (550):261–281.

22. Altschul SF, et al. (1997) Gapped BLAST and PSI-BLAST: a new generation of protein database search programs. *Nucleic Acids Res* 25:3389–3402.

23. IUCN (2016) IUCN RedList of Threatened Species. Version 2016.2. Available at: http://www.iucnredlist.org/initiatives/mammals.

24. Wilson DE, Reeder DM (2005) *Mammal species of the world: a taxonomic and geographic reference, 3rd ed.* (Johns Hopkins University Press, Baltimore, MD). 3rd Ed.

25. Wilman H, et al. (2014) EltonTraits 1.0: Species-level foraging attributes of the world's birds and mammals. *Ecology* 95(7):2027–2027.

26. Meyer C, Kreft H, Guralnick R, Jetz W (2015) Global priorities for an effective information basis of biodiversity distributions. *Nat Commun* 6:8221.

27. Burgin CJ, Colella JP, Kahn PL, Upham NS (2018) How many species of mammals are there? *J Mammal* 99(1):1–14.

28. Mammal Diversity Database (2018) American Society of Mammalogists, Mammal Diversity Database. Available at: https://mammaldiversity.org/ [Accessed June 2, 2018].

29. IUCN (2008) IUCN Redlist of Threatened Species, 2008 Assessments.

30. Nilsson RH, et al. (2006) Taxonomic Reliability of DNA Sequences in Public Sequence Databases: A Fungal Perspective. *PLoS ONE* 1(1). doi:10.1371/journal.pone.0000059.

31. Valkiūnas G, Atkinson CT, Bensch S, Sehgal RNM, Ricklefs RE (2008) Parasite misidentifications in GenBank: how to minimize their number? *Trends Parasitol* 24(6):247–248.

32. Bridge PD, Roberts PJ, Spooner BM, Panchal G (2003) On the unreliability of published DNA sequences. *New Phytol* 160(1):43–48.

33. Ranwez V, Harispe S, Delsuc F, Douzery EJP (2011) MACSE: Multiple Alignment of Coding SEquences Accounting for Frameshifts and Stop Codons. *PLOS ONE* 6(9):e22594.

34. Katoh K, Standley DM (2013) MAFFT Multiple Sequence Alignment Software Version 7: Improvements in Performance and Usability. *Mol Biol Evol* 30(4):772–780.

35. Löytynoja A (2014) Phylogeny-aware alignment with PRANK. *Methods Mol Biol Clifton NJ* 1079:155–170.

36. Capella-Gutiérrez S, Silla-Martínez JM, Gabaldón T (2009) trimAl: a tool for automated alignment trimming in large-scale phylogenetic analyses. *Bioinformatics* 25(15):1972–1973.

37. Stamatakis A (2014) RAxML version 8: a tool for phylogenetic analysis and post-analysis of large phylogenies. *Bioinformatics* 30(9):1312–1313.

38. Field DJ, et al. (2014) Toward consilience in reptile phylogeny: miRNAs support an archosaur, not lepidosaur, affinity for turtles. *Evol Dev* 16(4):189–196.

39. Wilkinson M (1996) Majority-rule reduced consensus trees and their use in bootstrapping. *Mol Biol Evol* 13(3):437–444.

40. Aberer AJ, Krompass D, Stamatakis A (2013) Pruning Rogue Taxa Improves Phylogenetic Accuracy: An Efficient Algorithm and Webservice. *Syst Biol* 62(1):162–166.

41. Sanderson MJ, Shaffer HB (2002) Troubleshooting Molecular Phylogenetic Analyses. *Annu Rev Ecol Syst* 33(1):49–72.

42. Brown JM, Thomson RC (2016) Bayes factors unmask highly variable information content, bias, and extreme influence in phylogenomic analyses. *Syst Biol*. doi:10.1093/sysbio/syw101.

43. Sanderson MJ, McMahon MM, Steel M (2011) Terraces in phylogenetic tree space. *Science* 333(6041):448–450.

44. R Core Team (2017) *R: A language and environment for statistical computing* (Vienna, Austria).

45. Revell LJ (2012) phytools: an R package for phylogenetic comparative biology (and other things). *Methods Ecol Evol* 3:217–223.

46. Kearse M, et al. (2012) Geneious Basic: an integrated and extendable desktop software platform for the organization and analysis of sequence data. *Bioinforma Oxf Engl* 28(12):1647–1649.

47. Pyron RA, Burbrink FT, Wiens JJ (2013) A phylogeny and revised classification of Squamata, including 4161 species of lizards and snakes. *BMC Evol Biol* 13:93.

48. Wiens JJ, Morrill MC (2011) Missing Data in Phylogenetic Analysis: Reconciling Results from Simulations and Empirical Data. *Syst Biol*:syr025.

49. Roure B, Baurain D, Philippe H (2013) Impact of Missing Data on Phylogenies Inferred from Empirical Phylogenomic Data Sets. *Mol Biol Evol* 30(1):197–214.

50. Lanfear R, Calcott B, Ho SYW, Guindon S (2012) PartitionFinder: Combined Selection of Partitioning Schemes and Substitution Models for Phylogenetic Analyses. *Mol Biol Evol* 29(6):1695–1701.

51. Lanfear R, Calcott B, Kainer D, Mayer C, Stamatakis A (2014) Selecting optimal partitioning schemes for phylogenomic datasets. *BMC Evol Biol* 14(1):82.

52. Yang Z (2006) *Computational Molecular Evolution* (Oxford University Press, Oxford, New York).

53. Jetz W, Pyron RA (2018) The interplay of past diversification and evolutionary isolation with present imperilment across the amphibian tree of life. *Nat Ecol Evol*.

54. Miller MA, Pfeiffer W, Schwartz T (2010) Creating the CIPRES Science Gateway for inference of large phylogenetic trees. *Proceedings of the Gateway Computing Environments Workshop (GCE), 14 Nov. 2010, New Orleans, LA*, pp 1–8.

55. Paradis E, Claude J, Strimmer K (2004) APE: Analyses of Phylogenetics and Evolution in R language. *Bioinformatics* 20:289–290.

56. Churakov G, et al. (2010) Rodent Evolution: Back to the Root. *Mol Biol Evol* 27(6):1315–1326.

57. Steppan SJ, Schenk JJ (2017) Muroid rodent phylogenetics: 900-species tree reveals increasing diversification rates. *PLOS ONE* 12(8):e0183070.

58. Jansa SA, Goodman SM, Tucker PK (2005) Molecular Phylogeny and Biogeography of the Native Rodents of Madagascar (Muridae: Nesomyinae): A Test of the Single-Origin Hypothesis. *Cladistics* 15(3):253–270.

59. Shi JJ, Rabosky DL (2015) Speciation dynamics during the global radiation of extant bats. *Evolution* 69(6):1528–1545.

60. Amador LI, Arévalo RLM, Almeida FC, Catalano SA, Giannini NP (2018) Bat Systematics in the Light of Unconstrained Analyses of a Comprehensive Molecular Supermatrix. *J Mamm Evol* 25(1):37–70.

61. Teeling EC, Jones G, Rossiter SJ (2016) Phylogeny, Genes, and Hearing: Implications for the Evolution of Echolocation in Bats. *Bat Bioacoustics*:25–54.

62. Brace S, et al. (2016) Evolutionary History of the Nesophontidae, the Last Unplaced Recent Mammal Family. *Mol Biol Evol* 33(12):3095–3103.

63. Feigin CY, et al. (2018) Genome of the Tasmanian tiger provides insights into the evolution and demography of an extinct marsupial carnivore. *Nat Ecol Evol* 2(1):182–192.

64. Fontanesi L, et al. (2016) LaGomiCs—Lagomorph Genomics Consortium: An International Collaborative Effort for Sequencing the Genomes of an Entire Mammalian Order. *J Hered* 107(4):295–308.

65. Cusimano N, Stadler T, Renner SS (2012) A New Method for Handling Missing Species in Diversification Analysis Applicable to Randomly or Nonrandomly Sampled Phylogenies. *Syst Biol* 61(5):785–792.

66. Brown WM, Prager EM, Wang A, Wilson AC (1982) Mitochondrial DNA sequences of primates: Tempo and mode of evolution. *J Mol Evol* 18(4):225–239.

67. Philippe H, Zhou Y, Brinkmann H, Rodrigue N, Delsuc F (2005) Heterotachy and long-branch attraction in phylogenetics. *BMC Evol Biol* 5(1):50.

68. Lepage T, Bryant D, Philippe H, Lartillot N (2007) A General Comparison of Relaxed Molecular Clock Models. *Mol Biol Evol* 24(12):2669–2680.

69. Zhou C-F, Wu S, Martin T, Luo Z-X (2013) A Jurassic mammaliaform and the earliest mammalian evolutionary adaptations. *Nature* 500(7461):163–167.

70. Benton MJ, et al. (2015) Constraints on the timescale of animal evolutionary history. *Palaeontol Electron* 18(1).

71. Phillips MJ (2015) Four mammal fossil calibrations: balancing competing palaeontological and molecular considerations. *Palaeontol Electron* 18(1):1–16.

72. Parham JF, et al. (2012) Best practices for justifying fossil calibrations. *Syst Biol* 61:346–359.

73. Flynn JJ, Parrish JM, Rakotosamimanana B, Simpson WF, Wyss AR (1999) A Middle Jurassic mammal from Madagascar. *Nature* 401(6748):57–60.

74. Luo Z-X, Kielan-Jaworowska Z, Cifelli RL (2002) In quest for a phylogeny of Mesozoic mammals. *Acta Palaeontol Pol* 47(1):1–78.

75. Luo Z-X, Yuan C-X, Meng Q-J, Ji Q (2011) A Jurassic eutherian mammal and divergence of marsupials and placentals. *Nature* 476(7361):442–445.

76. Luo Z-X, Chen P, Li G, Chen M (2007) A new eutriconodont mammal and evolutionary development in early mammals. *Nature* 446(7133):288–293.

77. Phillips MJ, Bennett TH, Lee MSY (2009) Molecules, morphology, and ecology indicate a recent, amphibious ancestry for echidnas. *Proc Natl Acad Sci* 106(40):17089–17094.

78. Beck RMD (2012) An ‘ameridelphian’ marsupial from the early Eocene of Australia supports a complex model of Southern Hemisphere marsupial biogeography. *Naturwissenschaften* 99(9):715–729.

79. Prideaux GJ, Warburton NM (2010) An osteology-based appraisal of the phylogeny and evolution of kangaroos and wallabies (Macropodidae: Marsupialia). *Zool J Linn Soc* 159(4):954–987.

80. Fox RC, Scott CS, Rankin BD (2010) New Early Carnivoran Specimens from the Puercan (Earliest Paleocene) of Saskatchewan, Canada. *Httpdxdoiorg10166609-1651*. doi:10.1666/09-165.1.

81. Gheerbrant E (2009) Paleocene emergence of elephant relatives and the rapid radiation of African ungulates. *Proc Natl Acad Sci* 106(26):10717–10721.

82. Bergqvist LP, Abrantes E, Avilla L dos S (2004) The Xenarthra (Mammalia) of São José de Itaboraí Basin (upper Paleocene, Itaboraian), Rio de Janeiro, Brazil. *Geodiversitas* 26(2):323–337.

83. Gunnell GF, Simmons NB (2005) Fossil Evidence and the Origin of Bats. *J Mamm Evol* 12(1–2):209–246.

84. Rose KD, et al. (2008) Early Eocene lagomorph (Mammalia) from Western India and the early diversification of Lagomorpha. *Proc R Soc Lond B Biol Sci* 275(1639):1203–1208.

85. Marivaux L, Vianey-Liaud M, Jaeger JJ (2004) High-level phylogeny of early Tertiary rodents: dental evidence. *Zool J Linn Soc* 142:105–134.

86. Antoine P-O, et al. (2012) Middle Eocene rodents from Peruvian Amazonia reveal the pattern and timing of caviomorph origins and biogeography. *Proc R Soc B-Biol Sci* 279:1319–1326.

87. Seiffert ER, et al. (2005) Basal Anthropoids from Egypt and the Antiquity of Africa’s Higher Primate Radiation. *Science* 310(5746):300–304.

88. Seiffert ER, Simons EL, Attia Y (2003) Fossil evidence for an ancient divergence of lorises and galagos. *Nature* 422(6930):421–424.

89. Seiffert ER (2006) Revised age estimates for the later Paleogene mammal faunas of Egypt and Oman. *Proc Natl Acad Sci* 103(13):5000–5005.

90. Bajpai S, Gingerich PD (1998) A new Eocene archaeocete (Mammalia, Cetacea) from India and the time of origin of whales. *Proc Natl Acad Sci* 95(26):15464–15468.

91. O’Leary MA, Uhen MD (1999) The time of origin of whales and the role of behavioral changes in the terrestrial-aquatic transition. *Paleobiology* 25(4):534–556.

92. Wesley-Hunt GD, Flynn JJ (2005) Phylogeny of the carnivora: Basal relationships among the carnivoramorphans, and assessment of the position of 'miacoidea' relative to carnivora. *J Syst Palaeontol* 3(1):1–28.

93. Ho SYW, Phillips MJ (2009) Accounting for Calibration Uncertainty in Phylogenetic Estimation of Evolutionary Divergence Times. *Syst Biol* 58(3):367–380.

94. Pyron RA (2011) Divergence Time Estimation Using Fossils as Terminal Taxa and the Origins of Lissamphibia. *Syst Biol* 60(4):466–481.

95. Ronquist F, et al. (2012) A Total-Evidence Approach to Dating with Fossils, Applied to the Early Radiation of the Hymenoptera. *Syst Biol* 61(6):973–999.

96. Heath TA, Huelsenbeck JP, Stadler T (2014) The fossilized birth–death process for coherent calibration of divergence-time estimates. *Proc Natl Acad Sci* 111(29):E2957–E2966.

97. Zhang C, Stadler T, Klopfstein S, Heath TA, Ronquist F (2016) Total-Evidence Dating under the Fossilized Birth–Death Process. *Syst Biol* 65(2):228–249.

98. Ronquist F, Lartillot N, Phillips MJ (2016) Closing the gap between rocks and clocks using total-evidence dating. *Phil Trans R Soc B* 371(1699):20150136.

99. Lee MSY (2016) Multiple morphological clocks and total-evidence tip-dating in mammals. *Biol Lett* 12(7):20160033.

100. Rieux A, Balloux F (2016) Inferences from tip-calibrated phylogenies: a review and a practical guide. *Mol Ecol* 25(9):1911–1924.

101. Slater GJ (2013) Phylogenetic evidence for a shift in the mode of mammalian body size evolution at the Cretaceous-Palaeogene boundary. *Methods Ecol Evol* 4(8):734–744.

102. Close RA, Friedman M, Lloyd GT, Benson RBJ (2015) Evidence for a Mid-Jurassic Adaptive Radiation in Mammals. *Curr Biol* 25(16):2137–2142.

103. Luo Z-X, Gatesy SM, Jenkins FA, Amaral WW, Shubin NH (2015) Mandibular and dental characteristics of Late Triassic mammaliaform Haramiyavia and their ramifications for basal mammal evolution. *Proc Natl Acad Sci*:201519387.

104. Zheng X, Bi S, Wang X, Meng J (2013) A new arboreal haramiyid shows the diversity of crown mammals in the Jurassic period. *Nature* 500(7461):199.

105. Drummond AJ, Suchard MA, Xie D, Rambaut A (2012) Bayesian phylogenetics with BEAUti and the BEAST 1.7. *Mol Biol Evol* 29:1969–1973.

106. Tonini JFR, Beard KH, Ferreira RB, Jetz W, Pyron RA (2016) Fully-sampled phylogenies of squamates reveal evolutionary patterns in threat status. *Biol Conserv* 204:23–31.

107. Redding DW, Mooers AØ (2006) Incorporating Evolutionary Measures into Conservation Prioritization. *Conserv Biol* 20(6):1670–1678.

108. Quintero I, Jetz W (2018) Global elevational diversity and diversification of birds. *Nature*.

109. Steel M, Mooers A (2010) The expected length of pendant and interior edges of a Yule tree. *Appl Math Lett* 23(11):1315–1319.

110. Ferger WF (1931) The Nature and Use of the Harmonic Mean. *J Am Stat Assoc* 26:36–40.

111. Rabosky DL (2014) Automatic detection of key innovations, rate shifts, and diversity-dependence on phylogenetic trees. *PLoS ONE* 9:e89543.

112. Huelsenbeck JP, Larget B, Swofford D (2000) A Compound Poisson Process for Relaxing the Molecular Clock. *Genetics* 154(4):1879–1892.

113. Moore BR, Höhna S, May MR, Rannala B, Huelsenbeck JP (2016) Critically evaluating the theory and performance of Bayesian analysis of macroevolutionary mixtures. *Proc Natl Acad Sci* 113(34):9569–9574.

114. Rabosky DL, Mitchell JS, Chang J (2017) Is BAMM flawed? Theoretical and practical concerns in the analysis of multi-rate diversification models. *Syst Biol*. doi:10.1093/sysbio/syx037.

115. Quental TB, Marshall CR (2009) Extinction During Evolutionary Radiations: Reconciling the Fossil Record with Molecular Phylogenies. *Evolution* 63(12):3158–3167.

116. Maddison WP, Midford PE, Otto SP, Oakley T (2007) Estimating a Binary Character's Effect on Speciation and Extinction. *Syst Biol* 56(5):701–710.

117. Beaulieu JM, O'Meara BC (2016) Detecting Hidden Diversification Shifts in Models of Trait-Dependent Speciation and Extinction. *Syst Biol* 65(4):583–601.

118. Rabosky DL (2017) 9. Advanced analysis options — bamm 2.5.0 documentation. Available at: http://bamm-project.org/advanced.html?highlight=uncertainty [Accessed April 2, 2017].

119. Rabosky DL, et al. (2014) BAMMtools: an R package for the analysis of evolutionary dynamics on phylogenetic trees. *Methods Ecol Evol* 5:701–707.

120. Rabosky DL, Lovette IJ (2008) Explosive evolutionary radiations: decreasing speciation or increasing extinction through time? *Evolution* 62:1866–1875.

121. Rabosky DL (2017) 11. Frequently Asked Questions — bamm 2.5.0 documentation. Available at: http://bamm-project.org/faq.html [Accessed April 5, 2017].

122. Rabosky DL (2017) 8. Analyzing BAMM output with BAMMtools — bamm 2.5.0 documentation. Available at: http://bamm-project.org/postprocess.html [Accessed April 5, 2017].

123. May MR, Höhna S, Moore BR (2016) A Bayesian approach for detecting the impact of mass-extinction events on molecular phylogenies when rates of lineage diversification may vary. *Methods Ecol Evol* 7(8):947–959.

124. Höhna S, May MR, Moore BR (2016) TESS: an R package for efficiently simulating phylogenetic trees and performing Bayesian inference of lineage diversification rates. *Bioinformatics* 32(5):789–791.

125. Morlon H, Parsons TL, Plotkin JB (2011) Reconciling molecular phylogenies with the fossil record. *Proc Natl Acad Sci* 108(39):16327–16332.

126. Morlon H, et al. (2016) RPANDA: an R package for macroevolutionary analyses on phylogenetic trees. *Methods Ecol Evol* 7(5):589–597.

127. Condamine FL, Rolland J, Höhna S, Sperling FAH, Sanmartín I (2018) Testing the Role of the Red Queen and Court Jester as Drivers of the Macroevolution of Apollo Butterflies. *Syst Biol*. doi:10.1093/sysbio/syy009.

128. Rabosky DL (2006) Likelihood methods for detecting temporal shifts in diversification rates. *Evolution* 60:1152–1164.

129. Harcourt-Brown KG (2002) Tree Balance, Time Slices, and Evolutionary Turnover in Cretaceous Planktonic Foraminifera. *Syst Biol* 51(6):908–916.

130. Ruta M, Pisani D, Lloyd GT, Benton MJ (2007) A supertree of Temnospondyli: cladogenetic patterns in the most species-rich group of early tetrapods. *Proc R Soc Lond B Biol Sci* 274(1629):3087–3095.

131. Bernardi M, Angielczyk KD, Mitchell JS, Ruta M (2016) Phylogenetic Stability, Tree Shape, and Character Compatibility: A Case Study Using Early Tetrapods. *Syst Biol* 65(5):737–758.

132. Tarver JE, Donoghue PCJ (2011) The Trouble with Topology: Phylogenies without Fossils Provide a Revisionist Perspective of Evolutionary History in Topological Analyses of Diversity. *Syst Biol* 60(5):700–712.

133. Mazel F, et al. (2017) Global patterns of β-diversity along the phylogenetic time-scale: The role of climate and plate tectonics. *Glob Ecol Biogeogr* 26(10):1211–1221.

134. Pagel M (1994) Detecting correlated evolution on phylogenies: a general method for the comparative analysis of discrete characters. *Proc R Soc Lond B* 255(1342):37–45.

135. Pinheiro J, Bates D, DebRoy S, Sarkar D, R Core Team (2018) *nlme: Linear and Nonlinear Mixed Effects Models* Available at: R package version 3.1-137, https://CRAN.R-project.org/package=nlme.

136. Ho LST, Ané C (2014) A Linear-Time Algorithm for Gaussian and Non-Gaussian Trait Evolution Models. *Syst Biol* 63(3):397–408.

137. Orme CDL (2018) *The Caper Package: Comparative Analysis of Phylogenetics and Evolution in R* Available at: https://www.researchgate.net/publication/265617017_The_Caper_Package_Comparative_Analysis_of_Phylogenetics_and_Evolution_in_R [Accessed May 8, 2018].

138. Harmon LJ, Weir JT, Brock CD, Glor RE, Challenger W (2008) GEIGER: investigating evolutionary radiations. *Bioinformatics* 24:129–131.

139. McPeek MA, Brown JM (2007) Clade age and not diversification rate explains species richness among animal taxa. *Am Nat* 169.

140. Rabosky DL, Slater GJ, Alfaro ME (2012) Clade age and species richness are decoupled across the eukaryotic tree of life. *PLoS Biol* 10:e1001381.

141. Alroy J (2014) Accurate and precise estimates of origination and extinction rates. *Paleobiology* 40(3):374–397.

142. Foote M (2000) Origination and extinction components of taxonomic diversity: general problems. *Paleobiology* 26(sp4):74–102.

143. Jones KE, et al. (2009) PanTHERIA: a species-level database of life history, ecology, and geography of extant and recently extinct mammals. *Ecology* 90(9):2648–2648.

144. Faurby S, Svenning J-C (2016) Resurrection of the Island Rule: Human-Driven Extinctions Have Obscured a Basic Evolutionary Pattern. *Am Nat* 187(6):812–820.

145. Smith FA, et al. (2003) Body mass of late Quaternary mammals. *Ecology* 84:3402 (updated version obtained from senior author).

146. Goolsby EW, Bruggeman J, Ané C (2017) Rphylopars: fast multivariate phylogenetic comparative methods for missing data and within-species variation. *Methods Ecol Evol* 8(1):22–27.

147. Verheyen W, et al. (2011) Contribution to the systematics and zoogeography of the East-African Acomys spinosissimus Peters 1852 species complex and the description of two new species (Rodentia: Muridae). *TERMS USE*:36.

148. QGIS Development Team (2017) *QGIS Geographic Information System* (Open Source Geospatial Foundation Project) Available at: http://qgis.osgeo.org.

149. Jetz W, Carbone C, Fulford J, Brown JH (2004) The scaling of animal space use. *Science* 306(5694):266–268.

150. Claramunt S, Derryberry EP, Remsen JV, Brumfield RT (2012) High dispersal ability inhibits speciation in a continental radiation of passerine birds. *Proc R Soc Lond B Biol Sci* 279(1733):1567–1574.

151. Whitmee S, Orme CDL (2013) Predicting dispersal distance in mammals: a trait-based approach. *J Anim Ecol* 82(1):211–221.

152. Wei T (2017) An introduction to corrplot package. Available at: https://cran.r-project.org/web/packages/corrplot/vignettes/corrplot-intro.html [Accessed May 12, 2018].

153. McNab BK (1979) The Influence of body Size on the Energetics and Distribution of Fossorial and Burrowing Mammals. *Ecol Lett* 60:1010–1021.

154. Cooper N, Purvis A (2010) Body size evolution in mammals: complexity in tempo and mode. *Am Nat* 175:727–738.

155. Smith FA, Lyons SK (2013) *Animal body size: linking pattern and process across space, time, and taxonomic group* (University of Chicago Press, Chicago, IL).

156. Lemon J, Bolker B, Oom S (2017) Package "plotrix." Available at: https://cran.r-project.org/web/packages/plotrix/plotrix.pdf [Accessed May 12, 2018].

157. Lewin-Koh N (2018) Hexagon binning: an overview. Available at: https://cran.r-project.org/web/packages/hexbin/vignettes/hexagon_binning.pdf [Accessed May 12, 2018].

158. Freckleton RP, Phillimore AB, Pagel M (2008) Relating Traits to Diversification: A Simple Test. *Am Nat* 172(1):102–115.

159. Pagel M (1997) Inferring evolutionary processes from phylogenies. *Zool Scr* 26(4):331–348.

160. Matthews LJ, Arnold C, Machanda Z, Nunn CL (2011) Primate extinction risk and historical patterns of speciation and extinction in relation to body mass. *Proc R Soc Lond B Biol Sci* 278(1709):1256–1263.

161. Kozak KH, Wiens JJ (2012) Phylogeny, ecology, and the origins of climate–richness relationships. *Ecology* 93(sp8):S167–S181.

162. Dugo-Cota Á, Castroviejo-Fisher S, Vilà C, Gonzalez-Voyer A (2015) A test of the integrated evolutionary speed hypothesis in a Neotropical amphibian radiation. *Glob Ecol Biogeogr* 24(7):804–813.

163. Harvey MG, et al. (2017) Positive association between population genetic differentiation and speciation rates in New World birds. *Proc Natl Acad Sci* 114(24):6328–6333.

164. Rabosky DL, Huang H (2016) A Robust Semi-Parametric Test for Detecting Trait-Dependent Diversification. *Syst Biol* 65(2):181–193.

165. Maddison WP, FitzJohn RG (2015) The Unsolved Challenge to Phylogenetic Correlation Tests for Categorical Characters. *Syst Biol* 64(1):127–136.

166. Shipley B (2000) Cause and correlation in biology a user's guide to path analysis, structural equations, and causal inference /.

167. von Hardenberg A, Gonzalez-Voyer A (2013) Disentangling Evolutionary Cause-Effect Relationships with Phylogenetic Confirmatory Path Analysis. *Evolution* 67(2):378–387.

168. Gonzalez-Voyer A, von Hardenberg A (2014) An Introduction to Phylogenetic Path Analysis. *Modern Phylogenetic Comparative Methods and Their Application in Evolutionary Biology*, ed Garamszegi LZ (Springer Berlin Heidelberg, Berlin, Heidelberg), pp 201–229.

169. van der Bijl W (2018) phylopath: Easy phylogenetic path analysis in R. *PeerJ* 6:e4718.

170. Shipley B (2013) The AIC model selection method applied to path analytic models compared using a d-separation test. *Ecology* 94(3):560–564.

171. Shipley B (2009) A New Inferential Test for Path Models Based on Directed Acyclic Graphs. *Struct Equ Model*. doi:10.1207/S15328007SEM0702_4.

172. Cusimano N, Renner SS (2010) Slowdowns in Diversification Rates from Real Phylogenies May Not be Real. *Syst Biol* 59(4):458–464.

173. Brock CD, Harmon LJ, Alfaro ME (2011) Testing for Temporal Variation in Diversification Rates When Sampling is Incomplete and Nonrandom. *Syst Biol*:syr007.

174. Sanmartín I, Meseguer AS (2016) Extinction in Phylogenetics and Biogeography: From Timetrees to Patterns of Biotic Assemblage. *Evol Popul Genet*:35.

175. Rabosky DL (2015) No substitute for real data: A cautionary note on the use of phylogenies from birth–death polytomy resolvers for downstream comparative analyses. *Evolution* 69(12):3207–3216.

176. Title PO, Rabosky DL (2017) Do Macrophylogenies Yield Stable Macroevolutionary Inferences? An Example from Squamate Reptiles. *Syst Biol* 66(5):843–856.

177. dos Reis M, et al. (2012) Phylogenomic datasets provide both precision and accuracy in estimating the timescale of placental mammal phylogeny. *Proc R Soc Lond B Biol Sci* 279(1742):3491–3500.

178. Romiguier J, Ranwez V, Delsuc F, Galtier N, Douzery EJP (2013) Less Is More in Mammalian Phylogenomics: AT-Rich Genes Minimize Tree Conflicts and Unravel the Root of Placental Mammals. *Mol Biol Evol* 30(9):2134–2144.

179. Foley NM, Springer MS, Teeling EC (2016) Mammal madness: is the mammal tree of life not yet resolved? *Phil Trans R Soc B* 371(1699):20150140.

180. Tarver JE, et al. (2016) The Interrelationships of Placental Mammals and the Limits of Phylogenetic Inference. *Genome Biol Evol* 8(2):330–344.

181. Esselstyn JA, Oliveros CH, Swanson MT, Faircloth BC (2017) Investigating Difficult Nodes in the Placental Mammal Tree with Expanded Taxon Sampling and Thousands of Ultraconserved Elements. *Genome Biol Evol* 9(9):2308–2321.

182. Scornavacca C, Galtier N (2017) Incomplete Lineage Sorting in Mammalian Phylogenomics. *Syst Biol* 66(1):112–120.

183. Graur D, Hide WA, Li W-H (1991) Is the guinea-pig a rodent? *Nature* 351:649–652.

184. Puttick MN, Thomas GH, Benton MJ (2016) Dating placentalia: Morphological clocks fail to close the molecular fossil gap. *Evol Int J Org Evol* 70(4):873.

185. Beck RMD, Baillie C (2018) Improvements in the fossil record may largely resolve the conflict between morphological and molecular estimates of mammal phylogeny. *bioRxiv*:373191.

186. Guillerme T, Cooper N (2016) Assessment of available anatomical characters for linking living mammals to fossil taxa in phylogenetic analyses. *Biol Lett* 12(5):20151003.

187. Halliday TJD, Upchurch P, Goswami A (2017) Resolving the relationships of Paleocene placental mammals. *Biol Rev* 92(1):521–550.

188. Liu L, et al. (2017) Genomic evidence reveals a radiation of placental mammals uninterrupted by the KPg boundary. *Proc Natl Acad Sci*:201616744.

189. Springer MS, et al. (2017) Waking the undead: Implications of a soft explosive model for the timing of placental mammal diversification. *Mol Phylogenet Evol* 106:86–102.

190. Phillips MJ (2016) Geomolecular Dating and the Origin of Placental Mammals. *Syst Biol* 65(3):546–557.

191. Phillips MJ, Fruciano C (2018) The soft explosive model of placental mammal evolution. *BMC Evol Biol* 18(1):104.

192. Gatesy J, Springer MS (2017) Phylogenomic red flags: Homology errors and zombie lineages in the evolutionary diversification of placental mammals. *Proc Natl Acad Sci* 114(45):E9431–E9432.

193. Alroy J, et al. (2018) Taxonomic occurrences of Mammalia recorded in Fossilworks, the Evolution of Terrestrial Ecosystems database, and the Paleobiology Database. Fossilworks. http://fossilworks.org.

194. Brown JW, Rest JS, García-Moreno J, Sorenson MD, Mindell DP (2008) Strong mitochondrial DNA support for a Cretaceous origin of modern avian lineages. *BMC Biol* 6(1):6.

195. Cifelli RL (2004) Chapter 5: Marsupial Mammals from the Albian–Cenomanian (Early–Late Cretaceous) Boundary, Utah. *Bull Am Mus Nat Hist* 285:62–79.

196. Davis BM (2007) A revision of "pediomyid" marsupials from the Late Cretaceous of North America. *ACTA Palaeontol Pol*:40.

197. Purvis A, Fritz SA, Rodríguez J, Harvey PH, Grenyer R (2011) The shape of mammalian phylogeny: patterns, processes and scales. *Philos Trans R Soc Lond B Biol Sci* 366(1577):2462–2477.

198. Beaulieu JM, O'Meara BC (2015) Extinction can be estimated from moderately sized molecular phylogenies. *Evolution* 69(4):1036–1043.

199. Rabosky DL (2016) Challenges in the estimation of extinction from molecular phylogenies: A response to Beaulieu and O'Meara. *Evolution* 70(1):218–228.

200. Nee S, Holmes EC, May RM, Harvey PH (1994) Extinction rates can be estimated from molecular phylogenies. *Philos Trans R Soc Lond B-Biol Sci* 344:77–82.

201. Stadler T (2011) Simulating trees with a fixed number of extant species. *Syst Biol* 60:676–684.

202. Höhna S, May MR, Moore BR (2015) Phylogeny Simulation and Diversification Rate Analysis with TESS. Available at: https://cran.r-project.org/web/packages/TESS/vignettes/Bayesian_Diversification_Rate_Analysis.pdf.

203. Renne PR, et al. (2013) Time Scales of Critical Events Around the Cretaceous-Paleogene Boundary. *Science* 339(6120):684–687.

204. Wilson GP, et al. (2012) Adaptive radiation of multituberculate mammals before the extinction of dinosaurs. *Nature* 483(7390):457–460.

205. Wilson GP (2013) Mammals across the K/Pg boundary in northeastern Montana, U.S.A.: dental morphology and body-size patterns reveal extinction selectivity and immigrant-fueled ecospace filling. *Paleobiology* 39(3):429–469.

206. Wilson GP (2014) Mammalian extinction, survival, and recovery dynamics across the Cretaceous-Paleogene boundary in northeastern Montana, USA. *Geol Soc Am Spec Pap* 503:365–392.

207. Grossnickle DM, Newham E (2016) Therian mammals experience an ecomorphological radiation during the Late Cretaceous and selective extinction at the K–Pg boundary. *Proc R Soc B* 283(1832):20160256.

208. Foley NM, et al. (2018) Growing old, yet staying young: The role of telomeres in bats' exceptional longevity. *Sci Adv* 4(2):eaao0926.

209. Murray SW, et al. (2012) Molecular phylogeny of hipposiderid bats from Southeast Asia and evidence of cryptic diversity. *Mol Phylogenet Evol* 62(2):597–611.

210. Loss AC, Leite YLR (2011) Evolutionary diversification of *Phyllomys* (Rodentia: Echimyidae) in the Brazilian Atlantic Forest. *J Mammal* 92:1352–1366.

211. Upham NS, Patterson BD (2015) Evolution of caviomorph rodents: a complete phylogeny and timetree for living genera. *Biology of Caviomorph Rodents: Diversity and Evolution*, eds Vassallo AI, Antenucci D (SAREM Series A, Buenos Aires, Argentina), pp 63–120.

212. Emmons LH, Fabre P (2018) A Review of the *Pattonomys/Toromys* Clade (Rodentia: Echimyidae), with Descriptions of a New *Toromys* Species and a New Genus. *Am Mus Novit* 3894(3894):1–52.

213. Voss RS, Jansa SA (2009) Phylogenetic relationships and classification of didelphid marsupials, and extant radiation of New World methatherian mammals. *Bull Am Mus Nat Hist* 32:1–177.

214. Díaz-Nieto JF, Jansa SA, Voss RS (2016) DNA sequencing reveals unexpected Recent diversity and an ancient dichotomy in the American marsupial genus Marmosops (Didelphidae: Thylamyini). *Zool J Linn Soc* 176(4):914–940.

215. Pavan SE, Voss RS (2016) A revised subgeneric classification of short-tailed opossums (Didelphidae, Monodelphis). (American Museum novitates, no. 3868). *Subgenera of shorttailed opossums (Monodelphis)*. Available at: http://digitallibrary.amnh.org/handle/2246/6692 [Accessed December 22, 2017].

216. Rasoloarison RM, Weisrock DW, Yoder AD, Rakotondravony D, Kappeler PM (2013) Two New Species of Mouse Lemurs (Cheirogaleidae: Microcebus) from Eastern Madagascar. *Int J Primatol* 34(3):455–469.

217. Zachos FE, et al. (2013) Species inflation and taxonomic artefacts—A critical comment on recent trends in mammalian classification. *Mamm Biol - Z Für Säugetierkd* 78(1):1–6.

218. Groves CP (2014) Primate Taxonomy: Inflation or Real? *Annu Rev Anthropol* 43(1):27–36.

219. Muldoon KM (2010) Paleoenvironment of Ankilitelo Cave (late Holocene, southwestern Madagascar): implications for the extinction of giant lemurs. *J Hum Evol* 58(4):338–352.

220. Brown JH, Stevens GC, Kaufman DM (1996) The geographic range: Size, Shape, Boundaries, and Internal Structure. *Annu Rev Ecol Syst* 27(1):597–623.

221. Lomolino MV (2005) Body size evolution in insular vertebrates: generality of the island rule. *J Biogeogr* 32(10):1683–1699.

222. Rabosky DL (2015) No substitute for real data: A cautionary note on the use of phylogenies from birth–death polytomy resolvers for downstream comparative analyses. *Evolution* 69(12):3207–3216.

223. Harvey MG, Rabosky DL (2018) Continuous traits and speciation rates: Alternatives to state-dependent diversification models. *Methods Ecol Evol* 9(4):984–993.

224. Esselstyn JA, Maharadatunkamsi, Achmadi AS, Siler CD, Evans BJ (2013) Carving out turf in a biodiversity hotspot: multiple, previously unrecognized shrew species co-occur on Java Island, Indonesia. *Mol Ecol* 22(19):4972–4987.

225. Rowe KC, Achmadi AS, Esselstyn JA (2014) Convergent evolution of aquatic foraging in a new genus and species (Rodentia: Muridae) from Sulawesi Island, Indonesia. *Zootaxa* 3815(4):541–564.

226. Groves C, Grubb P (2011) *Ungulate Taxonomy* (JHU Press).

227. Gutiérrez EE, Garbino GST (2018) Species delimitation based on diagnosis and monophyly, and its importance for advancing mammalian taxonomy. *Zool Res*:97.

228. Pimm SL, et al. (2014) The biodiversity of species and their rates of extinction, distribution, and protection. *Science* 344(6187):1246752.